Modelling Non-linear and Distributed Elements in Transient State Estimation

Alejandro Castellanos Escamilla

A thesis presented for the degree of
Doctor of Philosophy
in
Electrical and Computer Engineering
at the
University of Canterbury,
Christchurch, New Zealand.

2015

ABSTRACT

Power quality state estimation (PQSE) is a set of techniques with the objective to estimate diverse power quality phenomena in electric power systems; transient state estimation (TSE) being one such technique. Its objective is to estimate node voltage waveforms in a network after it has been subject to an electromagnetic transient. This work focuses on TSE using the numerical integrator substitution (NIS) method to model the system transients. The objective of this work is to further extend TSE with NIS, to include non-linear and distributed parameter elements.

The intended application for TSE is to serve as an analysis tool for post-disturbance root cause analysis. The technique can be considered under development but in the future must be capable, considering certain requirements are met for measurements and system modelling, to help in the identification of the cause(s) for failure or malfunction when electromagnetic transients are recorded. The use of TSE removes the need of multiple simulation runs that are currently required in order to find the cause of disturbance (each simulation with a different system configuration trying to match measured waveforms).

The contributions of this work include: analysis of numerical oscillation in TSE with NIS using single-phase circuits, the application of TSE with NIS to non-linear branches using the piecewise linear method, the development of an extended observability analysis capable of identifying unobservable islands, the application of virtual measurements to linear and lumped circuits, and the application of TSE with NIS to transmission lines modelled with distributed parameters.

ACKNOWLEDGEMENTS

This work was supported by Mexico's National Council for Science and Technology (CONACyT) through a PhD scholarship. The author would like to thank CONACyT for its financial support.

To my supervisor Professor Neville Watson; my infinite gratitude for his guidance, advice, and patience.

To the people that enriched this experience, many of them my colleagues in the pursuit of a post-grad degree in electric power systems at Canterbury. Thank you for being there. The following is an extensive but certainly incomplete list: Bhaba Das, Zhiyang Jin, Kalyan Malla, Michael Hwang, Parash Achrya, Pat Bodger, Andrew Lapthorn, Edsel Villa, Ken Smart, Giang Dang, Lance Frater, Jorge Celis, Kelvin Gong, Harry Li, Yanosh Irani, Sheejan Pandey, Rabia Nazir, Eduardo Benitez Sandoval, Pablo Torres Lepe, Denise Arroyo Lambaer, Diwakar Brunel, Yiwei Hu, Yuheng Lu, Xueshu Cao, Josh Schipper, Jiaksan Tan, Rahman Peimankar, Patrick Chen, Ali Farzanehrafat, Steffen Fischer, Ming Zhong, and James Ormrod.

GLOSSARY

Abbreviations

CT	Current Transformer
CVT	Capacitor Voltage Transformer
dB	Decibel
EMS	Energy Management Systems
EMTP	ElectroMagnetic Transients Program
GPS	Global Positioning System
IED	Intelligent Electronic Device
KCL	Kirchhof's Current Law
NIS	Numerical Integrator Substitution
NRMSE	Normalised Root Mean Square Error
PQSE	Power Quality State Estimation
RMS	Root Mean Square
SCADA	Supervisory Control And Data Acquisition
SNR	Signal-to-Noise Ratio
SVD	Singular Value Decomposition
TSE	Transient State Estimation

Nomenclature

$\mathbf{z}$	Measurements vector
$\mathbf{H}$	Measurements matrix
$\mathbf{x}$	State variables vector
$\mathbf{w}$	Measurement's Gaussian white noise
$\mathbf{G}$	Gain matrix
$\mathbf{H}^T$	Transpose of matrix $\mathbf{H}$
$\mathbf{H}^{-1}$	Inverse of matrix $\mathbf{H}$
$\det(\mathbf{H})$	Determinant of matrix $\mathbf{H}$
$\text{rank}(\mathbf{H})$	Rank of matrix $\mathbf{H}$
$\text{null}(\mathbf{H})$	Nullity of matrix $\mathbf{H}$
v_k	Voltage at node k
i_{jk}	Current flow in branch jk, positive direction from j to k
R	Resistance
L	Inductance
C	Capacitance
t	Time
$\frac{d}{dt}$	Ordinary derivative
Δt	Time interval magnitude or time-step
$\int_a^b f(t)dt$	Definite integral
$v_{k(t)}$	Discrete voltage at node k at time t
$\frac{\partial}{\partial t}$	Partial derivative
$R^{'}$	Resistance per unit length
Z_c	Characteristic impedance, transmission line
ν	Wave phase velocity, transmission line
τ	Wave travelling time, transmission line
$\mathbf{Y}$	Equivalent conductance matrix
$\mathbf{U}$	Right eigenvectors matrix, SVD
$\mathbf{V}$	Left eigenvectors matrix, SVD
$\mathbf{S}$	Singular values diagonal matrix, SVD
$\mathbf{H}^+$	Pseudo-inverse of matrix $\mathbf{H}$
σ	Standard deviation
σ^2	Variance
$A_{PEAKsignal}$	Signal amplitude, peak value
$A_{RMSsignal}$	Signal amplitude, RMS value

CONTENTS

LIST OF FIGURES

LIST OF TABLES

Chapter 1

INTRODUCTION

1.1 GENERAL OVERVIEW

Electric power systems, along with other systems, are the backbone of modern society. Modern life would be impossible without electric motors, major internet server facilities, public lighting, traffic control centres, homes, etc, receiving energy from the network with the expected power quality, in a reliable and cost effective way. Electric power systems are in continuous change and new technologies are being implemented all the time. However, the main infrastructure (e.g., transmission lines, substations, power generation plants) is in most cases old and its replacement or enhancement is slow and sometimes barely matches the growing demand. Alongside this, modern society is increasing its use of devices that when connected to the network produces "pollution" and increase the stress on the existing infrastructure. In this scenario the network has to work as close to its limits as possible. To achieve this, the monitoring of the existing conditions (the state of the system) is of paramount importance, as are estimation tools to find the causes of malfunctions or failures in the system as soon as possible to avoid future service interruptions. Power quality state estimation (PQSE) is a group of tools that aims at these objectives through the use of field measurements; measurements which are becoming more available as the grid changes.

Transient state estimation (TSE) is one of these tools, and could be used to find causes of malfunctions or failures by estimating voltage waveforms based on recorded current and voltage transient waveforms. The technique is based on well established theories like state estimation and electromagnetic transient simulation for power systems. The technique is still under development, with two main approaches used to model the transient behaviour: the state-space formulation, and the numerical integrator substitution (NIS) method. Both approaches have their merits and limitations, but the main limitation for the state-space formulation is a higher complexity to model non-linear and distributed parameter elements. This, combined with the fact that NIS is the standard method to simulate electromagnetic transients in power systems, resulted in the current work in TSE using the NIS methodology.

To have a TSE method that can be applied to any power system subjected to any kind of electromagnetic transient, more improvements are required. The work presented in this thesis puts TSE closer to this general objective.

1.2 OBJECTIVES

The two main objectives of this work are: the inclusion of non-linear elements in TSE with NIS, and the application of the estimation method to transmission lines modelled with distributed parameters.

To achieve these objectives the NIS formulation for both non-linear and distributed parameter elements are reviewed and modified for its application in TSE. During the process that finally ended in the objectives, areas of improvement for the existing TSE with NIS method were identified and modifications were proposed. Some of the proposed modifications ended in further contributions.

1.3 CONTRIBUTIONS

The contributions of this work are (in order of importance):

- Application of TSE with NIS to transmission lines modelled with distributed parameters. This is the main contribution of this work and allows the use of TSE with NIS for transmission systems.

- Development of an extended observability analysis capable of identifying unobservable islands in circuits with linear and lumped elements. Due to lumped parameter formulation in TSE with NIS, it is possible to have unobservable islands that contain measurements; a problem which has not been previously identified.

- Application of virtual measurements to linear and lumped circuits. It is used, when possible, to make a previously unobservable island become observable.

- Application of TSE with NIS to non-linear branches. A first for TSE, and is based on the well known piecewise method.

- Application of half-step interpolation to remove numerical oscillations created by measurement's white noise in inductive branches. Although the problem of numerical oscillations has been previously dealt with for simulation, the use of interpolation for TSE with NIS is new.

- Analysis of initial conditions effect on single-phase circuits TSE. This has not been previously reported for TSE with NIS. Its importance becomes clear in circuits modelled with distributed parameters (including three-phase circuits).

1.4 THESIS LAYOUT

The thesis is organised as follows:

Chapter 2

Starts with a brief review of PQSE techniques, this introduces ideas and concepts that are used through the thesis. Followed by a short introduction to NIS methodology. This chapter ends with a brief review of TSE with NIS existing formulation, for circuits with linear and lumped parameter elements.

Chapter 3

First noise modelling is reviewed and its effects are analysed using a simple single-phase circuit. Then the use of half-step interpolation is introduced as a solution to the problem generated of numerical oscillation in TSE with NIS. Finally, the modelling of non-linear elements with the piecewise linear method is presented and applied to TSE.

Chapter 4

Begins with the review of the existing observability analysis method based on singular value decomposition (SVD) matrices, followed by a discussion of the reasons behind partial observability in circuits with linear and lumped parameters. Then the observability method is extended to detect unobservable island. Finally the introduction of virtual measurement in TSE is presented.

Chapter 5

Opens with a revision of the Bergeron model with losses for transmission lines (with distributed parameters); followed by its inclusion in TSE. Finally, the accuracy of the proposed method is investigated; using as input measurements obtained from simulation results using different models (better models that include frequency-dependent parameters).

Chapter 6

This chapter presents the recommended future work for TSE with NIS, and final conclusions are given.

Chapter 2

BACKGROUND

2.1 POWER QUALITY STATE ESTIMATION

Power quality state estimation is an extension of the concept of steady-state estimation that has been to include power quality related indices and data. The classic steady-state estimation can be seen as the part of power quality state estimation that deals with over and under steady-state voltages. This method was developed in the 1960's by Schweppe [Schweppe and Wildes, 1970, Schweppe and Rom, 1970, Schweppe, 1970]. Its goal is to provide the best possible data as input to monitor and control an electric power system and was implemented in power systems control rooms in the early 1970's [Schweppe and Handschin, 1974]. The steady-state estimation deals with the estimation of values based on the power-flow problem, i.e. it takes a "snapshot" of the system and provides the best estimate of the busbar voltage and angle magnitudes based on measurements obtained by the supervisory control and data acquisition (SCADA) system at a certain time. In the 1980's, Heydt was the first to apply the concept of state estimation to harmonics [Heydt, 1989], with the primary objective of identifying harmonic sources at non-monitored load buses, i.e. load buses without harmonic measurement equipment. This was later extended as a complete (including all buses) state estimation. The technique has been implemented for testing purposes in Japan using field synchronised measurements [Kanao et al., 2005]. The transient state estimation has been proposed by Yu and Watson [Yu and Watson, 2007]. This technique estimates the voltage and current waveforms at non-monitored parts of the systems when subject to a transient phenomena such as a fault or switching condition. The first aim of this technique was to identify a fault location [Yu and Watson, 2005]. The last technique that can be catalogued as power quality state estimation is voltage sag/dip state estimation, where voltage dips frequency and parameters are estimated at non-monitored points [Wang et al., 2005, Espinosa-Juarez and Hernandez, 2007].

Figure 2.1 presents the theoretical framework of PQSE. The relationship between estimation and simulation for different phenomena is presented, as well as the use of control theory (and state estimation) concepts that are applicable to all PQSE's techniques. These concepts are defined in the next subsection. At the figure centre the types of PQSE are presented; to their left (and

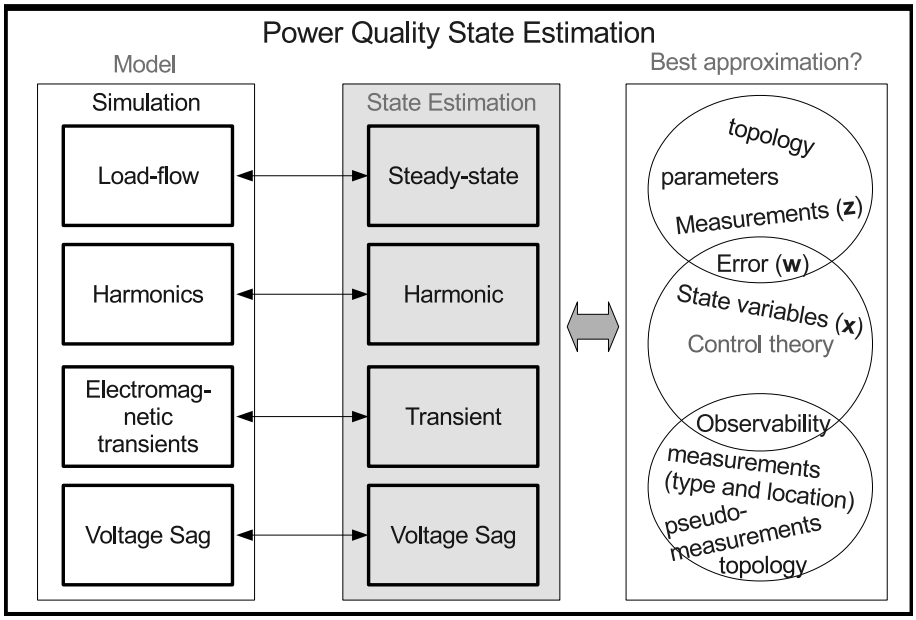

Figure 2.1 PQSE's theoretical framework.

connected by small two-way arrows) are the related power system simulation analysis, these are used in estimation to represent the system in each technique (and relate measurements with state variables); and in the right side (connected by a big two-way arrow) the state estimation theory concepts that define requirements for measurements and state variables in order to obtain a estimation.

2.1.1 Power systems steady-state estimation

2.1.1.1 Least-squares estimation; from astronomy to electric power systems

The method of least squares was developed by Karl Friedrich Gauss in 1795 while working on an astronomical problem [Sorenson, 1970] [Jazwinski, 1970, p.142]. The motion of planets and comets can be characterised by six parameters and the problem was to determine the values of the parameters from the measurement (or observation) data. Gauss argued that all our measurements are approximations to the truth, i.e. they contain errors, so the same must be true for the calculations which are based on them. Therefore, the goal of the calculations must be to approximate, as best as possible, the truth. The objective of the least-squares method is to minimise the sum of the squares of the difference between the estimated and measured values (the difference is also know as residual). According to Gauss, this will provide the *most probable value* for the wanted parameters.

Gauss's work served as a base for future developments. The second world war brought advancements in the control theory area of estimation when the problem related to the aiming of

weapons was dealt with [Bennett, 1993, pp.164-185]. After the war, the concept of state was introduced in control theory to model a multiple inputs/outputs system [Smith, 2012] [Bennett, 1993, pp.200-205]. During the 1960's, work was done on estimation related to navigation, in particular dealing with space-craft and missile navigation [Handschin, 1971,Smith, 2012][1]; Fred S. Schweppe defined the power systems steady-state estimator as "a data processing algorithm for converting redundant meter readings and other available information into an estimate of the state of the static-state vector" [Schweppe and Wildes, 1970,Schweppe and Rom, 1970,Schweppe, 1970].

2.1.1.2 State estimation and the electric power systems monitoring and control

The state of a power system refers to its operating condition [Wu, 1990], which is relative to the power flowing in, and voltages at, the different system components. If the bus voltage magnitudes and phase angles are know, at a certain time, then the power flow and voltages can be determined for the entire system, at that time. Hence, in steady-state, the complex bus voltages (voltage phasors) are the state variables, because from its knowledge the state of the system can be determined.

To monitor and control an electric power network, energy management systems (EMS) are utilised at the energy control centres. The SCADA system is that part of the EMS that collects the field measurements, mainly real and reactive power flows which are also used for revenue metering and recording purposes. Other information collected includes currents, bus voltage magnitudes or bus phase angles. The SCADA system also provides status information such as transformer tap positions and power circuit breakers on/off status that determine the network configuration. With this information as an input, the steady-state estimation algorithm provides the most probable values of the bus voltage magnitudes and phase angles that will serve as input for further EMS functions such as load frequency control and/or security assessment that are performed on-line [Abur and Exposito, 2004, pp.2-7] [Grainger and Stevenson, 1994, p.664] [Schweppe and Handschin, 1974]. Schweppe's genius resided in his ability to understand the need for a reliable real-time data to be fed to the control centres[2], before steady-state estimation the control centres would take the data directly from measurements and perform the EMS functions calculations [Stagg et al., 1970]. Sometimes the received data was compared against expected results from load-flow simulations or be "evaluated" by the operator based on experience [Handschin, 1971, p.57].

[1] In 1960 R.E. Kalman published a paper in the ASME Journal of Basic Engineering entitled "A new approach to linear filtering and prediction problems" in which Kalman introduced the design equations for the discrete Kalman filter, which can be regarded as an efficient computational solution of Gauss least-squares method [Sorenson, 1970].

[2] The term "real-time" used here means that the data been used in the control centre was taken from the field a few seconds or minutes before. This delay is caused by the time required to measure, sent the data to the control centre, pre-process the data and finally perform the state estimation.

2.1.1.3 The steady state estimation problem

The state estimation relates the measurements vector $\mathbf{z}$ to the state variables vector $\mathbf{x}$ by

$$\mathbf{z} = \mathbf{h}(\mathbf{x}) + \mathbf{w} \tag{2.1}$$

where $\mathbf{w}$ is the measurements error vector and $\mathbf{h}(\mathbf{x})$ is a vector of non-linear scalar functions of $\mathbf{x}$ determined by the system relation between the measurements and the state variables. Because the most commonly available data are power flows, the non-linear equations have a similar formulation to the load-flow problem [Wu, 1990, Handschin, 1971, Schweppe and Rom, 1970]. The number of state variables is equal to n, and because the swing bus angle value is zero[3]

$$\dim[\mathbf{x}] = n = 2N - 1$$

where N is the number of buses. The number of measurements is m and hence

$$\dim[\mathbf{z}] = m$$

the vector $\mathbf{w}$ is also m-dimensional.

In steady-state estimation, the system is considered balanced, symmetric and operating at constant frequency. Load-flow calculations consider that the input data does not contain observation errors and the number of given quantities equals the number of unknown bus voltages, i.e. $m = n$. In order to obtain an improved solution in state estimation, the input data should contain redundancy, i.e. the number of measurements m should be larger than the number of state variables n ($m > n$). The output of the estimator $\hat{\mathbf{x}}$, which are the values of the state variables that minimise the errors, gives complete information about the state of the system [Handschin, 1971].

The errors $\{w_1, w_2, \ldots, w_m\}$ are assumed to be independent Gaussian random variables with zero mean. The variance σ_i^2 of the measurement error w_i, provides an indication of the certainty or degree of confidence about that particular measurement [Wu, 1990]. The measurement error covariance matrix $\mathbf{R}$ is

$$\mathbf{R} = E\{\mathbf{w}\mathbf{w}^T\} = \begin{bmatrix} \sigma_1^2 & & & 0 \\ & \sigma_2^2 & & \\ & & \ddots & \\ 0 & & & \sigma_m^2 \end{bmatrix}. \tag{2.2}$$

In (2.1), $\mathbf{x}$ is a deterministic quantity. Because the errors $\mathbf{w}$ are random variables, the measure-

[3]The swing bus (or slack bus) is a reference bus for which voltage magnitude and angle are 1 p.u. and 0 rad respectively, in a load-flow simulation.

ments $\mathbf{z}$ are also random variables. It can be shown than $\mathbf{z}$ has a Gaussian distribution with mean $\mathbf{h}(\mathbf{x})$ and covariance $\mathbf{R}$. The probability density function of $\mathbf{z}$ can be written as [Handschin, 1971]

$$p(\mathbf{z}) = \frac{e^{-\frac{1}{2}[\mathbf{z}-\mathbf{h}(\mathbf{x})]^T\mathbf{R}^{-1}[\mathbf{z}-\mathbf{h}(\mathbf{x})]}}{(2\pi)^{\frac{m}{2}}(\det\mathbf{R})^{\frac{1}{2}}}. \tag{2.3}$$

For the state estimation problem, a set of measurements $\mathbf{z}$ has been observed based on the fact that it is desired to estimate the state $\mathbf{x}$. An $\mathbf{x}$ is selected which makes the observed $\mathbf{z}$ most likely to have been observed, i.e. the $\mathbf{x}$ which maximises the probability density function (2.3). An estimate $\hat{\mathbf{x}}$ thus obtained is called the maximum likelihood estimate [Wu, 1990].
To maximise $p(\mathbf{z})$ in (2.3) it is necessary to minimise the quadratic term in the exponent, i.e.

$$\min_x \mathbf{J}(\mathbf{x}) = \frac{1}{2}[\mathbf{z}-\mathbf{h}(\mathbf{x})]^T\mathbf{R}^{-1}[\mathbf{z}-\mathbf{h}(\mathbf{x})] \tag{2.4}$$

$$= \sum_{i=1}^{m}\frac{1}{2}\frac{\{z_i - h_i(\mathbf{x})\}^2}{\sigma_i^2}. \tag{2.5}$$

Because the maximum likelihood estimate in this case minimises the error squared weighted by the measurement accuracy, it is commonly called the weighted least squares (WLS) estimate [Wu, 1990][4].

The following condition has to be satisfied [Abur and Exposito, 2004, p.18]

$$g(\hat{\mathbf{x}}) = \frac{\partial\mathbf{J}}{\partial\mathbf{x}} = -\boldsymbol{H}^T(\hat{\mathbf{x}})\mathbf{R}^{-1}[\mathbf{z}-\mathbf{h}(\hat{\mathbf{x}})] = 0 \tag{2.6}$$

$$\text{where} \qquad \boldsymbol{H}(\mathbf{x}) = \left[\frac{\partial\mathbf{h}(\mathbf{x})}{\partial\mathbf{x}}\right].$$

Expanding the non-linear function $g(\mathbf{x})$ using Taylor's series around $\mathbf{x}^k$

$$g(\mathbf{x}) = g(\mathbf{x}^k) + \mathbf{G}(\mathbf{x}^k)(\mathbf{x}-\mathbf{x}^k) + \cdots = 0.$$

Using Newton's method and ignoring the second derivative and higher terms:

$$\mathbf{x}^{k+1} = \mathbf{x}^k - \left[\mathbf{G}(\mathbf{x}^k)\right]^{-1} g(\mathbf{x}^k)$$

where k is the iteration index,
$\mathbf{x}^k$ is the solution vector at iteration k,

$$\mathbf{G}(\mathbf{x}^k) = \frac{\partial g(\mathbf{x}^k)}{\partial\mathbf{x}} = \boldsymbol{H}^T(\mathbf{x}^k)\mathbf{R}^{-1}\boldsymbol{H}(\mathbf{x}^k)$$

[4]The methods of least squares and maximum likelihood only produce the same result under the conditions presented in page 8 for the errors and measurements, see "Estimation by least-squares and by maximum likelihood" by J. Berkson in Proceedings of the Third Berkeley Symposium on Mathematical Statistics and Probability (1954/1955) Vol. I pp. 1-11.

$$g(\mathbf{x}^k) = -\boldsymbol{H}^T(\mathbf{x}^k)\mathbf{R}^{-1}[\mathbf{z} - \mathbf{h}(\mathbf{x}^k)]$$

$\mathbf{G}(\mathbf{x})$ is the gain matrix, which is sparse, positive definite, symmetric and non-singular if the measurements are sufficient and well distributed, i.e. the system is fully observable.

The matrix $\mathbf{G}(\mathbf{x})$ is typically not inverted, instead it is decomposed into triangular factors and the following set of equations are solved using forward/back substitutions at each iteration

$$\left[\mathbf{G}(\mathbf{x}^k)\right] \Delta\mathbf{x}^{k+1} = \boldsymbol{H}^T(\mathbf{x}^k)\mathbf{R}^{-1}[\mathbf{z} - \mathbf{h}(\mathbf{x}^k)] \tag{2.7}$$

where $\Delta\mathbf{x}^{k+1} = \mathbf{x}^{k+1} - \mathbf{x}^k$. Equation 2.7 is know as the Normal Equation [Abur and Exposito, 2004, p.18].

Beside the actual estimation of the state variables vector the following functions are also performed by the state estimator in the EMS [Abur and Exposito, 2004, p.4]:

- Topology processor. Receives the status information from the SCADA system and utilise it to create a one-line diagram of the present network, i.e. transform the bus-section/ switching-device model into a bus/branch model [Monticelli, 1999, p.4]. The parameters of the network (e.g., line impedances) are considered to be correct and known.

- Observability analysis. With the available measurements and one-line diagram, this determines unobservable branches and islands in the system if they exist. The observability analysis is run off-line mainly to determine the optimal location of measurements, but is run on-line to indicate how current changes in the network affect the system observability. A system is observable when "the set of available measurements, together with any equality constraints imposed on network flows, is sufficient to calculate the entire static-state vector of the network uniquely" [Clements, 1990]. A unique solution exists when the rank of $\mathbf{G}$ is n. A necessary but not sufficient condition is that $m \geq n$. It is not sufficient because linear dependencies can exist in the rows of $\mathbf{G}$. The necessary measurements to make a network observable can be obtained by making use of manufactured data, such as generator output or substation load demand, that are based on historical data or the dispatcher's objective guesses, called *pseudo measurements*, or information that does not require metering such as zero injections at a switching station, called *virtual measurements* [Wu, 1990]. Some methods developed for the observability analysis and optimal meter placement can be found in [Clements, 1990, Monticelli and Wu, 1985].

- Bad data processing. Detects, identifies and eliminates bad measurements which are outliers with gross errors contained in the field measurements set. The presence of those outliers invalidates the assumption of a Gaussian distribution. Under a linear approximation and considering no bad data is present, the residual has a Gaussian distribution with zero mean and covariance $\mathbf{R} - \boldsymbol{H}\mathbf{G}^{-1}\boldsymbol{H}^T$. This can be used to detect the existence of bad

data. To identify the bad data it is sufficient to compare the normalised residuals when the bad data is non-interacting. The largest corresponds to a bad measurement. After the bad measurement has been identified, it can be eliminated but it is possible that its elimination will affect the network observability. When there are several bad measurements and they interact, other techniques are required [Wu, 1990].

- Parameter and structural error processing. Estimates network parameters and detects structural errors caused by erroneous status information. Measurement redundancy and an extended model are required. The extended model includes the status and network parameters as state variables, i.e. $\mathbf{h}(\mathbf{x}, \mathbf{s}, \mathbf{y})$ where $\mathbf{s}$ is the flow through modelled switches and $\mathbf{y}$ is the flow through network impedances of uncertain value [Alsaç et al., 1998].

2.1.2 Harmonic state estimation

2.1.2.1 The use of power measurements

Gerald T. Heydt [Heydt, 1991, Introduction] changed his research interest from stochastic power-flow to harmonic power-flow studies in 1981 following the needs of the North America electric power industry (receiving funding from the Electric Power Research Institute) and introduced him into the power quality area. As a result of his involvement in the area, Heydt published [Heydt, 1989] which extended the application of state estimation from the fundamental frequency to harmonic frequencies. His intention was to "identify the source of harmonic injection given certain (and perhaps limited) bus and line measurements". The estimation considers the network as being linear and power is conserved at a specific frequency without distortion from other harmonic frequencies. Furthermore, the lines are considered to have lumped parameters. Finally, a least-squares estimation is applied only to a few pre-selected, non-monitored buses. Complex volt-amperes at certain harmonic frequencies are estimated. The measurements correspond to monitored buses and lines complex volt-amperes at the same frequencies. Measurement errors are not considered. An active power injection at a certain frequency reveals a harmonic injection with that frequency on that particular bus. The method is based on the harmonic power-flow formulation.

In 1994 Beides and Heydt presented [Beides and Heydt, 1991], here (2.1) is used in conjunction with an equation that describes the dynamic of the power system. The measurements are voltages and powers at harmonic frequencies and the state variables are the buses' harmonic voltage magnitudes and phases. The system is solved using a Kalman filter and provides a dynamic estimation, i.e. a continuously changing snapshot of the network harmonics.

The main motivation behind the estimation of harmonics is the identification of harmonic sources. Such a task is usually required after the presence of harmonics is detected due, for

example, to equipment failure or protection scheme activation. If simulations are run trying to recreate the cause of the fault, a series of guesses would have to be done as to where to place the harmonics source and its type, until the simulation output matches the suspected cause of the problem (providing an exact knowledge of the system topology and parameters is available). Another reason is the enforcement of harmonic limits in non-monitored parts of the system [Najjar and Heydt, 1991] and, finally, its introduction into EMSs to monitor the entire system harmonics and maybe replace the steady-state estimation.

2.1.2.2 Power system harmonic state estimation

Meliopoulos, Zhang and Zelingher published their work [Meliopoulos et al., 1994] with the idea that if only the fundamental frequency was presented in the measurements, the resulting estimation could replace the one obtained by an EMS using steady-state estimation. The algorithm is based on (2.1) with the following modifications over the steady-state estimation:

- Multi-phase model. A three-phase model is required to include asymmetrical conditions that are of importance and can no longer be rejected when harmonics are presented.

- Voltage and current waveform measurements. Because, there is not a globally accepted definition for reactive power when harmonics are presented.

- Multi-frequency model. No longer is only one frequency considered. The values of the network parameters are required at each harmonic frequency used.

- Synchronized measurements. Achieved by the use of a global positioning system (GPS), this guarantees that the measurements will be taken at the same instant in time (within some accuracy). This is required as the harmonic measurements demand the computation of quantities which are perform in local equipment before been sent to a data concentrator.

The state vector is the bus voltages and because the measurements are voltage and currents only, (2.1) becomes a linear equation

$$\mathbf{z} = \mathbf{H}\mathbf{x} + \mathbf{w} \tag{2.8}$$

where $\mathbf{H}$ is the measurement matrix. In [Meliopoulos et al., 1994] a least-squares solution is obtained by separating the variables into real and imaginary parts. Another solution in the WLS sense is obtained by replacing $\mathbf{h}(\mathbf{x})$ by $\mathbf{H}$ as shown in (2.8) into (2.6), which produces [Arrillaga et al., 2000, p.232]

$$\mathbf{H}^T\mathbf{R}^{-1}\mathbf{H}\hat{\mathbf{x}} = \mathbf{H}^T\mathbf{R}^{-1}\mathbf{z}. \tag{2.9}$$

Typically the number of measurements in the harmonic case is lower than the number of state variables $m < n$ and to obtain a solution virtual measurements are included. Pseudo measurements are generally not available as historical harmonics data is not commonly available. Another way to address this problem is to reduce the number of state variables to include only buses that are know or suspected to have devices that produce harmonics [Arrillaga et al., 2000, p.234] [Du et al., 1996], which is similar to the approach used by Heydt in [Heydt, 1989].

If the error vector in (2.8) is included in $\mathbf{z}$, then:

$$\mathbf{z} = \mathbf{H}\mathbf{x}. \tag{2.10}$$

Equation 2.10 is known as the measurement equation which can be solved for $\mathbf{x}$ using singular value decomposition (SVD) when $m < n$. The technique will provide particular solutions for the observable islands [Arrillaga et al., 2000, p.242]. In [Matair et al., 2000], a methodology based on this approach is presented. The use of SVD also provides information about the system observability.

The approach discussed is called Wide harmonic state estimation. Another kind of harmonic state estimation is know as Point harmonic state estimation and deals with the estimation of harmonics based on waveform measurement at one point of the system (e.g., one bus) [Watson and Arrillaga, 2003a,Soliman et al., 1990]. One method used for Point harmonic state estimation is the phasor estimation by least-squares, which is briefly presented in appendix C.

2.1.3 Voltage sag/dip state estimation

It is necessary to know the frequency of occurrence of voltage sags (or dips) in the network as well as their parameters, depth magnitude and duration, because they can have a negative impact on some equipment. This knowledge allows corrective or preventive actions to be taken, i.e. if sensitive equipment is going to be connected to a bus that is known to have a high occurrence of sags, it would have to be specified to withstand the sags frequency and severity expected, or have a mitigation device in place [IEEE, 2007, pp.129-138].

There are measurement equipment available and capable of keeping track of the number of sags and sags parameters at a network point, but it is impractical from an economic point of view to have such devices installed at all points. Most sags are caused by short circuits and as such can be simulated using short circuit analysis to calculate their magnitude. A method to estimate the location of the fault needed to produce a given sag magnitude on a radial network is available. Also available are methods to estimate the number of sags due to short circuit frequency [IEEE, 2007, pp.140-151]. The methods are based on work done by M. H. J. Bollen and L. Conrad.

Two techniques have been presented to deal with voltage sag inspired on power system steady-

state estimation. In [Wang et al., 2005] the sag magnitude is estimated as it propagates on a distribution feeder by the use of a least-squares method. The technique is based on the estimation of the voltage profile along a feeder using a limited number of measurements on the feeder. It only considers sags created by short circuits on a radial configuration. In [Espinosa-Juarez and Hernandez, 2007] the number of sags at non-monitored buses is estimated from the sags frequency at monitored buses. It uses (2.8) but ignores $\mathbf{w}$ (with $m < n$) and uses linear integer programming to solve the undetermined system.

2.1.4 Transient state estimation

While short circuit analysis is used to estimate the magnitude of voltage sags, a better approach would be to simulate the transient which, beside the approximate duration, also provide the waveform associated with a fault at a certain location. It is capable of doing so in any configuration (radial or ring). Transient analysis is not only applicable to faults but also the calculation of waveforms created by switching operations, lightning strikes and controllers action (each phenomenon with a different time scale). Therefore estimation of the transient state of a power system would be a valuable tool to obtain other power quality indices (from the estimated waveforms). It can also be applied, in the similar way harmonic state estimation determines harmonic sources, to determine the cause of failure (as indicated on section 2.1.2.1).

In recent years the Smart Grid concept has become popular. The concept captures the trend behind the increase in the requisition and installation of intelligent electronic devices (IEDs) in power systems, for monitoring and control. The presence of IEDs in the systems also means an increase in the amount of data collected, and the possibility of accessing and using such data remotely. Increasing the number of existing devices such as event recorders and digital relays capable of capturing and storing event waveforms (the storage is trigger by event detection). Smart Grid also means the push towards a widespread use of GPS time stamping in the recordings and the use of sensors that are more reliable and accurate (e.g., optical instrument transformers). All of the above is needed for TSE application, because time stamped waveforms obtained with high frequency sampling rates from remote locations are required.

2.1.4.1 The state-space approach

The concept of transient state estimation was introduced by Kent K. C. Yu and Neville R. Watson [Yu and Watson, 2007, Watson and Yu, 2008, Yu, 2005, Yu and Watson, 2005]. To relate the measurements to the state variables in the transient state, a dynamic model is required. Such a model is not required in steady-state estimation or harmonic state estimation as the system is considered quasi-static which allows the use of phasors to describe the variables. In

state variable formulation, the following equations are used to represent the system:

$$\frac{d\mathbf{x}}{dt} = \dot{\mathbf{x}} = \mathbf{A}\mathbf{x} + \mathbf{B}\mathbf{u} \tag{2.11a}$$

$$\mathbf{y} = \mathbf{C}\mathbf{x} + \mathbf{D}\mathbf{u}. \tag{2.11b}$$

In (2.11), $\mathbf{y}$ is the output variables vector, $\mathbf{u}$ is the inputs vector and $\mathbf{x}$ is the state variables vector [Watson and Arrillaga, 2003b, pp.11-12].

In [Yu and Watson, 2007], the selected state variables are bus voltages and branch currents which are calculated in a iterative way. Virtual measurements are taken from the previous iteration values. Inductance and capacitance remain constant in an iteration step, but can be modified in the next step to represent time dependent parameters. $\mathbf{H}$ is formed at each iteration, (2.9) is used to estimate the state variables also at each iteration.

In [Watson and Yu, 2008] a diakoptical segregation methodology is used to achieve an efficient formulation of the network equations. The state variables are capacitive node voltages and inductive branch currents. The derivative of voltage and current measurements are utilised as extra information to achieve observability. After forming the measurement matrix, the measurement equation is solved as

$$\mathbf{x} = \left(\mathbf{H}^T\mathbf{H}\right)^{-1}\mathbf{H}^T\mathbf{z}.$$

It is also possible to solve using $\mathbf{x} = \mathbf{H}^+\mathbf{z}$ where $\mathbf{H}^+$ is the pseudo-inverse of $\mathbf{H}$ [Watson, 2010].

2.1.4.2 Numerical integrator substitution approach

The numerical integration substitution method was introduced by Hermann W. Dommel in 1969 [Dommel, 1969]. The method is the basis for EMTP-type (ElectroMagnetic Transients Program) programs which are the standard means of simulating electromagnetic transients in the electric power industry. The method is based on Bergeron's model for distributed parameters and the trapezoidal integration rule for lumped parameters. It is possible to include time-varying and non-linear elements.

In [Watson, 2010] the method is used to estimate the state of a single-phase circuit with lumped parameters that is subject to a short circuit. Work was done by Ali Farzanehrafat, while working towards his PhD under Neville R. Watson, to extend its application to distribution systems. It has been extended to three-phase distribution systems using PI models for transformers and lines [Watson et al., 2012, Farzanehrafat and Watson, 2013, Watson and Farzanehrafat, 2014, Farzanehrafat, 2014].

The use of backward Euler method and root-matching to avoid numerical oscillation associated with the trapezoidal rule in NIS was presented in [Watson and Farzanehrafat, 2013], for three-

Table 2.1 PQSE's main characteristics.

State estimation	State variables	Measurement equation	Measurements	Remarks
Steady-state	$\|V\|$, δ_V	Non-linear ($m > n$)	P, Q, $\|I\|$, $\|V\|$, δ_V	Phasors at nominal frequency[a]
Harmonic	$\bar{V}_k$	Linear ($m < n$)	$\bar{I}_k$, $\bar{V}_k$	Phasors at harmonic frequencies[b]
Voltage sag	$\text{Sags}_{A\%}$	Linear ($m < n$)	$\text{Sags}_{A\%}$	Sag characteristics or number
Transient	v	Linear ($m < n$)	i, v	Waveforms overtime

[a] $\bar{V} = |V| \angle\delta_V$, is the voltage phasor defined by magnitude (RMS) and angle. P and Q are the real and reactive power.

[b] k index indicates harmonic order.

phase distribution systems.

With NIS it is possible (and expected) to have less measurements than state variables, so to have a general solution method the use of pseudo-inverse by SVD has become the preferred solution technique.

Table 2.1 presents the main characteristics of all PQSE techniques, and in doing so highlights their differences. Note that all other state variables can be computed (except perhaps by number of sags) from the estimated waveforms using TSE. Examples where sag characteristics and harmonics are obtained from TSE results will be presented in chapter 5.

2.2 NUMERICAL INTEGRATOR SUBSTITUTION METHOD

For lumped parameter elements the NIS method uses the trapezoidal rule to discretise or convert the differential equations that describe the power system elements to difference equations. The Bergeron method (or characteristics method) is applied to elements modelled with distributed parameters.

2.2.1 Lumped parameters

For a lumped inductor, the voltage difference at its terminals (j and k) is proportional to the inductance (L, given in Henries) times the derivative of the current against time:

$$v_L = v_j - v_k = L\frac{di_{jk}}{dt}. \tag{2.12}$$

The current at time $t - \Delta t$ is

$$i_{jk(t-\Delta t)} = \frac{1}{L} \int_{t_0}^{t-\Delta t} (v_j - v_k) dt \tag{2.13}$$

where t_0 is the initial time. From this point in time the current at time t is

$$\begin{aligned} i_{jk(t)} &= \frac{1}{L} \int_{t_0}^{t} (v_j - v_k) dt = \frac{1}{L} \left\{ \int_{t_0}^{t-\Delta t} (v_j - v_k) dt + \int_{t-\Delta t}^{t} (v_j - v_k) dt \right\} \\ &= i_{jk(t-\Delta t)} + \frac{1}{L} \int_{t-\Delta t}^{t} (v_j - v_k) dt. \end{aligned} \tag{2.14}$$

Thus the current at time t is the current in the previous time, $i_{jk(t-\Delta t)}$, plus the definite integral of the voltage difference at the discretise interval divided by the inductance. The definite integral for the interval $[t - \Delta t, t]$ can be approximated using the trapezoidal rule as follows

$$\begin{aligned} i_{jk(t)} &= i_{jk(t-\Delta t)} + \frac{1}{L} \int_{t-\Delta t}^{t} (v_j - v_k) dt \\ &= i_{jk(t-\Delta t)} + \frac{1}{L} \left[t - (t - \Delta t) \right] \frac{\left[v_{j(t-\Delta t)} - v_{k(t-\Delta t)} \right] + \left[v_{j(t)} - v_{k(t)} \right]}{2} \\ &= i_{jk(t-\Delta t)} + \frac{\Delta t}{2L} \left\{ \left[v_{j(t-\Delta t)} - v_{k(t-\Delta t)} \right] + \left[v_{j(t)} - v_{k(t)} \right] \right\}. \end{aligned} \tag{2.15}$$

The differential equation has been converted to a difference equation and only information at the extremes of the interval is available (the interval magnitude being Δt). The current and voltages at the beginning of the interval are grouped together and called the current history term. Furthermore, an equivalent resistance R_{eff} is defined as equal to $2L/\Delta t$ [Dommel, 1969]. Thus

$$i_{jk(t)} = I_{\text{History}(t)} + \frac{1}{R_{\text{eff}}} \left[v_{j(t)} - v_{k(t)} \right] \tag{2.16a}$$

$$I_{\text{History}(t)} = i_{jk(t-\Delta t)} + \frac{1}{R_{\text{eff}}} \left[v_{j(t-\Delta t)} - v_{k(t-\Delta t)} \right]. \tag{2.16b}$$

Equations 2.16 can be represented as a equivalent resistance, R_{eff}, in shunt connection with a current source of magnitude $I_{\text{History}(t)}$ between circuit terminals j and k. This can be seen in figure 2.2, which is know as the Norton equivalent or circuit companion for the element.

Following a similar procedure the equations for a capacitor, are [Dommel, 1969]

$$i_{jk(t)} = I_{\text{History}(t)} + \frac{1}{R_{\text{eff}}} \left[v_{j(t)} - v_{k(t)} \right] \tag{2.17a}$$

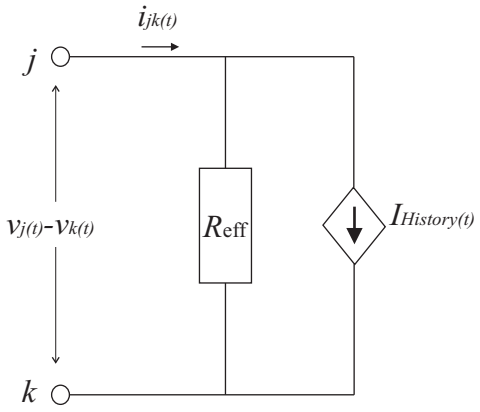

Figure 2.2 Norton equivalent.

$$I_{\text{History}(t)} = -i_{jk(t-\Delta t)} - \frac{1}{R_{\text{eff}}}\left[v_{j(t-\Delta t)} - v_{k(t-\Delta t)}\right] \tag{2.17b}$$

$$R_{\text{eff}} = \frac{\Delta t}{2C}. \tag{2.17c}$$

Finally, the equation for the resistance of value R in ohms is [Dommel, 1969]

$$i_{jk(t)} = \frac{1}{R}\left[v_{j(t)} - v_{k(t)}\right] \tag{2.18}$$

in this case R_{eff} is simply R and the history current is zero.

A known problem with NIS using the trapezoidal rule is the occurrence of numerical chatter, this is caused by sudden changes in voltage (resulting in capacitor currents with chatter) or current (inductor voltage with chatter). Many solutions have been proposed to solve this problem for simulation. They can be classified in three groups: the ones requiring circuit modification (e.g., parallel damping [Dommel, 1987]), the ones requiring modification of the integration step and method (e.g., critical damping adjustment [Marti and Lin, 1989]), and the ones requiring an alternative formulation (e.g., root-matching [Watson and Arrillaga, 2003b]). To keep the same accuracy obtained with original NIS, in the first case a judicious selection of added element parameters has to be performed as to minimise the effect during small variations and maximise it after a discontinuity (large variation). In the second case, the use of other integration formulations affect the accuracy and the overall stability of the simulation (the trapezoidal rule is an A-stable method, meaning no run off is possible). So different time-steps are required to obtain the same accuracy and avoid instability. In the particular case of root-matching, its accuracy is excellent (even with larger time-steps) it is also stable and can be added to a program using NIS with trapezoidal rule. But it can only be applied to element combinations (e.g., RL or RLC combinations), which makes it a supplement to NIS instead of a substitute.

2.2.2 Distributed parameters

For a single-phase transmission line with $L^{'}$, $R^{'}$, $C^{'}$ and $G^{'}$ (inductance, resistance, capacitance an conductance per unit length), the differential equations that model its behaviour are [Branin, 1967b][5]:

$$-\frac{\partial v}{\partial x} = L^{'}\left(\frac{\partial i}{\partial t}\right) + R^{'}i \tag{2.19a}$$

$$-\frac{\partial i}{\partial x} = C^{'}\left(\frac{\partial v}{\partial t}\right) + G^{'}v \tag{2.19b}$$

where x is the distance from the origin point (line's sending end) to any other point in the line. In general the parameters are not constant but change with frequency (and for not uniform lines change with distance as well), which further complicates its solution. A common assumption in transmission lines is to consider $C^{'}$ as constant and $G^{'} = 0$. The wave equations are obtained from (2.19), after some manipulation. The Bergeron solution method is presented in the next section.

2.2.2.1 Lossless line

For a lossless line ($R^{'}= G^{'}=0$) with constant parameters the wave equations for voltage and current are:

$$-\frac{\partial v}{\partial x \partial x} = L^{'}C^{'}\left(\frac{\partial v}{\partial t \partial t}\right) \tag{2.20a}$$

$$-\frac{\partial i}{\partial x \partial x} = C^{'}L^{'}\left(\frac{\partial i}{\partial t \partial t}\right), \tag{2.20b}$$

the solution to equation 2.20 is[6]

$$v\left(x,t\right) = f_1\left(x - \nu t\right) + f_2\left(x + \nu t\right) \tag{2.21a}$$

$$i\left(x,t\right) = \frac{1}{Z_c}\left[f_1\left(x - \nu t\right) - f_2\left(x + \nu t\right)\right] \tag{2.21b}$$

where f_1 and f_2 are arbitrary functions. $Z_c = \sqrt{L^{'}/C^{'}}$ is the characteristic impedance and $\nu = 1/\sqrt{L^{'}C^{'}}$ is the phase velocity. Physically $f_1\left(x - \nu t\right)$ is a wave travelling in the forward direction and $f_2\left(x + \nu t\right)$ is a wave travelling in the opposite direction.

[5] (2.19a) and (2.19b) are known as Telegrapher's equations to honour Oliver Heaviside (1850-1925), whom formulated the equations while working on telephonic line disturbances for a telegraph company. Simplifications in geometry (e.g., perfectly horizontal cable) and electrical parameters (e.g., uniform ground conductivity) are required to formulate them.

[6] This solution is associated with the name D'Alembert, after the French mathematician Jean-le-Ront D'Alembert (1717-1783).

If (2.21a) is multiplied by $(1/Z_c)$ and added and subtracted to (2.21b), then

$$\left(\frac{1}{Z_c}\right) v\,(x,t) + i\,(x,t) = \left(\frac{2}{Z_c}\right) f_1\,(x-\nu t) \tag{2.22a}$$

$$\left(\frac{1}{Z_c}\right) v\,(x,t) - i\,(x,t) = -\left(\frac{2}{Z_c}\right) f_2\,(x+\nu t) \tag{2.22b}$$

in equation 2.22a $(1/Z_c)v\,(x,t)+i\,(x,t)$ is constant if $(x-\nu t)$ is constant, and in equation 2.22b $(1/Z_c)v\,(x,t)-i\,(x,t)$ is constant if $(x+\nu t)$ is constant,

$$x - \nu t = c \tag{2.23a}$$

$$x + \nu t = c \tag{2.23b}$$

where c is any constant, are called the characteristics of the differential equations. The time to travel the line full length (d) is:

$$\tau = d/\nu = d\sqrt{L'C'}, \tag{2.24}$$

then an observer, travelling at the same speed and direction as the forward travelling wave, will find that the expression $(1/Z_c)v\,(x,t)+i\,(x,t)$ at node j at the time $t-\tau$ will be the same at node k at time t. So the equations are now only function of time, in discrete-time form this is[7]:

$$\left(\frac{1}{Z_c}\right) v_{j(t-\tau)} + i_{jk(t-\tau)} = \left(\frac{1}{Z_c}\right) v_{k(t)} + [-i_{kj(t)}] \tag{2.25}$$

rearranging

$$i_{kj(t)} = \left(\frac{1}{Z_c}\right) v_{k(t)} - \left(\frac{1}{Z_c}\right) v_{j(t-\tau)} - i_{jk(t-\tau)} \tag{2.26}$$

as before, a current history term can be defined as

$$I_{k(t-\tau)} = -\left(\frac{1}{Z_c}\right) v_{j(t-\tau)} - i_{jk(t-\tau)} \tag{2.27}$$

finally, the two equations for the currents at both ends of the line are

$$i_{jk(t)} = \left(\frac{1}{Z_c}\right) v_{j(t)} + I_{j(t-\tau)} \tag{2.28a}$$

$$i_{kj(t)} = \left(\frac{1}{Z_c}\right) v_{k(t)} + I_{k(t-\tau)} \tag{2.28b}$$

where

$$I_{j(t-\tau)} = -\left(\frac{1}{Z_c}\right) v_{k(t-\tau)} - i_{kj(t-\tau)} \tag{2.29}$$

[7]Dommel took the idea from L. Bergeron, "Du coup de bélier en hydraulique au coup de foudre en èlectricitè: mèthode graphique gènèrale," 1949. (Water hammer in hydraulics and wave surges in electricity) English version by editorial Wiley, 1961.

$$I_{k(t-\tau)} = -\left(\frac{1}{Z_c}\right) v_{j(t-\tau)} - i_{jk(t-\tau)}. \tag{2.30}$$

These equations are the simplest representation for distributed parameter lines in the NIS method.

The equations for the inductor (2.16) and capacitor (2.17) require information from the interval start. This means that the currents and voltages in the previous step, the previously calculated values or initial condition, have to be used to calculate the currents and voltages at the present time. The value of the equivalent resistance depends on Δt so this value will be constant for a linear and time-invariant branch as long as the integration step or time-step, Δt, does not change. For distributed parameters information is needed from previous time-steps (see equations 2.28a and 2.28b); the number of steps to keep is the result of dividing the travelling time (τ) by the integration time-step. This also means that the formulation is only needed when the travelling time is larger than the simulation time-step ($\tau > \Delta t$), otherwise a series RL combination or a PI model is used to represent transmission lines.

The selection of Δt, also affects simulation accuracy. The larger the time-step the less accurate the simulation result is. For transients classified as slow front surges (e.g., faults in overhead lines) the time step is in the range of microseconds (a typical value is 50 μs). This value can become as small as a few nanosecond for fast front surges events (e.g., lightning) in order to capture the transient waveform. Also the model used for the same element subject to different transients changes, an obvious example is the need of distributed parameter model for a transmission line (with fixed length) if Δt becomes smaller than τ.

In EMTP-like programs, the equivalent resistance values are used to generate an equivalent conductance matrix, $\mathbf{Y}$, which relates the node voltages to the currents that flow in the elements/branches connected to the corresponding nodes.

$$\mathbf{Yv} = \mathbf{i} + \mathbf{I}_{\text{History-nodal}} \tag{2.31}$$

where $\mathbf{v}$ is the vector of the node voltages, $\mathbf{i}$ is the vector of the nodal currents and $\mathbf{I}_{\text{History-nodal}}$ is the vector of the nodal history terms, each element of which is the algebraic sum of the history terms of all elements connected to the corresponding node. Note that (2.31) is the result of applying Kirchhof's current law (KCL) to each node and that each element of $\mathbf{i}$ will be zero unless there is a voltage or current source (e.g., a generator) connected to the relevant node. To simulate a transient using Dommel's method, it is necessary to solve equation 2.31 for the node voltages $\mathbf{v}$. This is typically done using optimally ordered elimination in order to avoid the calculation of the inverse [Dommel, 1969] [Dommel, 1987] [Watson and Arrillaga, 2003b].

Figure 2.3 presents a simple flowchart showing NIS implementation to simulate electromagnetic transients.

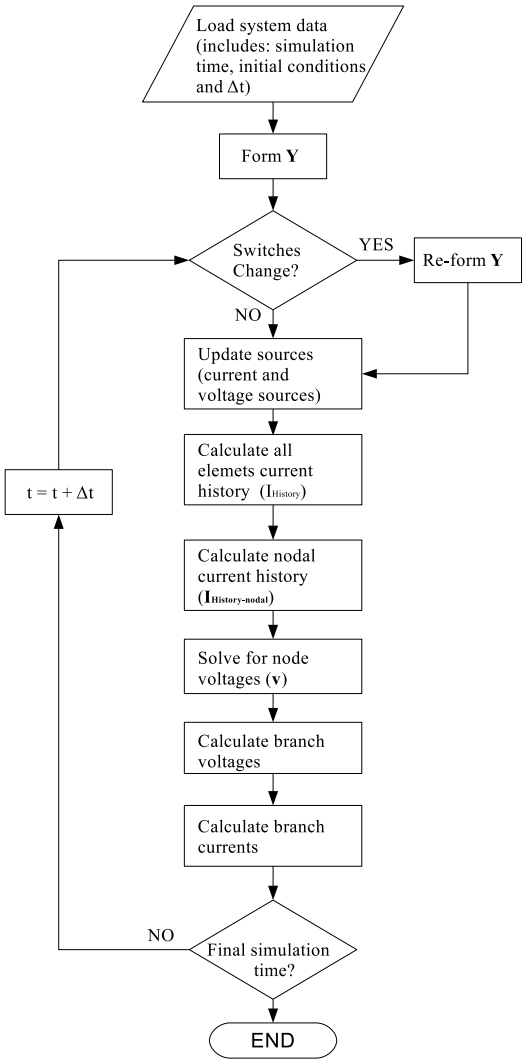

Figure 2.3 Flowchart for electromagnetic transient simulation with NIS.

2.3 TSE WITH NIS

2.3.1 Problem formulation

When applying the NIS method to TSE, it is necessary to create a measurement matrix, **H**, instead of the equivalent conductance matrix to solve equation 2.10. Because the state variables are the node voltages, then the following equations can be used to create **H** in the case of linear elements modelled with lumped parameters [Watson, 2010]:

- When the measurement m is the voltage at node j

$$h_{mj} = 1. \tag{2.32}$$

- When the measurement m is the voltage at branch jk

$$h_{mj} = 1 \tag{2.33a}$$

$$h_{mk} = -1. \tag{2.33b}$$

- When measurement m is the branch current through a resistor, inductor or capacitor between nodes j and k

$$h_{mj} = \frac{1}{R_{\text{eff}}} \tag{2.34a}$$

$$h_{mk} = -\frac{1}{R_{\text{eff}}}. \tag{2.34b}$$

All other $\mathbf{H}$ terms are zero.

According to equations 2.16 and 2.17, the currents measured for inductive and capacitive branches must include the respective history term, $I_{\text{History}(t)}$. Then, the basic equation for TSE using the NIS method is [Watson, 2010]:

$$\mathbf{z} - \mathbf{I}_{\text{History}} = \mathbf{H}\mathbf{x}. \tag{2.35}$$

When the NIS formulation changes the equations in this section are still valid, the modification (due to a different formulation or integration method) only affects the formulas for history terms and equivalent resistance.

In a three-phase system, the element/branch between buses j and k will have an equivalent resistance matrix with self and, possibly, mutual elements [Dommel, 1987]. In this case (2.32) and (2.34) will accommodate matrices [Watson and Farzanehrafat, 2013, Farzanehrafat and Watson, 2013, Watson and Farzanehrafat, 2014].

2.3.2 SVD solution

To solve 2.35 for $\mathbf{x}$, singular value decomposition (SVD) can be applied to $\mathbf{H}$ to determine its pseudo-inverse as typically the number of measurements is smaller than the number of state variables. In the case of TSE with NIS, in general, neither pseudo nor virtual measurements are available (later, a procedure to include virtual measurements will be presented). For linear and time-invariant lumped parameters $\mathbf{H}$, does not change over the entire estimation time, so its pseudo-inverse has to be calculated only once and the estimation consists of multiplying $\mathbf{z} - \mathbf{I}_{\text{History}}$ at each measurement time, or step, by $\mathbf{H}^{+}$ to obtain the node voltages. Before multiplying, the history term for inductors and capacitors must be calculated using the initial conditions in the case of the first measurement and using the estimated node voltages and the

measured branch current in the previous step for the next measurement. It is also possible to use the measured current and the previous step history current to calculate the new step $\mathbf{I}_{\text{History}(t)}$ for steps other than the first (in the first step the initial conditions are required), but this is not preferred as branch node voltages will be observable if the branch current is available as measurement and the error is smaller when using the estimated voltages[8].

Note that if a fault is located inside a measured element (e.g., a fault inside a line with current measurement), TSE does not provide an acceptable estimation because the model for such element (and the corresponding $\mathbf{H}$ terms) is no longer correct while the fault is on. When a transient includes breaker operation, matrix $\mathbf{H}$ has to change when an operation is detected if and only if the breaker is in the path of a measured current. A new pseudo-inverse calculation would be required each time a change is made in $\mathbf{H}$ (as well as the need to perform and observability analysis). TSE with NIS is still under development and a solution for these problems is not included in this thesis.

2.3.2.1 Singular value decomposition

The SVD factorization has the form:

$$\mathbf{H} = \mathbf{U}\mathbf{S}\mathbf{V}^T \tag{2.36}$$

where $\mathbf{U}$ is a $m \times m$ orthogonal matrix whose columns are the eigenvectors of $\mathbf{H}\mathbf{H}^T$, $\mathbf{V}$ is a $n \times n$ orthogonal matrix whose columns are the eigenvectors of $\mathbf{H}^T\mathbf{H}$, and $\mathbf{S}$ is a $m \times n$ diagonal matrix. The non-zero diagonal elements of $\mathbf{S}$ are the singular values of $\mathbf{H}$. The singular values are the square roots of the eigenvalues of $\mathbf{H}^T\mathbf{H}$.

The pseudo-inverse is:

$$\mathbf{H}^+ = \mathbf{V}\mathbf{S}^+\mathbf{U}^T \tag{2.37}$$

where $\mathbf{S}^+$ always exists and is the transpose of the matrix with diagonal elements equal to the reciprocals of the singular values and zero for the zero diagonal elements of $\mathbf{S}$. It can be proved that:

$$\hat{\mathbf{x}} = \mathbf{H}^+\mathbf{z} \tag{2.38}$$

is the least-squares solution of (2.10) that has the minimum norm [Anton and Busby, 2003]. This is true for any $m \times n$ matrix $\mathbf{H}$. If $\mathbf{H}$ has full column rank ($\text{rank}\,(\mathbf{H}) = n$), this case is possible when the number of measurements (m) is higher than the number of state variables (n), then the solution obtained by (2.38) is the least-squares solution (also $\hat{\mathbf{x}} = (\mathbf{H}^T\mathbf{H})^{-1}\mathbf{H}^T\mathbf{z}$). In the case when $\mathbf{H}$ does not have full column rank, this is always the case when $m < n$, ($\mathbf{H}^T\mathbf{H}$) is not invertible. So there are infinitely many solutions, but the use of the pseudo-inverse does

[8] The knowledge of one of the branch's node voltages (by estimation) is also required; more on observability in chapter 4.

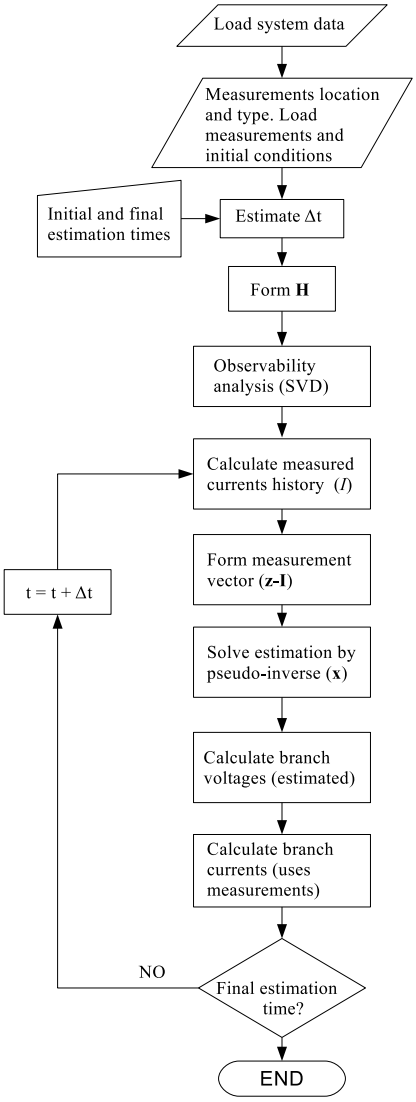

Figure 2.4 Flowchart for TSE with NIS.

provide the least-squares solution with minimum norm (a unique solution in the row space of $\mathbf{H}$).

When $m = n$ and rank $(\mathbf{H}) = n$, $\mathbf{H}$ is non-singular and $\mathbf{H}^{+} = \mathbf{H}^{-1}$. Here, $\mathbf{H}^{+}\mathbf{z}$ provides the unique solution of (2.10).

Figure 2.4 presents a simple flowchart for TSE with NIS, the changes against simulation can be seen by comparing with figure 2.3.

2.4 CONCLUSION

An overview of PQSE has been presented, and of the all four techniques described only TSE requires a transient model for the power system elements and the use of waveform discrete values while all other techniques use phasors with RMS values (in voltage sag estimation the number of sags can be the variable of interest). All techniques share the use of a measurement equation, for steady-state estimation this equation is non-linear since power measurements are used. For the application of TSE, the presence of devices capable of capturing and storing event waveforms at high sampling rates is required.

A brief description of the NIS method is given; this includes its formulation for simple lumped and distributed elements, and how to perform electromagnetic transient simulation. The element formulas do not change for estimation, but the problem formulation and solution process are different.

A revision of the state of the art for TSE with NIS is included; the method was demonstrated for three-phase distribution systems with linear, lumped, and time-invariant elements. The basic formulas for TSE with NIS are presented, including the measurement equation and how the measurement matrix is generated. TSE's preferred solution method has been explained as well; using the pseudo-inverse by SVD it is possible to estimate systems when the number of measurements is less than the number of state variables, and also provides information about system observability.

Chapter 3

NUMERICAL OSCILLATIONS, AND NON-LINEAR ELEMENTS

In this chapter noise modelling is presented and its effects are analysed using single-phase circuits. Then the use of interpolation is introduced as a solution to the problem generated by Gaussian white noise. Finally modelling of non-linear elements using the piecewise linear method in TSE is presented.

3.1 NOISE, NUMERICAL OSCILLATIONS, AND CHATTER IN TSE

The problem of numerical oscillations created by measurement's noise and wrong initial conditions is presented in this section. To start a brief description of noise and how it is simulated is presented, followed by the analysis of noise application and initial conditions mismatch in a single-phase circuit with linear and lumped parameter elements.

3.1.1 Noise definition and simulation

In this work Gaussian white noise is used to simulate measurement's noise. Is Gaussian because it has a normal or Gaussian probability distribution, and white refers to the ideal that the noise has uniform power in the entire signal frequency range[1]. A measurement (signal) with white noise is represented mathematically as [Ribeiro et al., 2014, p.80]:

$$\mathbf{z}_1 = \mathbf{y}_1 + \mathbf{w}_1 \tag{3.1}$$

where $\mathbf{z}_1$ is the observed discrete time measurement, $\mathbf{y}_1$ is the measurement without noise and $\mathbf{w}_1$ is the Gaussian white noise. The vectors' length depends on the time interval (estimation time) and the sampling rate (time-step). Therefore $\mathbf{w}_1$ is a random variable defined by mean and variance values (the variance is σ^2 where σ is the standard deviation). The mean value is zero

[1]For the mathematical definition of white noise please refer to [Jazwinski, 1970] pp. 81-85.

for Gaussian white noise. So, to completely define the noise a value for its standard deviation (and therefore variance) is needed.

For a random variable the following is true (normal white noise complies with the required conditions):

- Multiplying a random variable by a constant (c) increases the variance by the square of the constant. $\sigma^2_{c\mathbf{w}} = \mathrm{VAR}(c\mathbf{w}) = c^2\mathrm{VAR}(\mathbf{w})$.

Using this property, the standard deviation can be defined as the constant by which the random vector is multiplied as follows

$$\mathbf{z}_1 = \mathbf{y}_1 + (c \cdot \tilde{\mathbf{w}}_1) \tag{3.2}$$

where $\tilde{\mathbf{w}}_1$ is random with normal distribution, zero mean, and variance one[2]. Therefore noise standard deviation is c (its variance is $c^2 \times 1$).

Finally, in this work noise standard deviation (the constant c) is defined as a percentage of the maximum peak value obtained from the corresponding measurement ($\mathbf{y}_1$) steady-state (pre-fault) waveform. For example a measurement pre-fault peak value is 20 (can be Volts or Amperes, see figure 3.1), and it is decided a noise with standard deviation equal to 2 % pre-fault peak value is required to test the estimation algorithm. Then the measurement to be used is:

$$\mathbf{z}_1 = \mathbf{y}_1 + [(A_{PEAKpre-fault} \times c_p) \cdot \tilde{\mathbf{w}}_1] = \mathbf{y}_1 + [(20 \times 0.02) \cdot \tilde{\mathbf{w}}_1]\,. \tag{3.3}$$

This is the approach used for noise in this work; note that other definitions could be used[3]. A problem with (3.2) is the assumption that measurement's noise is the same over the entire estimation time. The noise normally changes with the measured signal amplitude, for example CT's accuracy is defined for a certain current's range and it is not the same for fault currents compared to steady-state currents (this changes with CT type, e.g., protection versus revenue). Instruments also can introduce gross errors, mainly due to saturation in CTs and CVTs. These problem are not included in this thesis, the main reason is that they can be solved in the measured signal conditioning process. There is also the existence of optical type instruments that do not present saturation and their accuracy does not change significantly with signal range [Ribeiro et al., 2014, ch.3].

[2] Using MATLAB (http://www.mathworks.com/products/matlab/) or Octave (http://www.gnu.org/software/octave/) function `randn`(N), where N is the size of the random vector to be generated, a vector with elements that follow a normal distribution with zero mean and variance equal to one is obtained.

[3] E.g., in [Farzanehrafat, 2014] a different approach is used, the random vector is multiplied by the signal value at each discrete point instead of pre-fault peak value $[z_{1(t)} = y_{1(t)}\left(1 + c_p \times \tilde{w}_{1(t)}\right)]$. Resulting in a larger noise variance for the same percentage value (variance value increases with signal peak value) and the problem that if the signal is zero the noise is also zero.

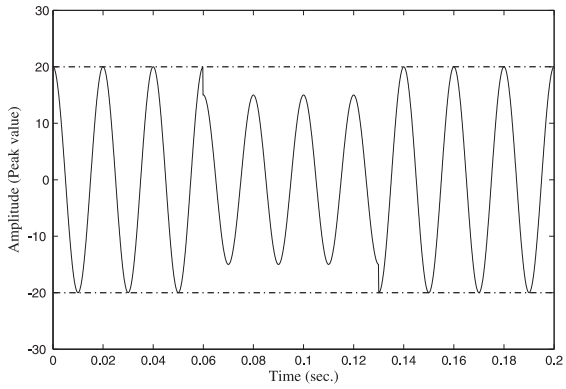

Figure 3.1 A simple waveform similar to voltage sag.

3.1.1.1 Signal-to-noise ratio

The signal-to-noise ratio (SNR) is defined as the ratio between signal and noise average powers. Typical values for SNR in power system measurements are >27 dB (40 dB being the one most used) [Ribeiro et al., 2014, p.80].

In particular if noise standard deviation is 1 % of pre-fault peak value, the measurements SNR is approximately 37 dB. This value can be easily obtained using SNR definition for a sinusoidal waveform and noise with standard deviation as in (3.3)

$$\text{SNR} = \frac{P_{signal}}{P_{noise}} = \left(\frac{A_{signal}}{A_{noise}}\right)^2 = \frac{A^2_{RMSsignal}}{\sigma^2_{noise}} \approx \frac{\left(\frac{A_{PEAKsignal}}{\sqrt{2}}\right)^2}{A^2_{PEAKsignal} \times 0.01^2} = \frac{1 \times 10^4}{2} = 5000$$

the value in decibels is $\text{SNR}_{\text{dB}} = 10 \times \log_{10}(\text{SNR}) \approx 37$ dB. The use of approximation in the above calculation is due to the fact that the transient deviations from steady-state value in the signal are being ignored to approximate the RMS value. In most cases the deviation from this value is small, for example the measurement point is away from the fault or disturbance location. When the measurement is a voltage and its waveform presents sags/dips then the SNR value will be smaller than 37 dB (depending on sag's duration and magnitude). When a measured current is carrying most of the fault current for a long time, the result is a larger SNR value because the signal power will become even larger than the noise power during the fault. See figures 3.1 and 3.2 as examples, the dotted line indicates the steady-state. Individual values for measurement's SNR ratios are not presented in this thesis.

After the information presented in this section, the range for noise standard deviation percentage (of steady-state peak value) to be used is between 0 and 3 %. Larger values for σ will result in SNR smaller than 27 dB. Typically the value of 1 % is used to approximate a SNR of 40 dB.

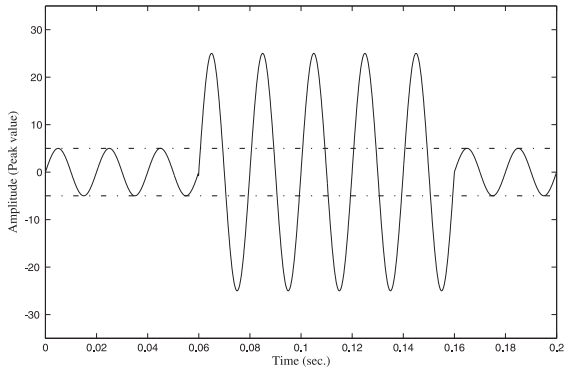

Figure 3.2 A simple waveform similar to short-circuit current.

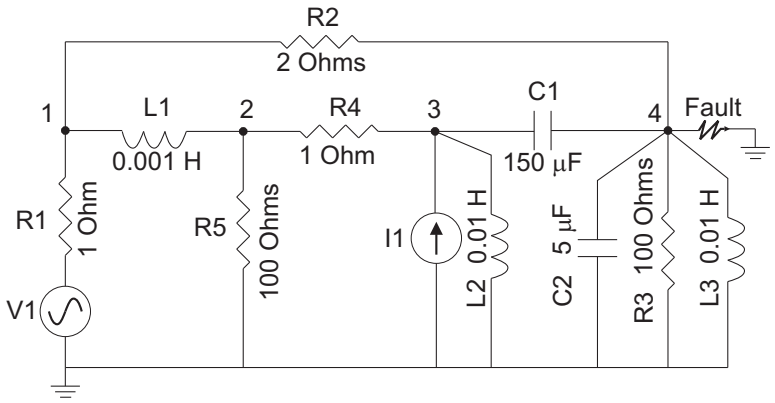

Figure 3.3 Single-phase circuit with linear and lumped parameter elements.

3.1.2 Numerical oscillations

As indicated in section 2.2, numerical chatter is a common problem in electromagnetic transient simulation using NIS. In this section the reason for numerical oscillation in TSE with NIS are investigated for simple elements in the context of a single-phase circuit.

Figure 3.3 presents a circuit used in [Watson, 2010] to introduce the concept of TSE with NIS. The values for the elements are indicated in the figure, the voltage source magnitude V1 is 220 V RMS and the current source magnitude I1 is 50 A RMS at 50Hz. Their waveforms are sinusoidal with zero and 90 degree start angles respectively. The fault is initiated at 20 ms and cleared 5 ms later. The simulation step time is 50 μs. All initial conditions are zero.

Using as measurements the currents in L2, C1, and R2, and the voltage at node 2; gives of a fully observable system. $\mathbf{H}$ is a matrix of $m \times n$ where $m = n$ (number of measurements equals the number of state variables) and its inverse exists (rank of $\mathbf{H}$ is n). The measurements are taken from results of two simulation programs, one created for the purpose of this work (based on Dommel's method) and the commercial software EMTDC/PSCAD. The figure 3.4 presents the result for node one voltage when only the "measured" C1's current is polluted with Gaussian

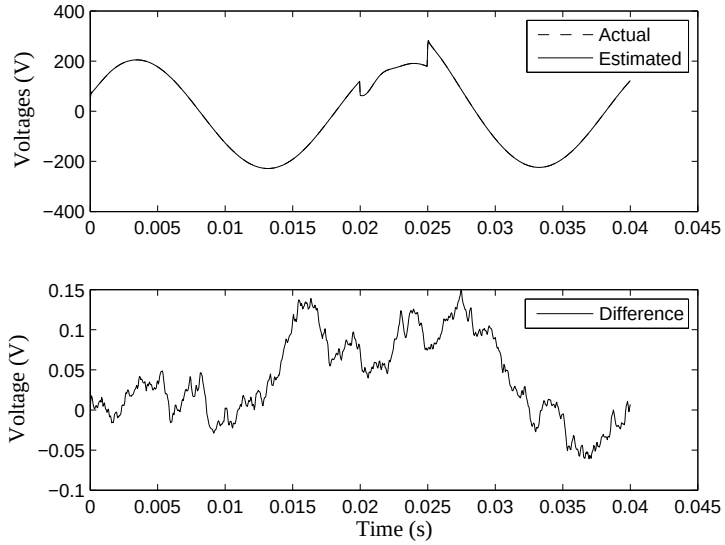

Figure 3.4 Voltage at node one for test circuit of figure 3.3, using measurements calculated with Dommel's method; C1's current contains white noise.

white noise, standard deviation equal to 1 % of current steady-state peak value calculated using the created simulation software or Dommel's method. The result is acceptable and the maximum error between the actual and estimated values is less than 0.07 % of the maximum pre-fault value in this case. Similar results are observed for the voltages at the other nodes.

When the results from EMTDC/PSCAD are used as measurements; using the same measurements as before but calculated using EMTDC/PSCAD and without introducing noise, the estimated voltage at node one (and all node voltages, except node two) presents oscillations that appear to be numerical chatter, see figure 3.5. Numerical chatter are oscillations around the true value [Watson and Arrillaga, 2003b, p.220] but, looking at the time interval when the fault is on, the average value of the estimated voltage has an offset, its average value is higher than the true value.

The oscillations, in the form of numerical chatter, are a common occurrence in EMPT-like simulations because they are inherent to the trapezoidal rule (see section 2.2). In particular voltage oscillations are triggered by sudden changes in currents flowing in inductive branches. The current in L2 can be replaced as measurement by the current in R4 and the estimated voltages do not present oscillations.

In this case, the reason for the chatter is that the simulated values calculated by EMTDC/PSCAD are different to the expected values or the values calculated using only the NIS method (no noise introduced in measurements). The difference is introduced by EMTDC/PSCAD interpolation sub-routines that are called when voltage and current steps are detected. In figure 3.5 there are three examples, when the simulation starts, the start of the fault and its removal (in figure 3.5

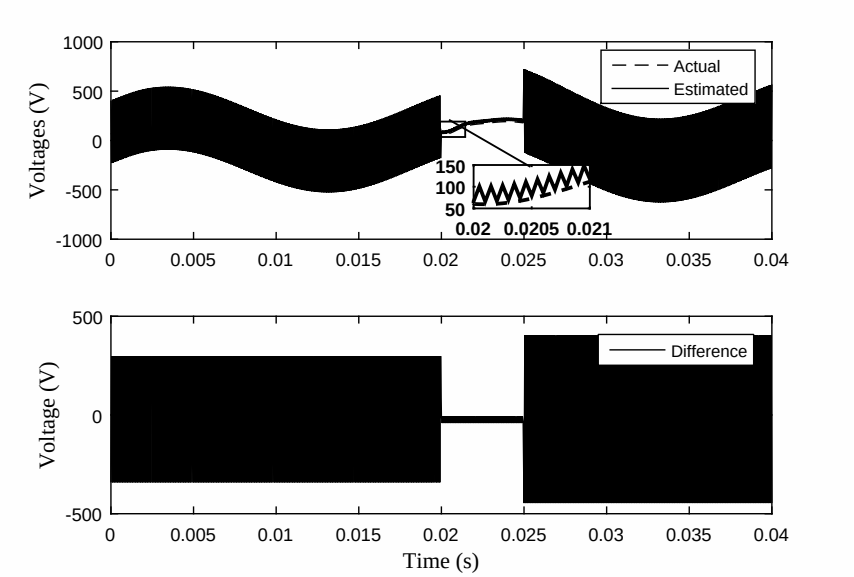

Figure 3.5 Voltage at node one for test circuit of figure 3.3, using measurements calculated with EMTDC/PSCAD; no noise introduced.

the three points are marked by the start of oscillations of different magnitude). The oscillations are created by the difference in the current measured for the inductor against its expected value (calculated using NIS).

To determine the offset, in figure 3.5, the initial conditions can be changed. For example, if the initial voltage of C1 is changed to a different value, the estimated voltages present an offset. Figure 3.6 is obtained using results from the created NIS simulation software; but the capacitor initial voltage has change from zero, the correct value, to 100 volts. If the capacitor initial current is changed the offset is small and the magnitude is equal to the difference from the real value times the capacitor equivalent resistance. From figure 3.3 the capacitor C1 is located between nodes three and four, but the offset is carried from node four to node one through R2. As there are no other measurements that would affect the estimation of the voltage, this can be inferred from the creation of the measurement matrix.

Figure 3.7 presents the result if the initial current value of L2 is changed by one ampere. The oscillations magnitude, in the form of numerical chatter, is the result of multiplying the difference in the initial current condition by the inductance equivalent resistance. In this case the oscillations are created for the estimated voltage in node two and spread to nodes four and one through C1 and R2.

If the initial voltage is changed instead of the initial current of L2, numerical chatter of magnitude equal to the difference between the used voltage and the true voltage occurs.

Incorrect values in the capacitor initial voltage produce an offset equal to the initial voltage error. If the error is in the initial current the offset is the result of the error multiplied by the capacitor

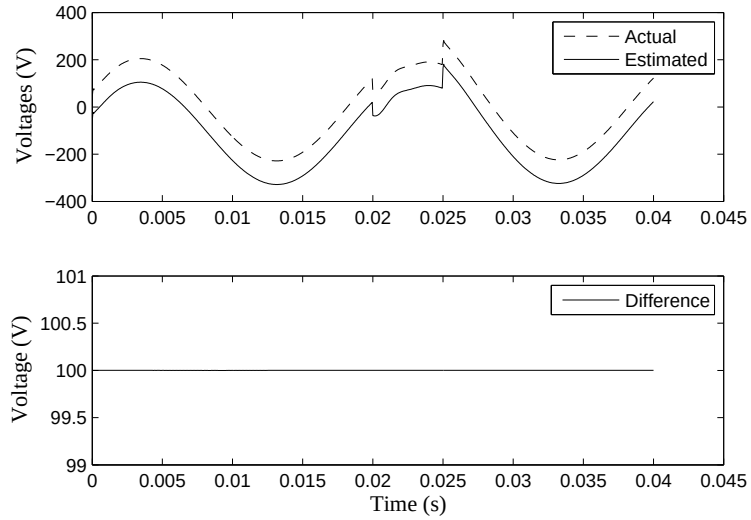

Figure 3.6 Voltage at node one for test circuit of figure 3.3, using measurements calculated with Dommel's method; no noise introduced but C1's initial voltage is 100 volts.

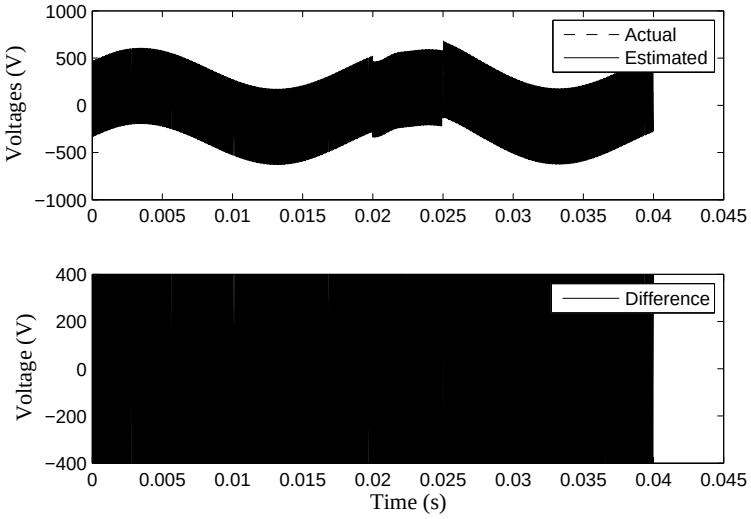

Figure 3.7 Voltage at node one for test circuit of figure 3.3, using measurements calculated with Dommel's method; no noise introduced but L2's initial current is one ampere.

R_{eff}. The error in initial conditions of inductances produces numerical chatter in a similar way. With reference to figure 3.5, the different magnitude of the oscillation after discontinuities is due to different initial conditions values than expected by NIS, at time zero; and different previous step voltage and current than expected by NIS at fault inception and removal.

In [Farzanehrafat and Watson, 2013] the authors recognise the importance of initial conditions and propose the use of a load-flow algorithm to calculate them to initialise the estimation. In the case of three-phase systems with lumped parameters, all initial conditions can be set to zero, the error decays rapidly in time due to the existence of mutual terms in the equivalent admittance

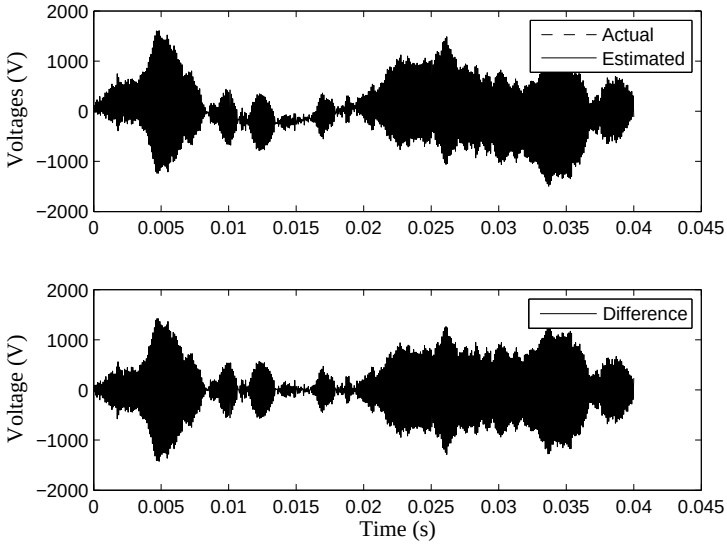

Figure 3.8 Voltage at node one for test circuit of figure 3.3, using measurements calculated with Dommel's method; noise introduced in L2's current.

matrices [Watson and Farzanehrafat, 2014, Farzanehrafat, 2014].

When applying noise to the measured current in an inductive branch, the noise is magnified due to the differentiator action of the inductor NIS formulation [Marti and Lin, 1989] [Dommel, 1987]. The oscillations are uneven and of greater magnitude. The results in figure 3.8 were estimated when white noise with σ equal to 0.1 % of the steady-state peak value is added to L2's current (calculated using Dommel's method).

Finally, figure 3.9 presents the estimated voltage at node one using as measurements the results from the created software, all measurements containing white noise with σ equal to 1 % of the steady-state peak value, but replacing L2's current by the current in R4. The white noise is visible and the maximum error is lower than five percent of the steady-state voltage. In the case of the resistor, the noise is just transferred to the voltage (the capacitor reduces it and the inductor magnifies it).

Table 3.1 summarises the results obtained in this section, indicating what kind of result is obtained from a given input using NIS with trapezoidal rule for simple R, L, and C elements. The presence of noise in a node voltage measurement, will affect the estimation result only for such node unless it is related (by current measurements) to other nodes.

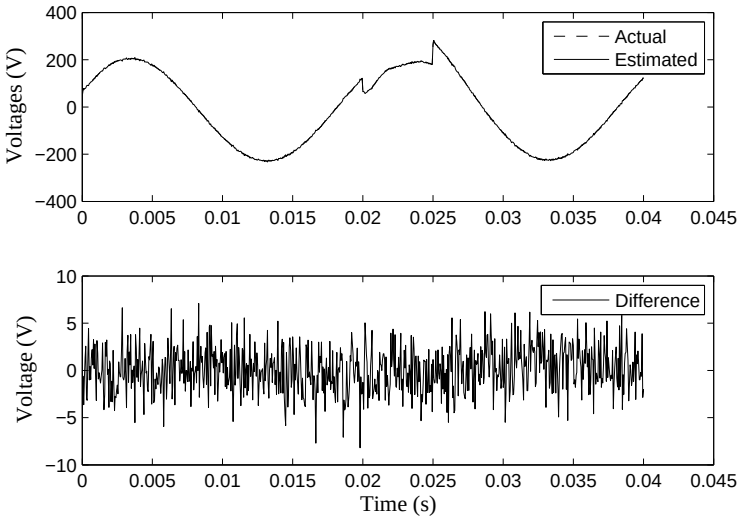

Figure 3.9 Voltage at node one for test circuit of figure 3.3, using measurements calculated with Dommel's method; noise introduced in all measurements, L2's current replaced by R4's current as measurement.

Table 3.1 Summary, error produced in estimated voltage versus input error for simple elements.

Error type	R	L	C
Wrong initial voltage	No effect	Numerical chatter	Constant offset
Wrong initial current	No effect	Numerical chatter	Constant offset
White noise in current measurement	Noise (similar)	Numerical oscillations (noise amplified)	Noise (reduced)

3.2 LINEAR INTERPOLATION

There are several approaches to deal with numerical oscillations in EMTP-like software [Marti and Lin, 1989] [Kuffel et al., 1995] [Watson and Irwin, 1998] [Gao et al., 2003] [Watson and Arrillaga, 2003b]. The simplest for simulation is to use a half-step linear interpolation because it does not require changes in Δt while keeping the trapezoidal rule [Kuffel et al., 1995,Watson and Arrillaga, 2003b]. For estimation, backward Euler integration (to replace trapezoidal rule) and root-matching were applied to three-phase distribution systems [Farzanehrafat, 2014, Watson and Farzanehrafat, 2013]. In this section the application of half-step interpolation to TSE with NIS is explained.

It involves a simple calculation of all variables involved in the estimation at half-step ($\Delta t/2$). As an example, the formula and procedure for a node voltage is as follows:

- For a time T, the estimation is normally performed but the voltage value is not saved.

- Instead, the voltage for time $T - \frac{\Delta t}{2}$ is calculated using (the saved value for the previous iteration is needed)

$$v_{(T-\frac{\Delta t}{2})} = v_{(T-\Delta t)} + \frac{1}{2}[v_{(T)} - v_{(T-\Delta t)}]. \tag{3.4}$$

- The value obtained above is used as input for a full iteration to estimate the voltage at time $T - \frac{\Delta t}{2} + \Delta t = T + \frac{\Delta t}{2}$.

- Using the values at the previous steps, $v_{(T-\frac{\Delta t}{2})}$ and $v_{(T+\frac{\Delta t}{2})}$, the true value at time T is calculated again using (3.4).

- The interpolated voltage is saved for output printing at time T and used in the next iteration.

An important difference, with respect to simulation, is the need to apply interpolation during the entire estimation instead of only steps when discontinuities are detected. Figure 3.10 shows a flowchart for TSE with NIS including interpolation. As can be seen half-step interpolation adds two extra iterations per sampling point to the estimation solution. First (with n = 0), all values are interpolated to the previous half-step ($t = t - (\Delta t/2)$). Then, a complete estimation iteration is performed ($t = t + (\Delta t/2)$ and n = 1). Finally all values are interpolated half-step back to the original time ($t = t$), only after which the state variables are saved.

3.2.1 Application example

Figure 3.11 shows the estimated voltage at node one (circuit in figure 3.3) after half-step interpolation is implemented to remove numerical chatter (compare with figure 3.5). Here the offset, a constant difference, between the estimated and calculated values can be seen without enlargement. However, when a step change happens, the interpolation is not able to follow the rapid change.

Figure 3.12 presents the result of using half-step interpolation when estimation uses results from EMTDC/PSCAD as measurements and white noise with σ equal to 0.1 % of the steady-state peak value is added to L2's current. This is a vast improvement over the result shown in figure 3.8.

Half-step interpolation is a solution for numerical oscillations in TSE. Table 3.2 present the resulting normalised root mean square error (NRMSE, see appendix A) for the entire estimation time, for measurements noise with three standard deviation values when TSE employs interpolation, backward Euler, and Gear 2$^{\text{nd}}$ order to eliminate numerical oscillations (all measurements with added noise; L2, C1, and R2 currents and node 2 voltage obtained from EMTDC/PSCAD). Note that exactly the same measurements (numerical values) were used for each noise level, to allow the direct comparison between estimation methods. The second column presents the error

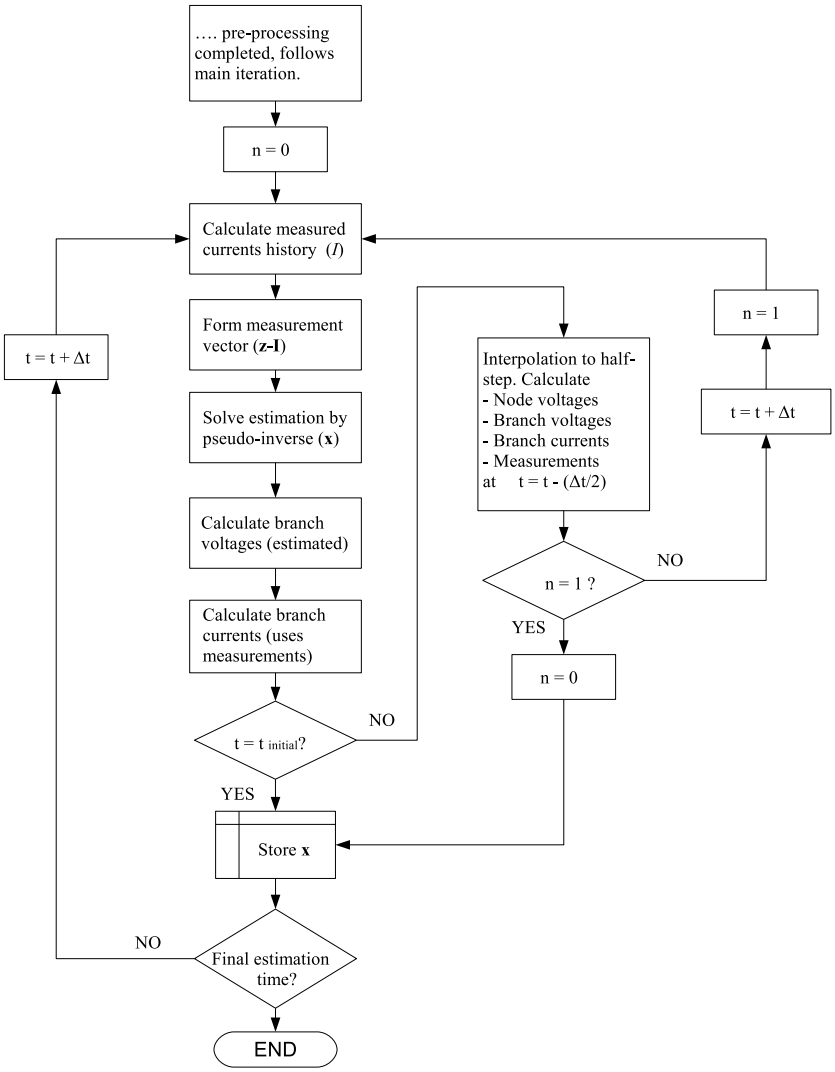

Figure 3.10 Flowchart for TSE with NIS using interpolation.

if TSE with NIS using trapezoidal rule is used without interpolation, noise σ 0.05 % of pre-fault peak value.

From table 3.2 it is possible to observe the following: the use of interpolation affects the waveform of all node voltages (not only the ones with numerical oscillations), see error for node 2; it is possible to say that interpolation provides similar results to Euler method; the difference between Euler and interpolation decreases when noise σ increases; and finally Gear 2^{nd} order is the worst solution of the three presented.

The reason behind results in table 3.2 can be explained by the difference in the formulations. For example, for an inductor, backward Euler history term only depends on the previous step inductor current, while Gear's history term depends not only in the previous step but in the

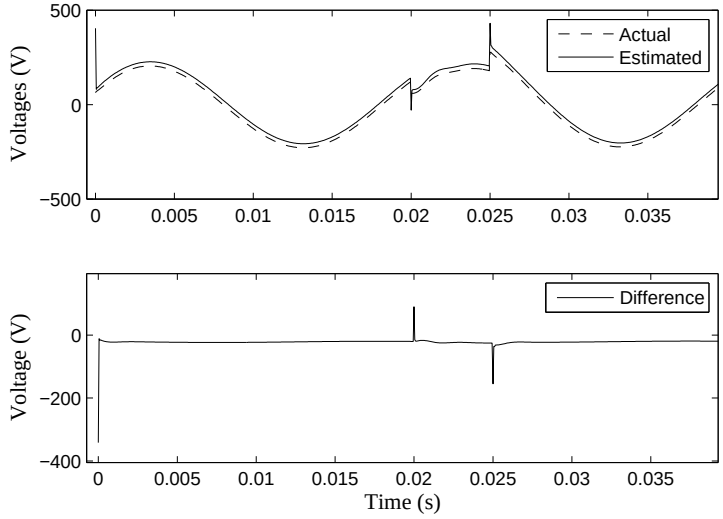

Figure 3.11 Voltage at node one for test circuit of figure 3.3, using measurements calculated by EMTDC/PSCAD; no noise introduced, half-step interpolation applied.

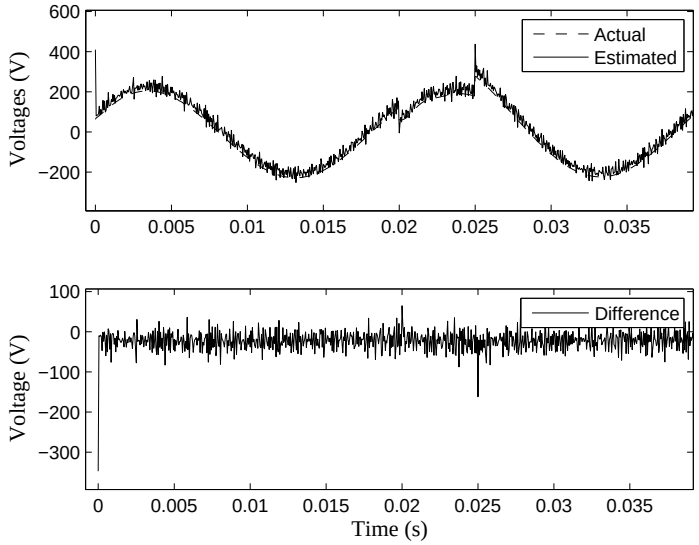

Figure 3.12 Voltage at node one for test circuit of figure 3.3, using measurements calculated by EMTDC/PSCAD; noise introduced in L2's current, half-step interpolation applied.

Table 3.2 Estimated node voltage NRMSE (%), for different noise σ and noise mitigation method.

	0.05 %				0.1 %			0.5 %		
Node	TSE	Interp.	Euler	Gear	Interp.	Euler	Gear	Interp.	Euler	Gear
1	186.79	12.80	11.58	15.37	15.36	14.29	21.38	54.55	53.99	96.72
2	0.04	1.33	0.04	0.04	1.33	0.08	0.08	1.38	0.42	0.42
3	186.54	7.67	5.86	11.71	11.44	10.22	18.91	53.54	53.06	96.21
4	186.79	12.65	11.58	15.37	15.24	14.29	21.38	54.49	53.99	96.73

inductor current two steps before as well. Trapezoidal rule uses both current and voltage in the previous step see equation 2.16 (for formulas of all three methods please refer to [Watson and Arrillaga, 2003b, table 4.1, p.72])[4]. Another possible use for interpolation is the estimation of breakers, controllers, protections, and switches exact operation time (if it happened in-between estimation steps), this could be explored in the future.

3.3 NON-LINEAR ELEMENTS

There are three main techniques to implement non-linear elements in EMTP-like programs [Watson and Arrillaga, 2003b, p.89] [Dommel, 1987, p. 12-1]; current source representation, compensation method, and piecewise linear. EMTP and EMTDC/PSCAD use the piecewise linear method to represent non-linear resistors like surge arresters. The compensation method is used to represent transformers saturation (non-linear inductor). And the current source representation method is no longer used. The above does not mean that the methods are exclusive for a certain type of element, but indicates the current practice to associate a particular method to an element type. In this section the application of the piecewise linear and compensation methods to TSE with NIS is investigated.

3.3.1 Non-linear resistors (piecewise method)

In this method the non-linear characteristic, a curve, is approximated by line segments (see figure 3.13). The voltage versus current relationship of a linear resistor is a straight line in which the resistance value is given by the slope of the line. To approximate a curve by linear segments, at least two points other than the origin on the curve are taken. As many points as desired can be taken; for example EMTDC/PSCAD can take up to 11 points. By using the point-slope equation

$$v - V_1 = R(i - I_1) \tag{3.5}$$

[4] An interesting discussion on transient simulation numerical oscillations causes and accuracy analysis for the integration methods used here is presented in [Marti and Lin, 1989].

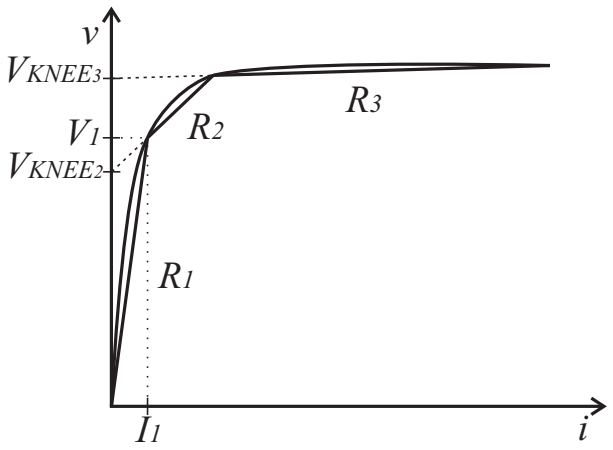

Figure 3.13 Piecewise linear resistance.

where the resistance value for each line piece is derived by using the end points. For example for the second line segment in figure 3.13

$$R_2 = \frac{V_2 - V_1}{I_2 - I_1}. \tag{3.6}$$

Figure 3.13 only indicates point (I_1, V_1), that defines the end of the first line approximation and the beginning of the second one. A voltage in series (or a shunt current source, equal to the voltage divided by the resistance) is necessary to keep the continuity of the pieces.

The series voltage required is indicated as V_{KNEE} in figure 3.13, and is calculated using (3.5) for the particular linear segment when the current is zero. For example, for the second line in the figure

$$V_{KNEE_2} = V_1 - R_2 I_1. \tag{3.7}$$

Taking the Norton companion used for linear elements (see figure 2.2) for a non-linear resistor, the history term is

$$I_{\text{History}} = -\frac{V_{KNEE_N}}{R_N} = i_1 - \frac{v_1}{R_N} \tag{3.8}$$

where (i_1, v_1) is the point at which the line of slope R_N begins.

3.3.1.1 Implementation in TSE with NIS

To estimate the voltage of a non-linear resistance, given the branch current as a measurement, it is necessary to use equation 2.34 to form the measurement matrix. However, the values of R_{eff} and I_{History} must change accordingly to the branch current magnitude. Therefore $\mathbf{H}$ must change and its pseudo-inverse calculated every time a change between the line pieces is detected. Note that if the curve is used the matrix and its pseudo-inverse has to be computed at every step.

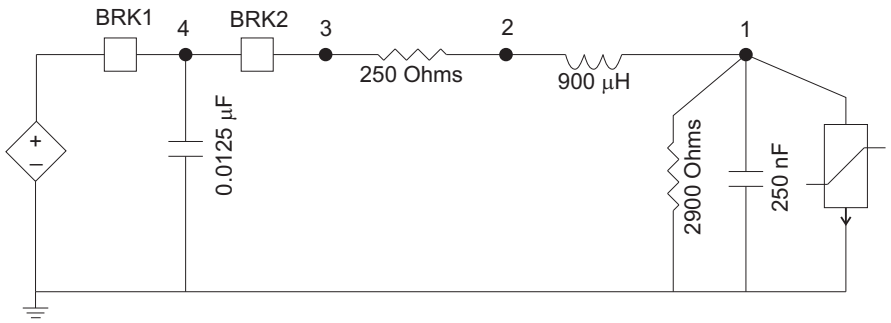

Figure 3.14 Equivalent circuit for an impulse generator, including a surge arrester (non-linear resistor).

3.3.1.2 Application example

In this example a simple equivalent circuit for an impulse generator is used [Thomason, 1934], and a surge arrester is included and modelled as a non-linear resistor (again, a simple representation); with the objective to test the implementation of the piecewise method in TSE. The circuit is presented in figure 3.14; the DC source charges the capacitor at node four to 1000 V then BRK1 is open and a few nanoseconds later BRK2 is closed, triggering an impulse waveform in node one (if the arrester is removed the impulse would be a 1.51×18.7 μs wave with a peak value of 1150 V). The arrester is defined by the following three points: (0.1, 700); (0.2, 800) and (2, 1800) [(Amperes, Volts)]. No air-gap is considered so the arrester is conducting all the time.

Figure 3.15 presents the estimated voltage at the arrester using its current calculated from EMTDC/PSCAD with a time step of 50 ns, white noise with standard deviation of 1 % of the maximum peak value (entire waveform, as for this case steady-state value is zero) is added to the measured current. Half-step interpolation is applied, although it is not required (the arrester formulation does not creates numerical oscillations).

Figure 3.15 is obtained by determining the arrester branch resistance based on current, which is the measurement (including noise). Another possibility is to define the resistance by looking at branch voltage, in this case there would be a one step delay in applying the change into **H**. Changing resistance based on voltage produces a larger difference between actual and estimated waveforms (larger residual).

Figure 3.16 presents a flowchart to implement the piecewise method in TSE with NIS. The same flowchart can be used for time-varying elements (e.g., circuit breakers), for this kind of elements the change detection is an option as well as it is the use of records indicating operation time (at which the breaker changed status). Non-linear resistors do not affect observability (in principle), at least there is always a non-zero value for the corresponding **H** elements (the column could become linearly dependent). But breakers or switches operation will affect observability as the open position would correspond to zero values in **H**. Note, it is possible to use the approach of a big resistance value for and open breaker but it could produce incorrect observability results.

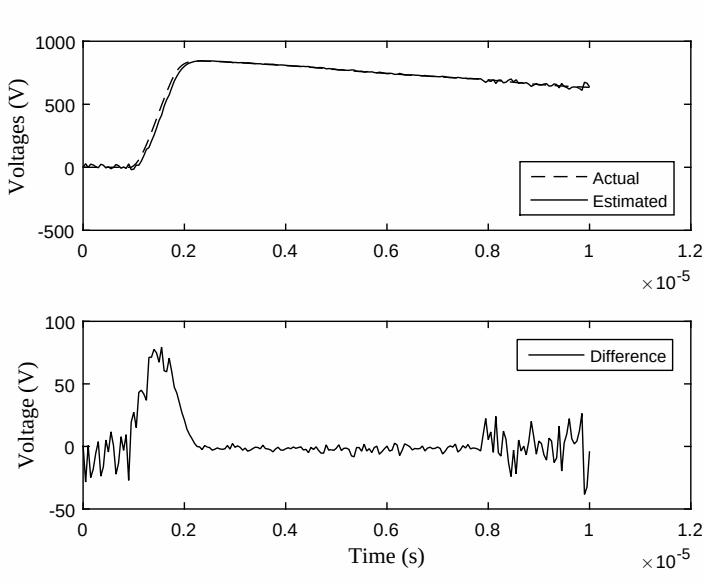

Figure 3.15 Voltage at node one for test circuit of figure 3.14, using measurements calculated by EMTDC/PSCAD.

It should be possible to represent the breaker operation (e.g., arc extinction or closing resistors). The modelling of time-varying elements in TSE needs to be investigated.

3.3.2 Non-linear inductors

For inductors the non-linear characteristic is defined in terms of flux linkage (λ) versus current, where the flux is related to the voltage as

$$v_{jk} = \frac{d\lambda}{dt}. \tag{3.9}$$

Because the simulation (estimation) is done in terms of voltage, (3.9) needs to be converted to a difference equation and its solution updated at each step (the conversion can be done using the procedure in section 2.2). The piecewise method explained before can thus be applied to a non-linear inductor.

3.3.2.1 Compensation method

The compensation method removes the non-linear element from the network and represents it as a current source, to calculate the value for such source the superposition principle is used [Watson and Arrillaga, 2003b, pp.89-91]. The element removal and the need to calculate a Thevenin resistance from the entire network (as seen from the removed element nodes), makes the application of the compensation method in TSE with NIS impossible. First there is not

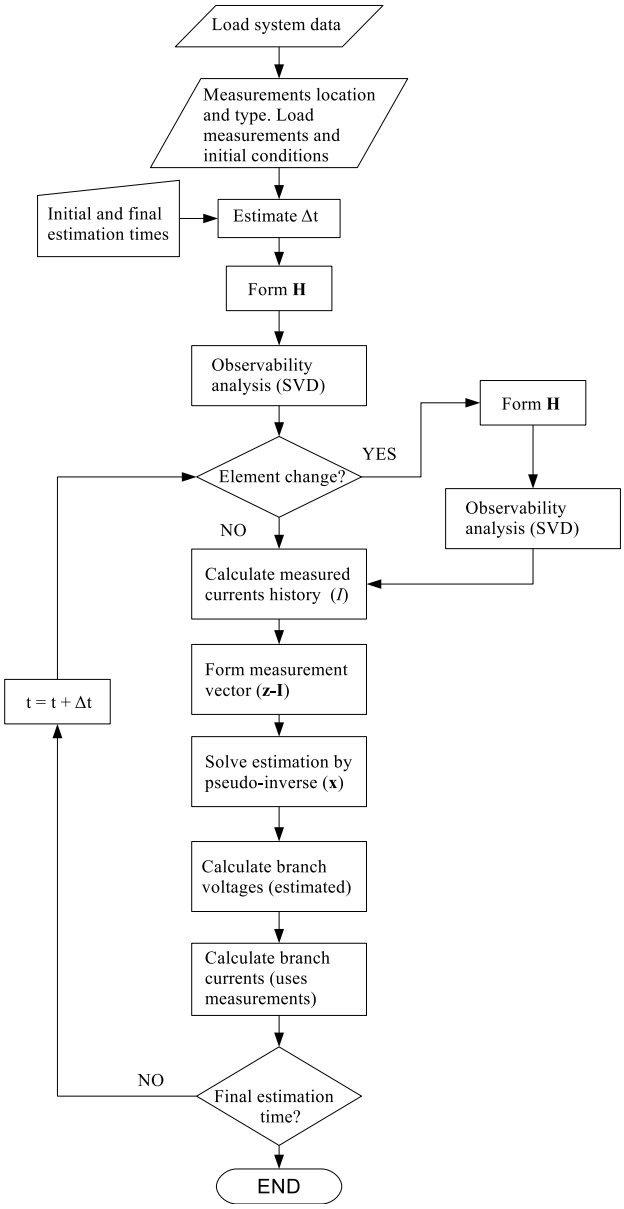

Figure 3.16 Flowchart for TSE with NIS for non-linear and time-varying elements.

direct equivalent resistance value to be used in **H**. And second (and perhaps more important), in TSE with NIS the equivalent resistance of all elements in the network is not know. For electromagnetic transients there is no general model for loads and the modelling complexity for generators increases if its controllers take action during a transient (transients of long duration). This makes the calculation of a Thevenin resistance impossible for practical cases.

3.4 CONCLUSION

In this chapter the use of interpolation to remove numerical oscillations in the estimated voltages is presented. Although interpolation is not the only solution to the problem, it is preferred because it is general and no major change is required in the solution process or problem formulation. Its application has been shown on a simple circuit.

In the next two chapters, half-step interpolation will be applied to three-phase systems estimation. Its algorithm does not change for multi-phase systems.

The inclusion of non-linear elements in TSE was presented and exemplified on an arrester connected to an impulse generator, the method used is the piecewise linear approximation. The compensation method is not suitable for TSE with NIS because it requires full system information to calculate Thevenin equivalents. More research is needed in this area, the focus should be on series elements (as transformers) because they provide more information (greater observability) for the estimation. The use of non-linear models for breakers should be investigated as well.

Chapter 4

OBSERVABILITY AND VIRTUAL MEASUREMENTS

In this chapter the problem of observability for TSE with NIS is revisited for circuits with linear and lumped parameters. First a review of the observability concept is given. Then the particular cases that result in partial system observability (i.e., the system being not fully observable), encountered in TSE with NIS with lumped parameters are presented. Later on the method for observability analysis using SVD matrices is reviewed. This is followed by the introduction of an extended observability analysis method capable to identify unobservable islands. Finally, the introduction of virtual measurement to improve the system observability is explained.

4.1 OBSERVABILITY ANALYSIS

In this section the observability analysis using SVD matrices is improved, first the existing method is explained and then an extension capable to identify unobservable islands is introduced.

4.1.1 Partial observability

A system is said to be observable if (2.10) has a unique solution for $\mathbf{x}$. It is possible to have a partially observable system with unobservable island(s). In general, for PQSE, the observability depends on the number type and location of measurements as well as network topology [Clements, 1990, Arrillaga et al., 2000]. For TSE in particular, a system is observable (or fully observable) if the measurement matrix ($\mathbf{H}$) has full column rank and is partially observable if rank $(\mathbf{H}) < n$. The number of singular values is equal to rank ($\mathbf{H}$). In TSE with NIS, in which the state variables are the node voltages, there are two main causes of partial observability:

- There is no measurement related to a given node. In this case, the column $\mathbf{h}_k$, related to the kth state variable, is a zero vector. Therefore, it is linearly dependent to any other column vector of $\mathbf{H}$. This case is only possible when $m < n$.

- One or more measurements produce linearly dependent column vectors in $\mathbf{H}$. For example, there may be one current measurement relating nodes j and k, without any other measurement (current or voltage) related to those nodes. This situation can be deduced from (2.34), because what is estimated is the voltage drop in the branch and it does not produce a good result for the node voltages unless at least one is known, i.e., a reference is needed.

In the first case, after (2.35) is solved using SVD, the result for x_k is zero over the entire estimation time [Watson, 2010]. In the second case, the use of SVD may not produce a zero-value solution. Here, the number of unobservable nodes is greater than the difference between the rank of $\mathbf{H}$ and the number of state variables (also called the nullity of $\mathbf{H}$, $\text{null}(\mathbf{H}) = n - \text{rank}(\mathbf{H})$). In this case, an unobservable island containing a measurement exists.

4.1.2 Observability analysis using SVD

The non-zero entries in the column vectors of $\mathbf{V}$ that correspond to the zero entries in the diagonal of $\mathbf{S}$ (the null space) indicate which state variables are not observable [Watson and Farzanehrafat, 2014]. For example, if $\mathbf{S}$ has the form

$$\mathbf{S} = \begin{bmatrix} s_1 & & & 0 & 0 & 0 \\ & s_2 & & & 0 & 0 \\ & & \ddots & & \vdots & \vdots \\ 0 & & & s_m & 0 & 0 \end{bmatrix} \tag{4.1}$$

and $\mathbf{V}$ is

$$\mathbf{V} = \begin{bmatrix} v_{1,1} & v_{1,2} & \cdots & v_{1,m} & 0 & 0 \\ v_{2,1} & v_{2,2} & \cdots & v_{2,m} & 0 & 0 \\ \vdots & \vdots & & \vdots & \vdots & \vdots \\ v_{j-1,1} & v_{j-1,2} & \cdots & v_{j-1,m} & 0 & 0 \\ v_{j,1} & v_{j,2} & \cdots & v_{j,m} & v_{j,m+1} & v_{j,n} \\ v_{j+1,1} & v_{j+1,2} & \cdots & v_{j+1,m} & 0 & 0 \\ \vdots & \vdots & & \vdots & \vdots & \vdots \\ v_{k-1,1} & v_{k-1,2} & \cdots & v_{k-1,m} & 0 & 0 \\ v_{k,1} & v_{k,2} & \cdots & v_{k,m} & v_{k,m+1} & v_{k,n} \\ v_{k+1,1} & v_{k+1,2} & \cdots & v_{k+1,m} & 0 & 0 \\ \vdots & \vdots & & \vdots & \vdots & \vdots \\ v_{n,1} & v_{n,1} & \cdots & v_{n,m} & 0 & 0 \end{bmatrix} \tag{4.2}$$

where $\mathbf{v}_{m+1}$ and $\mathbf{v}_n$ are the vectors that correspond to the null space and all of its terms are

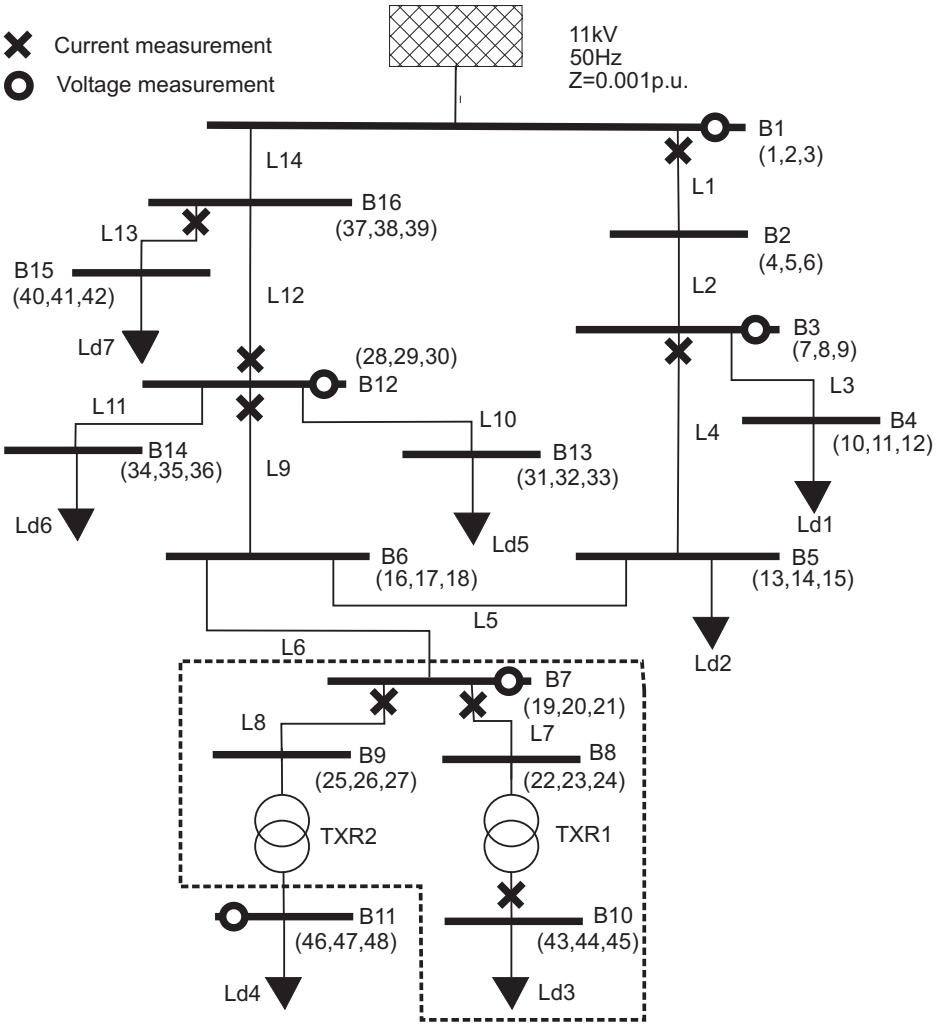

Figure 4.1 Killinchy distribution system.

zero except in positions j and k, then the state variables x_j and x_k are unobservable. Because the number of unobservable state variables is equal to $\mathbf{H}$ nullity, then the state variable is unobservable due to lack of measurement in both cases. Note that the columns of $\mathbf{V}$ that form the null space of $\mathbf{H}$ are not unique [Anton and Busby, 2003].

4.1.2.1 Application example

Figure 4.1 presents the one-line diagram of the Killinchy distribution system in South Canterbury, New Zealand [Watson and Farzanehrafat, 2014, Farzanehrafat and Watson, 2013]. Its parameters are presented in appendix B. The topology is known and is as illustrated in figure 4.1. The parameters of all distribution lines and transformers are known, the loads are simulated as static, and a Thevenin equivalent is used to represent the connection to the rest of the power system (its parameters are indicated in figure 4.1).

Using this information, a single-phase-to-ground fault will be simulated at bus 5 using the simulation software EMTDC/PSCAD. Several results of this simulation were then used as measurements inputs to the estimation (all available measurements are indicated in figure 4.1). Noise was introduced into the selected measurements as explained in section 3.1.1, noise had a standard deviation equal to 1 percent of each measurement's pre-fault peak value. Note that the noise for each available measurement was generated only once; therefore, for all the following cases the available measurements numerical values are the same. This guarantees than only the number of measurements used differs between cases.

For comparison, the average normalised root mean square error (NRMSE) for each bus is presented for each case (refer to appendix A for more details regarding the calculation of average NRMSE). The average NRMSE (over one cycle) was calculated for the pre-fault, fault, and post-fault estimated waveforms.

For the estimation, only transformers and lines are available as input. The transformers are modelled as ideal, and lines are represented by PI equivalents. In all cases, NIS with trapezoidal rule is applied. Because of the numerical oscillation created by the series inductance of the lines and inductances in transformer model, half-step interpolation is applied throughout the entire estimation time. The interpolation is applied to the (estimated) voltages as presented in section 3.2.

Case I (base scenario) Based on all measurements noted in figure 4.1[1], observability analysis indicates that buses 4, 13, and 14 are unobservable and that no measurement is associated with any of these buses. Figure 4.3 present the sparsity pattern for matrices **H**, **S**, and **V** for this case. It is easy to confirm that the analysis results are correct. By examining figure 4.3(b) it can be noticed that the system nullity is 9 (9 zero columns in **S**), and figure 4.3(c) indicates 9 unobservable buses (**V** null space); therefore, no unobservable bus has a related measurement. To identify the unobservable buses, it is necessary to consider the node numbers in figure 4.1 for each bus phase, which are indicated in parentheses below the bus number, and cross reference them with the row numbers of the non-zero entries in the null space of **V**. In this case, rows 10, 11, 12, 31, 32, 33, 34, 35, and 36 of **V** contain non-zero values, corresponding to buses 4 (10, 11, and 12), 13 (31, 32, and 33), and 14 (34, 35, and 36). Figure 4.2 presents the difference between the actual and estimated voltages at bus 5.

To further confirm the observability results, the average NRMSE per bus for this case is presented in the second (pre-fault) and third (fault) columns of table 4.1 on page 59. The post-fault values are not presented for any case because they are nearly identical to the pre-fault values. In table 4.1 the coloured-grey cells indicate an unobservable bus, note they also correspond to a

[1]The problem of measurement unit's optimal placement is not considered in this thesis. The measurements in figure 4.1 are placed per author's discretion and in such a way that permits the testing of the extended observability analysis.

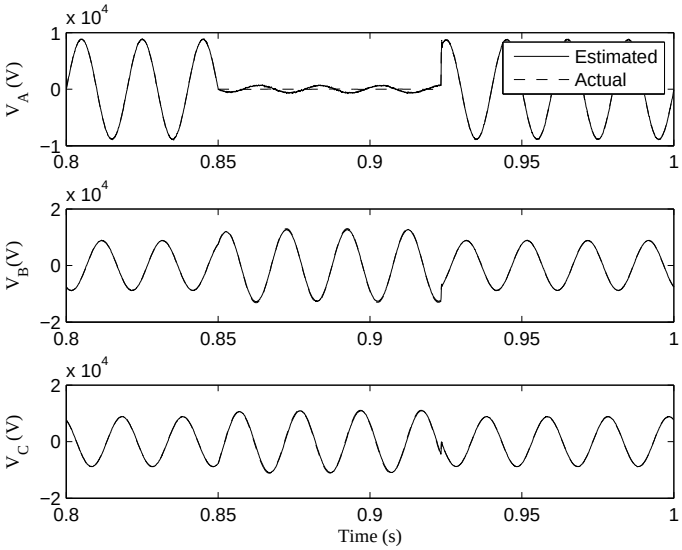

(a) Actual and estimated waveforms.

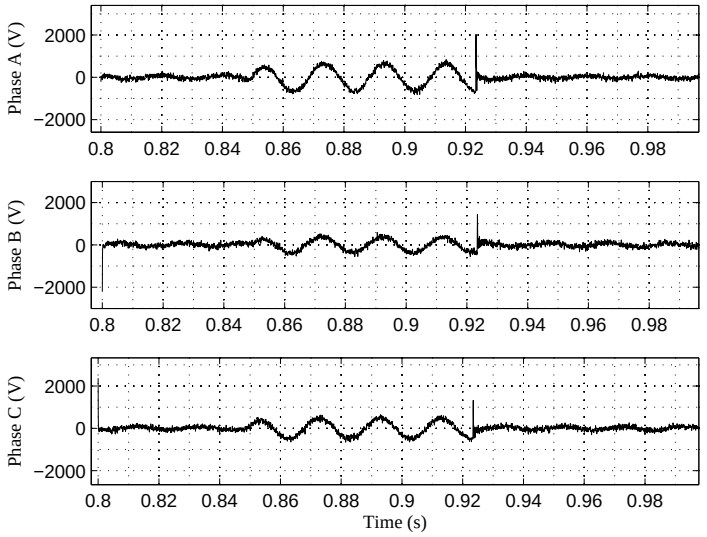

(b) Difference.

Figure 4.2 Difference between the actual and estimated voltages at bus 5 obtained using the measurements considered in Case I.

larger error. Buses 4, 13, and 14 clearly display large differences between the estimated and actual waveforms (the actual voltage waveforms are taken directly from the EMTDC/PSCAD simulation). The estimated voltages associated with buses 4, 13, and 14 are zero over all the estimation time.

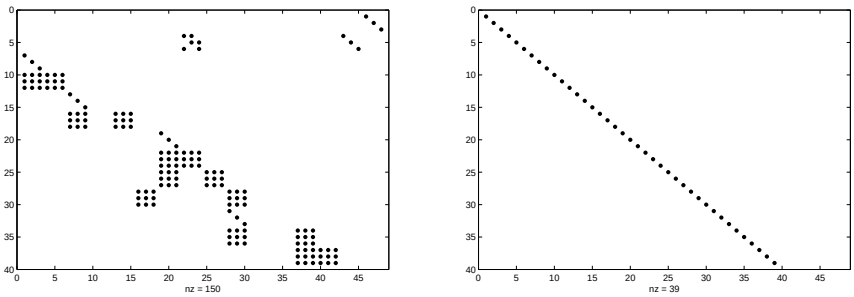

(a) Matrix **H**. (b) Matrix **S**.

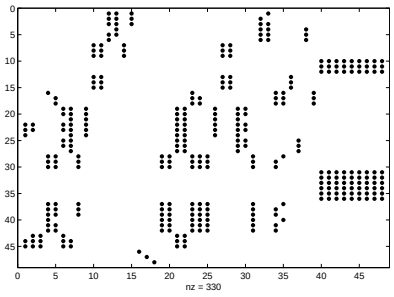

(c) Matrix **V**.

Figure 4.3 Matrix visualizations obtained using the measurements considered in Case I.

4.1.3 Identification of unobservable islands

When the number of unobservable nodes is greater than the nullity of **H**, more information is required to determine the underlying reason for the existence of unobservable state variables (i.e., the first or second of the cases presented above). In addition to SVD, it is therefore necessary to obtain the reduced row-echelon form of **H**, namely, $\mathbf{E}$[2]. By inspecting **E**, it is then possible to identify unobservable islands.

Now, consider a case in which the measurement locations and type have changed. **S** still has a

[2]The reduced row-echelon form is calculated by applying Gaussian reduction to the rows of **H**.

form similar to that of (4.1), but $\mathbf{V}$ is

$$\mathbf{V} = \begin{bmatrix} v_{1,1} & v_{1,2} & \cdots & v_{1,m} & 0 & 0 \\ v_{2,1} & v_{2,2} & \cdots & v_{2,m} & 0 & 0 \\ \vdots & \vdots & & \vdots & \vdots & \vdots \\ v_{j-1,1} & v_{j-1,2} & \cdots & v_{j-1,m} & 0 & 0 \\ v_{j,1} & v_{j,2} & \cdots & v_{j,m} & v_{j,m+1} & v_{j,n} \\ v_{j+1,1} & v_{j+1,2} & \cdots & v_{j+1,m} & v_{j+1,m+1} & v_{j+1,n} \\ v_{j+2,1} & v_{j+2,2} & \cdots & v_{j+2,m} & 0 & 0 \\ \vdots & \vdots & & \vdots & \vdots & \vdots \\ v_{k-1,1} & v_{k-1,2} & \cdots & v_{k-1,m} & 0 & 0 \\ v_{k,1} & v_{k,2} & \cdots & v_{k,m} & v_{k,m+1} & v_{k,n} \\ v_{k+1,1} & v_{k+1,2} & \cdots & v_{k+1,m} & 0 & 0 \\ \vdots & \vdots & & \vdots & \vdots & \vdots \\ v_{n,1} & v_{n,1} & \cdots & v_{n,m} & 0 & 0 \end{bmatrix} \tag{4.3}$$

all terms of $\mathbf{v}_{m+1}$ and $\mathbf{v}_n$ are now zero except in positions j, $j+1$, and k. In this case, rank $(\mathbf{H})$ is still m, and 3 unobservable state variables, with null $(\mathbf{H}) = n - m = 2$. Therefore, two of the three column vectors ($\mathbf{h}_j$, $\mathbf{h}_{j+1}$, and $\mathbf{h}_k$) are linearly dependent among themselves. The reduced row-echelon form of $\mathbf{H}$ in this particular case is

$$\mathbf{E} = \begin{bmatrix} 1 & 0 & \cdots & 0 & 0 & 0 & \cdots & 0 & 0 & 0 & \cdots & 0 \\ 0 & 1 & \cdots & 0 & 0 & 0 & \cdots & 0 & 0 & 0 & \cdots & 0 \\ \vdots & \vdots & \ddots & \vdots & \vdots & \vdots & & \vdots & \vdots & \vdots & & \vdots \\ 0 & 0 & \cdots & 1 & 0 & 0 & \cdots & 0 & 0 & 0 & \cdots & 0 \\ 0 & 0 & \cdots & 0 & 0_{(j,j)} & 1 & \cdots & 0 & -1_{(j,k)} & 0 & \cdots & 0 \\ \vdots & \vdots & & \vdots & \vdots & \vdots & \ddots & \vdots & \vdots & \vdots & & \vdots \\ 0 & 0 & \cdots & 0 & 0 & 0 & \cdots & 1 & 0 & 0 & \cdots & 0 \\ 0 & 0 & \cdots & 0 & 0 & 0 & \cdots & 0 & 0_{(k,k)} & 1 & \cdots & 0 \\ \vdots & \vdots & & \vdots & \vdots & \vdots & & \vdots & \vdots & \vdots & \ddots & \vdots \\ 0 & 0 & \cdots & 0 & 0 & 0 & \cdots & 0 & 0 & 0 & \cdots & 1_{(m,n)} \end{bmatrix}.$$

It is evident that $\mathbf{e}_j$ is a zero vector. All elements of the vector $\mathbf{e}_{j+1}$ are zeros except at for position j. The vectors $\mathbf{e}_{j+1}$ and $\mathbf{e}_k$ are linearly dependent because of a non-zero entry outside the diagonal (a -1 in position j of $\mathbf{e}_k$, in this case). Therefore, x_j is unobservable because there is no measurement is related to it, and x_{j+1} and x_k each have a related measurement but are linearly dependent; therefore, these nodes form an unobservable island. This information is important, because it will serve as an input to the location selection for the virtual measurements.

It is also possible to have an ill-conditioned measurement matrix. In this case, SVD will reveal a small singular value in **S** (small when numerically compared to the other singular values, i.e, the ratio with the previous singular value is greater than 1×10^2, where the singular values appear in decreasing order in **S**). Here, the use of **E** does not provide any additional information and is not required because the non-zero entries of the corresponding column vector of **V** will indicate the unobservable voltages.

4.1.4 Improved observability analysis procedure

The proposed procedure for observability analysis of TSE in distribution system is as follows:

1. Load **H**, **S** and **V**, all of which are available after SVD factorization is applied to **H**.
2. Inspect **S** for zero columns to identify the null space.
3. Inspect the null space of **V** for non-zero entries; the number of unobservable state-variables is a.
4. Inspect **H** for zero column vectors; the number of zero column vectors is b.
5. If $a = b$, then all unobservable nodes are attributable to a lack of measurements. The observability analysis is complete.
6. If $a \neq b$, then it is necessary to obtain **H** reduced row-echelon form, namely, **E**.
7. Inspect **E** for non-zero terms outside its diagonal.
8. Non-zero terms in the same rows of **E** indicate unobservable nodes that are linearly dependent among themselves, and thus form an unobservable island.
9. Inspect **S** for "small" singular values (i.e., $s_{j-1}/s_j > 1 \times 10^2$).
10. Inspect the **V** column vectors that correspond to "small" singular values for non-zero entries.
11. All unobservable nodes and islands have been identified.

4.1.4.1 Application Examples

The following two cases use the same system and measurements as in section 4.1.2.

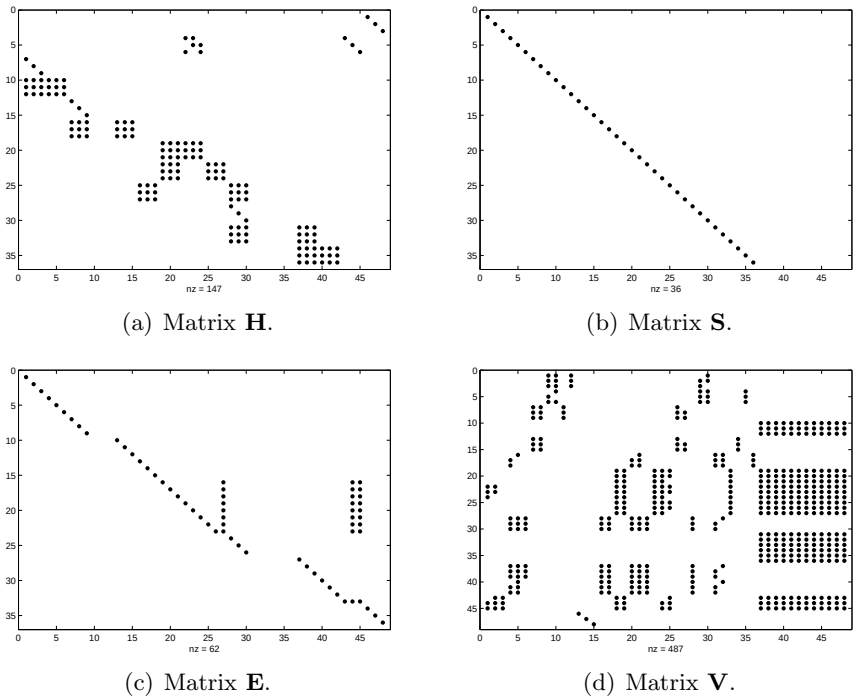

(a) Matrix **H**. (b) Matrix **S**.

(c) Matrix **E**. (d) Matrix **V**.

Figure 4.4 Matrix visualizations obtained based on the measurements considered in Case II.

Case II (an unobservable island) Here, the same measurements are used as in Case I, except that the voltage measurement at bus 7 is ignored. The observability analysis indicates that buses 4, 7, 8, 9, 10, 13, and 14 are not observable and that an unobservable island is created by buses 7, 8, 9, and 10.

This is an example of the second cause of partial observability (see section 4.1.1). When the voltage measurement at bus 7 is eliminated, an unobservable island is created, as indicated by the buses and elements enclosed by dashed lines in figure 4.1. In other words, all column vectors of **H** related to the buses in this island form a set that is linearly dependent.

Figure 4.4 presents the sparsity patterns for matrices **H**, **S**, **V** and **E** in this case. There are 12 zero columns in **S** [figure 4.4(b)] and 21 rows with non-zero terms in the null-space columns of **V** [figure 4.4(d)]. Therefore, matrix **E** contains non-zeros outside the diagonal, which correspond to nodes in the unobservable island, as shown in figure 4.4(c). Three columns with non-zero values outside the diagonal can be identified: numbers 27, 44, and 45. These non-zero values are located in rows that correspond to diagonal elements in the following columns: 19, 20, 21, 22, 23, 24, 25, 26, and 43. Therefore, the unobservable island consist of buses 7 (19, 20, and 21), 8 (22, 23, and 24), 9 (25, 26, and 27), and 10 (43, 44, and 45) (see figure 4.1).

Case III (two unobservable islands) In this case, the measurements are the same as those used in Case II, except that the voltage measurement at bus 3 is ignored. An additional unobservable island is created that contains buses 3 and 5. The observability analysis indicates that

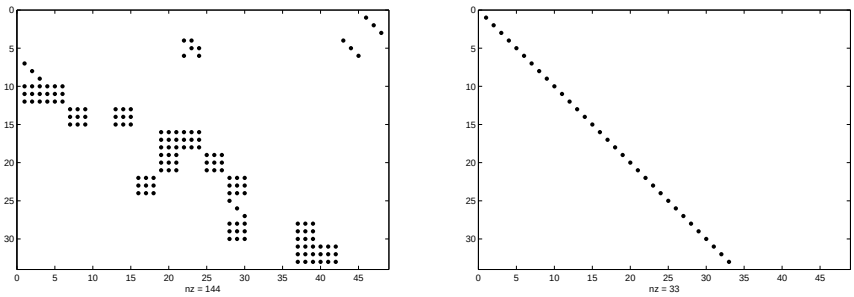

(a) Matrix **H**. (b) Matrix **S**.

(c) Matrix **E**. (d) Matrix **V**.

Figure 4.5 Matrix visualizations obtained based on measurements considered in Case III.

only buses 1, 2, 6, 11, 12, 15, and 16 are observable. Figure 4.5(c) shows the non-zero elements of matrix **E** for this case, indicating two unobservable islands.

4.2 VIRTUAL MEASUREMENTS

In [Schweppe and Wildes, 1970], the concept and types of pseudo-measurements for power systems steady-state estimation were introduced. A further classification was subsequently developed. Currently, virtual measurements a considered perfect pseudo-measurements, specially for zero power injection at buses without load or generation [Clements, 1990]. For harmonic state estimation, the harmonic nodal currents were initially used as measurements [Du et al., 1996]; subsequently, virtual measurements were defined as zero nodal harmonic current at nodes without harmonic sources connected [Matair et al., 2000]. In [Watson and Farzanehrafat, 2014], the authors suggest that virtual measurements are not appropriate for TSE. The virtual measurement proposed in this thesis is similar to that used in harmonic state estimation and is based on the application of Kirchhoff's current law (KCL) to a single node.

The results from the proposed observability analysis are used to identify candidate nodes at which virtual measurements can be applied to improve the system observability. Both the observability analysis and the virtual measurement fail if they are applied to faulted branches (e.g., a fault occurring in the middle of a distribution line), this remains an unsolved problem in TSE. The proposed observability analysis correctly identifies unobservable islands, including

faulted buses, although the proposed virtual measurement is limited to fault-free buses.

As in the case of harmonic state estimation [Du et al., 1996] [Matair et al., 2000], it is possible to include virtual measurements in TSE with NIS. When the branches are modelled with lumped parameters, Kirchoff's current law can be applied to certain nodes. The result is a zero added in the measurements vector $\mathbf{z}$ and a new row to $\mathbf{H}$ that is equal to the row corresponding to the same node voltage in the equivalent conductance matrix ($\mathbf{Y}$ in equation 2.31). Suppose that the virtual measurement is the nth measurement and is applied to node j which connects to nodes $k, l, \cdots, q$:

$$h_{nj} = \sum_{p=k}^{q} \frac{1}{R_{\text{eff},jp}} \tag{4.4a}$$

$$h_{nk} = -\frac{1}{R_{\text{eff},jk}} \tag{4.4b}$$

$$h_{nl} = -\frac{1}{R_{\text{eff},jl}} \tag{4.4c}$$

$$\vdots$$

$$h_{nq} = -\frac{1}{R_{\text{eff},jq}}. \tag{4.4d}$$

The current history term for each branch connected to node j must be computed, and all of these terms added to find the term $\mathbf{I}_{\text{History}}$ for equation 2.35.

In order to select where to apply this kind of virtual measurement, the following must be observed:

- No voltage or current sources are connected to the node (no power injections).
- The models and parameters of all elements/branches connected to the node are known.
- The selected node can be an unobservable node if and only if it is connected to a currently observable node.
- The selected node is connected to one or more unobservable nodes and at least one observable node.
- A new observability analysis must be applied to the new measurement matrix to ensure successful application.

Note that if a virtual measurement is performed at a faulted node and there is no other measurement related to the faulted node, the results will be a poor estimation, even though the node is observable (during the fault, the fault current is unknown). Using the results of the observability analysis and the knowledge of the system topology, it is possible to judiciously apply virtual measurements.

In Case II, the observability can be improved by applying a virtual measurement at bus 7 or 9; these buses are selected as candidates because they belong to the unobservable island but are also connected to currently observable nodes. The selection of candidate buses could be automated by using the branch-node incidence matrix (**A** in [Branin, 1967a]).

4.2.1 Application examples

The following five cases use the same Killinchy system and measurements as in section 4.1.2.

4.2.1.1 Case IV (virtual measurement at a faulted bus)

In this case, the same measurements are used as in Case I, with the additional application of KCL (a virtual measurement) at bus 5. The observability analysis result does not changed, despite the addition of three new rows to **H**, because they do not add any new information (bus 5 was already observable). This can be observed in figure 4.6(a), where the virtual measurement is responsible for the addition of the last three rows in **H**. Note that the columns with non-zero values for these three rows already have other non-zero values [see also figure 4.3(a)]. The null space of **V** is identical to that in Case I.

The error results are presented in table 4.1. Interestingly, the accuracy for bus 5 is negatively affected (average NRMSE from 4.0% to 6.2% during the fault), because bus 5 does not satisfy the conditions required for the application of a virtual measurement because of the lack of information regarding the branches connected to the bus (namely, load 2 and the fault). However, the increase in the error is limited by the existence of the current measurement in line 4.

4.2.1.2 Case V (virtual measurement at a previously observable bus)

Same measurements as in Case I are again considered, now with the addition of a virtual measurement at bus 6. The added measurement does not improve the observability. Figure 4.6(b) presents matrix **H** for this case, to which the virtual measurement has again added the last three rows. Based on this figure, a conclusion identical to that reached in Case IV can be drawn regarding observability.

The effect of the virtual measurement (correctly applied, although it does not improve observability) is to reduce the error from 2.5% to 0.9% at bus 6 during the fault (see table 4.1). The use of virtual measurements to improve accuracy is not recommended. Instead, virtual measurements should be applied to improve the observability. Particularly, must be used to obtain a solution for unobservable islands that contain measurements.

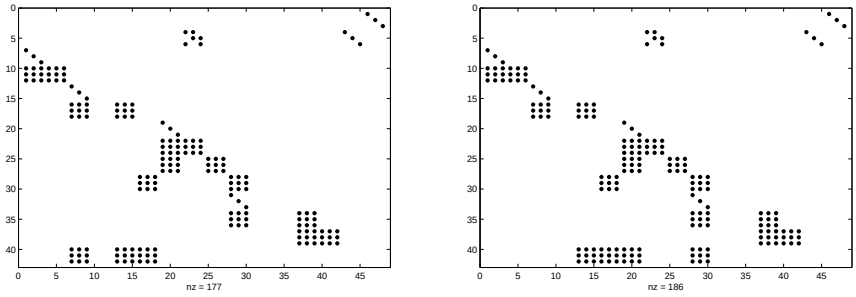

(a) Matrix **H** Case IV. (b) Matrix **H** Case V.

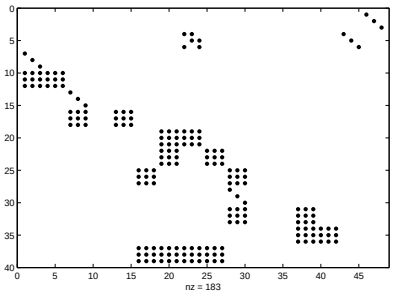

(c) Matrix **H** Case VI.

Figure 4.6 Matrix **H** visualizations obtained using the measurements considered in Cases IV, V, and VI.

4.2.1.3 Case VI (virtual measurement eliminating a previously unobservable island)

This case is identical to Case II except for the inclusion of a virtual measurement at bus 7. The observability analysis indicates that buses 4, 13, and 14 are unobservable. Thus, the previously unobservable island (buses 7, 8, 9, and 10) has now become observable. Figure 4.6(c) presents matrix **H** for this case, in which the virtual measurement has again added the last three rows. The non-zeros locations in the null space of matrix **V** are identical to those shown in figure 4.3(c). The errors are indicated in table 4.1, a larger error (during the fault) is obtained for the buses forming the previously unobservable island when comparing against results for Case I.

4.2.1.4 Case VII (virtual measurement resulting in an ill-conditioned matrix)

Here, the measurements are the same as in Case II, with the addition of a virtual measurement at bus 9. The observability analysis indicates that buses 4, 7, 8, 9, 13, and 14 are not observable and that buses 7, 8, and 9 form an unobservable island. In this case, the last singular value is very small: 2.19×10^{-5}. The corresponding column in **V** [column 39 in figure 4.7(d)] contains non-zero entries for buses 7, 8, and 9.

The errors for buses 7, 8, and 9 are very large (see table 4.1). These large errors can be attributed to the small singular value noted above, which results in an enormous value in the calculation of the pseudo-inverse of **S**. This is an example of an ill-conditioned measurement matrix.

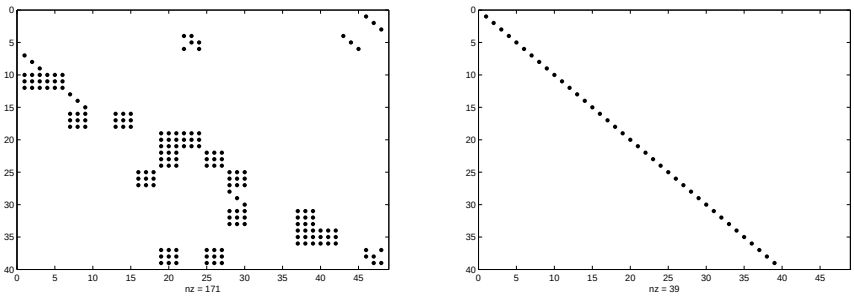

(a) Matrix **H**. (b) Matrix **S**.

(c) Matrix **E**. (d) Matrix **V**.

Figure 4.7 Matrix visualizations obtained based on the measurements considered in Case VII.

The cause of the unobservable island is the connection of transformer TXR2 (Dyn11, delta connecting to bus 9) because the measurement is applied to the delta side of the transformer. The application of a virtual measurement to bus 9 is equivalent to adding real current measurements between buses 9 and 11, and between buses 9 and 7. Therefore, the voltage difference between buses 11 and 9 is a function of a current measurement on the delta side of the transformer. The same problem has been reported in harmonic state estimation [Yu and Watson, 2004]. Additionally, it should be noted that bus 10 is observable and that its related measurement was performed on the star side (see figure 4.1).

4.2.1.5 Case VIII (unobservable islands that cannot be eliminated through virtual measurements)

The measurements are the same as those in Case III, with the addition of virtual measurements at buses 3 and 7. The observability analysis shows that buses 3, 4, 5, 13, and 14 are unobservable.

The virtual measurement at bus 3 fails to make the unobservable island previously containing buses 3 and 5 observable and instead adds bus 4 to it, as seen in figure 4.8(c). By looking at figure 4.8(a), it is possible to see that the application of KCL to bus 3 introduces non-zero values into the columns corresponding to bus 4. Bus 3 is a good candidate for a virtual measurement, but this measurements does not achieve its goal because the island is associated with two measurements (including the virtual one) and three buses. Therefore, it is impossible to eliminate the linear dependence among buses 3, 4, and 5 in this case.

Table 4.1 Average NRMSE values (%), Cases I to VIII.

	Case I		Case II		Case III		Case IV		Case V		Case VI		Case VII		Case VIII	
Bus	Pre-	Fault	Pre-	Fault	Pre-	Fault	Pre-	Fault	Pre-	Fault	Pre-	Fault	Pre-	Fault	Pre-	Fault
1	0.96	0.95	0.96	0.95	0.96	0.95	0.96	0.95	0.96	0.95	0.96	0.95	0.96	0.95	0.96	0.95
2	1.20	5.99	1.20	5.99	1.20	5.99	1.20	5.99	1.20	5.99	1.20	5.99	1.20	5.99	1.20	5.99
3	0.96	0.95	0.96	0.95	69.58	63.73	0.96	0.95	0.96	0.95	0.96	0.95	0.96	0.95	55.24	56.43
4	69.60	63.85	69.60	63.85	69.60	63.85	69.60	63.85	69.60	63.85	69.60	63.85	69.60	63.85	91.60	84.60
5	0.91	4.00	0.91	4.00	69.54	63.57	0.87	6.25	0.91	4.03	0.91	4.00	0.91	4.00	55.19	59.85
6	0.88	2.46	0.88	2.46	0.88	2.46	0.79	2.24	0.91	0.90	0.88	2.46	0.88	2.46	0.88	2.46
7	0.99	0.98	68.74	64.19	68.74	64.19	0.99	0.98	0.99	0.98	0.85	2.29	927.41	6194.69	0.85	2.29
8	1.02	1.01	68.51	64.01	68.51	64.01	1.02	1.01	1.02	1.01	0.94	2.30	927.41	6194.69	0.94	2.30
9	0.94	0.95	68.72	64.18	68.72	64.18	0.94	0.95	0.94	0.95	0.82	2.33	927.41	6194.69	0.82	2.33
10	0.93	0.85	68.51	60.81	68.51	60.81	0.93	0.85	0.93	0.85	0.85	0.75	0.91	0.90	0.85	0.75
11	0.93	0.92	0.93	0.92	0.93	0.92	0.93	0.92	0.93	0.92	0.93	0.92	0.93	0.92	0.93	0.92
12	0.96	0.98	0.96	0.98	0.96	0.98	0.96	0.98	0.96	0.98	0.96	0.98	0.96	0.98	0.96	0.98
13	69.14	65.66	69.14	65.66	69.14	65.66	69.14	65.66	69.14	65.66	69.14	65.66	69.14	65.66	69.14	65.66
14	69.06	65.58	69.06	65.58	69.06	65.58	69.06	65.58	69.06	65.58	69.06	65.58	69.06	65.58	69.06	65.58
15	0.96	0.99	0.96	0.99	0.96	1.01	0.96	0.99	0.96	0.99	0.96	0.99	0.96	0.99	0.96	1.01
16	0.96	0.99	0.96	0.99	0.96	0.99	0.96	0.99	0.96	0.99	0.96	0.99	0.96	0.99	0.96	0.99

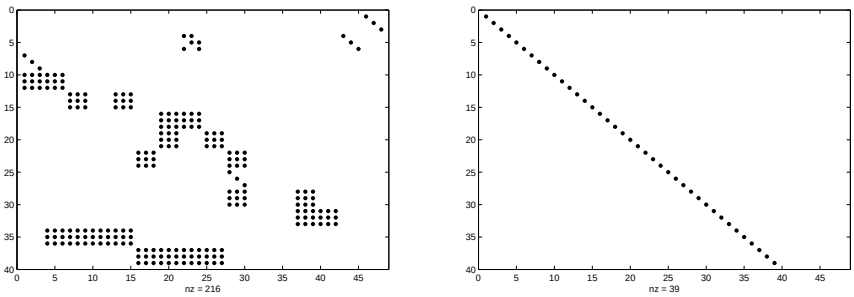

(a) Matrix **H**. (b) Matrix **S**.

(c) Matrix **E**. (d) Matrix **V**.

Figure 4.8 Matrix visualizations obtained using the measurements considered in Case VIII.

4.3 CONCLUSION

In solving the TSE problem using SVD it is possible to have a partially observable system. This is the case when the rank of **H** is less than the number of state variables. If the unobservable voltages are due to lack of measurements, then the obtained estimation for these voltages is zero over the entire estimation time; but a non-zero can be obtained if a measurement produces linearly dependent columns in **H** or the matrix is ill-conditioned. Therefore, it is imperative to know which state variables can be relied on and which cannot (that are unobservable), hence the importance of the observability analysis that has been developed and presented. The proposed observability analysis is capable of identifying not only unobservable buses but unobservable islands as well.

The use of virtual measurements to improve observability was discussed and demonstrated using an actual distribution system. Additionally, its limitations were highlighted. When correctly applied, virtual measurements can improve the observability of a distribution system, eliminating previously unobservable islands containing measurements.

Chapter 5

DISTRIBUTED PARAMETERS

In this chapter, a model used to represent distributed parameters (electrically long and medium transmission lines) in TSE with NIS is presented. As introduction, the model used in transients simulation is presented and then the changes required in the algorithm to apply it in estimation are discussed. The proposed method accuracy is investigated in different scenarios.

5.1 TRANSMISSION LINE MODELLING WITH NIS

For electromagnetic transient analysis and transient state estimation, short transmission lines can be represented by PI models (with lumped parameters) where the total inductance and resistance of the line are in series and the line total capacitance is split in two and located at each end of the line. Up to now, TSE has been applied to lines using lumped parameter models [Yu and Watson, 2007, Farzanehrafat and Watson, 2013]. These models do not take into account the distributed nature (or frequency dependence) of the line's parameters, and are valid for electrically short transmission lines (the waves travelling time is smaller than the estimation time step or measurement sampling time). For a sampling time of 50 μs, a line is short if its length is smaller than 15 km [Watson and Arrillaga, 2003b][1].

For long lines, the simplest model is based on the method of characteristics (or Bergeron's method) for the lossless line (see section 2.2.2.1). This provides an exact closed-form solution for the lossless uniform line. Further modification allows the inclusion of losses in the form of lumped resistances [Dommel, 1987, Watson and Arrillaga, 2003b].

[1] In general a line is short if its length is smaller than a quarter of the electromagnetic wave wavelength. Or $d << d_c$, where $d_c = c/4f$ (c is the wave velocity -close to the speed of light for overhead lines- and f its frequency -the maximum frequency of interest in the analysis-).

5.1.1 Bergeron model with losses

The Bergeron model with losses is an approximation based on Bergeron's solution to the lossless transmission line plus lumped resistances at both ends and the middle of the line (1/4 and 1/2 of the total line resistance respectively). The formulation uses the distributed parameters of the line at the nominal system frequency (50 or 60 Hz). The equations are [Dommel, 1969, Dommel, 1987, Watson and Arrillaga, 2003b]:

$$i_{jk(t)} = \left(\frac{1}{Z}\right) v_{j(t)} + I_{j(t-\tau)} \tag{5.1a}$$

$$i_{kj(t)} = \left(\frac{1}{Z}\right) v_{k(t)} + I_{k(t-\tau)} \tag{5.1b}$$

where

$$Z = Z_c + \frac{R}{4} = \sqrt{\frac{L'}{C'}} + \frac{R}{4} \tag{5.2}$$

is the equivalent impedance (Z_c is the characteristic impedance) and L' and C' are the per unit length line's inductance and capacitance, R is the total line resistance, and the history terms are

$$I_{j(t-\tau)} = \left[\frac{(1+a)}{2}\right]\left[-\frac{1}{Z}\cdot v_{k(t-\tau)} - a\cdot i_{kj(t-\tau)}\right] + \left[\frac{(1-a)}{2}\right]\left[-\frac{1}{Z}\cdot v_{j(t-\tau)} - a\cdot i_{jk(t-\tau)}\right] \tag{5.3a}$$

$$I_{k(t-\tau)} = \left[\frac{(1+a)}{2}\right]\left[-\frac{1}{Z}\cdot v_{j(t-\tau)} - a\cdot i_{jk(t-\tau)}\right] + \left[\frac{(1-a)}{2}\right]\left[-\frac{1}{Z}\cdot v_{k(t-\tau)} - a\cdot i_{kj(t-\tau)}\right] \tag{5.3b}$$

where $a = [Z_c - (R/4)] / [Z_c + (R/4)]$, and $\tau = d\sqrt{L'C'}$ is the travelling time (see equation 2.24 in page 20). The previous model is valid if $R/4 << Z_c$.

Equations 5.1a and 5.1b are valid for a single conductor line. When dealing with multiconductor lines, modal analysis is required to decouple the equations and obtain the travelling times and impedance for each mode. One way (used in this work) to obtain the modal transformation matrices is as follows: first the voltage transformation matrix ($\mathbf{T}_v$) is calculated. To accomplish this, a $\mathbf{T}$ is found (using eigenvalue analysis) such that[2]

$$\mathbf{T}^{-1}\left(\mathbf{Z}'_{ph}\mathbf{Y}'_{ph}\right)\mathbf{T} = \mathbf{\Lambda},$$

where $\mathbf{Z}'_{ph}$ and $\mathbf{Y}'_{ph}$ are the line's per unit length phase impedance and admittance, and $\mathbf{\Lambda}$ is a diagonal matrix. Then, the imaginary part is discarded, $\mathbf{T}_v = \mathrm{Re}\,(\mathbf{T})$. Finally, the current

[2] Another way to obtain the modal transformation matrices, without the need of eigenvalue analysis, is the use of the perturbation approach as show in "Modal analysis of untransposed bilateral three-phase lines, a perturbation approach" by Brandão Faria J. A. and Briceño Mendez J. H. in IEEE Transactions on Power Delivery, Vol 12, No. 1, January 1997, pp. 497-504. Its use produces a $\mathbf{T}$ numerically close to the one obtained by eigenvalue analysis; the other steps in the process remain the same.

transformation matrix is $\mathbf{T}_i = (\mathbf{T}_v^{-1})^T$. The use of these transformation matrices allows the application of (5.2) and (5.3) to each mode. After solving for each mode, the solution vector is transformed back to the phase domain. The modal transformation matrices are complex, but only the real part is used in transient simulation because all variables are real (for a transposed line Clarke's matrix is used) [Dommel, 1987].

5.2 INCLUSION OF DISTRIBUTED PARAMETER LINES IN TSE

In chapter 2, the formulas used to form $\mathbf{H}$ are presented for lumped parameters; in particular, if measurement m is the voltage at node k, then the measurement matrix element $h_{m,k}$ is equal to one. If measurement m is the current from node j to node k through a lumped parameter branch, then $h_{m,k} = -h_{m,j}$ where $h_{m,j}$ is equal to the branch equivalent conductance (according to the NIS formulation).

For a line with distributed parameters, if the measurement m is the current at terminal k (i_{kj}), then

$$h_{m,k} = \frac{1}{Z} \tag{5.4}$$

and $h_{m,j} = 0$ [Z is defined in (5.2)]. The reason for this is the topological disconnection between line terminals in the Bergeron model. The connection between the terminals is modeled by the history terms (5.3) (i.e., the current sources in Fig. 5.1). This means that at least one measurement is required on each side of the line. The need for measurements at each line end has implications for system observability (see section 5.4).

With multiconductor lines, (5.4) becomes a matrix equation. This matrix is obtained after transformation, to the phase domain, of the diagonal matrix containing the equivalent impedances for each mode. This is

$$\mathbf{H}_{KK} = \mathbf{T}_i \mathbf{Y}_{mo} \mathbf{T}_v^{-1} \tag{5.5}$$

where $\mathbf{Y}_{mo}$ is diagonal, and its elements are $y_{mo\ l,l} = 1/Z_l$, where l is the particular mode (there are the same number of modes as phases). As an example, if the voltages at the ends of a transmission line are to be estimated on the basis of on current (at one end) and voltage (at the other end) measurements, equation 2.35 takes the form

$$\begin{bmatrix} \mathbf{z}_1 \\ \mathbf{z}_2 \end{bmatrix} - \begin{bmatrix} \mathbf{I}_{\text{History 1}} \\ \mathbf{0} \end{bmatrix} = \begin{bmatrix} \mathbf{H}_{11} & \mathbf{0} \\ \mathbf{0} & \mathbf{H}_{22} \end{bmatrix} \begin{bmatrix} \mathbf{x}_1 \\ \mathbf{x}_2 \end{bmatrix} \tag{5.6}$$

where $\mathbf{z}_1$ is the vector with current measurements (from bus 1 to 2 for all phases); $\mathbf{z}_2$ is the vector of voltage measurements at bus 2; $\mathbf{I}_{\text{History 1}}$ is the vector of history terms corresponding to measurement $\mathbf{z}_1$; $\mathbf{0}$ indicates a null vector or matrix; $\mathbf{x}_1$ and $\mathbf{x}_2$ are the voltages (to be estimated) at bus 1 and 2 respectively; $\mathbf{H}_{11}$ is obtained from (5.5); and $\mathbf{H}_{22}$ is an identity matrix.

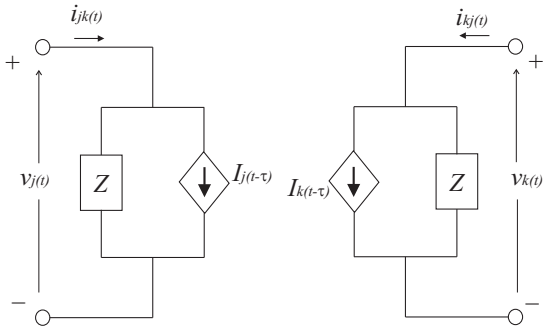

Figure 5.1 Bergeron transmission line equivalent circuit.

5.3 ESTIMATION SOLUTION

In general, the number of measurements m is expected to be lower than the number of state variables n ($\mathbf{H}$ is a $m \times n$ matrix). To solve the measurement equation (2.35) for $\mathbf{x}$ in such a case, SVD can be used on $\mathbf{H}$ to find its pseudo-inverse $\mathbf{H}^+$ (refer to section 2.3.2.1). A flowchart for TSE with NIS including elements modelled with distributed parameters is presented in figure 5.2. Note that if a fault occurs inside a transmission line with a current measurement, TSE does not provide an acceptable estimation because the model for such a line is no longer correct while the fault is active (same as with lumped parameter models).

5.3.1 Initial condition

The initial condition is important for TSE with NIS; in single-phase circuits, an incorrect value creates an error that depends on the branch element type (see table 3.1). In the case of three-phase systems with lumped parameters, the error decays rapidly in time owing to the existence of mutual terms in the equivalent admittance matrices [Farzanehrafat and Watson, 2013]. This is not true for the distributed parameter line; an error in the initial condition (the initial condition being a vector instead of the single value for lumped parameters) creates numerical oscillations that can grow in time during the estimation.

The initial condition for distributed parameter lines is calculated using the long transmission line steady-state equation (two-port equation, the equivalent PI model), after estimating the phasors of available measurements [three possible combinations, (i_{jk}, v_k), (v_j, i_{kj}), and (i_{jk}, i_{kj})] for each line modelled as distributed[3].

[3] As an example, when the available measurements are (v_j, i_{kj}) the two-port equation takes the form

$$\begin{bmatrix} \bar{V}_{k_l} \\ \bar{I}_{jk_l} \end{bmatrix} = \begin{bmatrix} 1/\cosh(\gamma d) & \mathbb{Z}_c \tanh(\gamma d) \\ (1/\mathbb{Z}_c)\tanh(\gamma d) & -1/\cosh(\gamma d) \end{bmatrix} \begin{bmatrix} \bar{V}_{j_l} \\ \bar{I}_{kj_l} \end{bmatrix}.$$

Note that it is a phasor equation in the modal domain, γ and $\mathbb{Z}_c$ are calculated from the line series impedance and shunt admittance at the nominal frequency for the particular mode l.

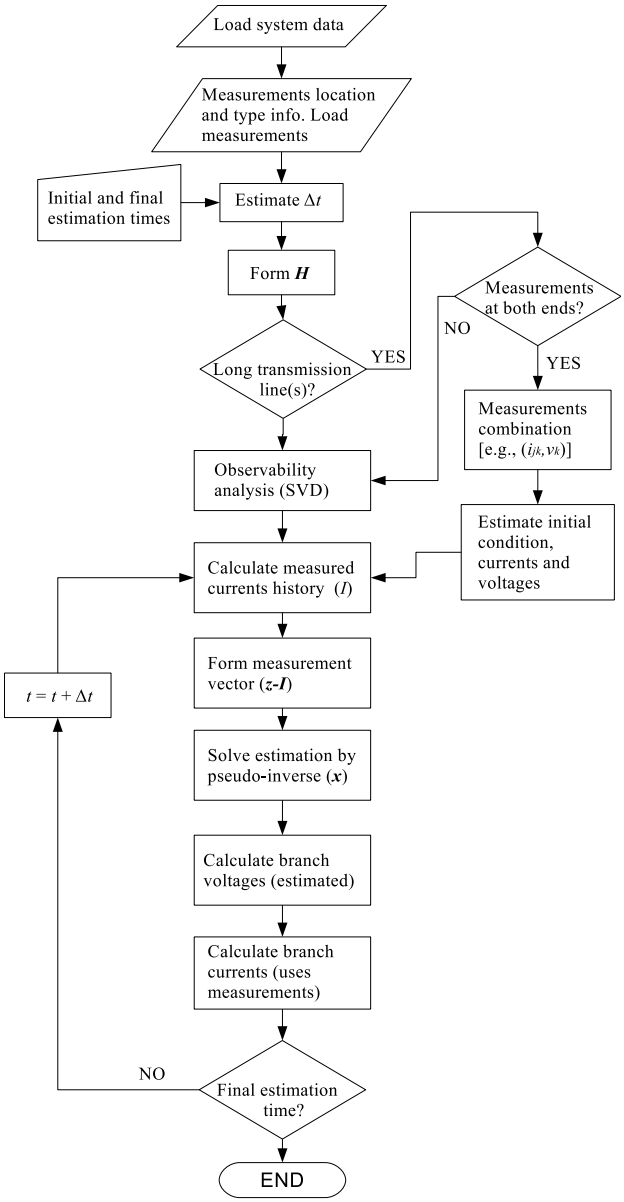

Figure 5.2 Simple flowchart for TSE with NIS with distributed parameters elements.

In this work the phasors are estimated using least squares for the fundamental frequency [Ribeiro et al., 2014, pp.215-216], which is presented in appendix C. Therefore, measurements must include at least one cycle previous to the event start. Then the initial condition is calculated up to N steps before the initial estimation time, where N is the number of time-steps (the time-step is estimated from the measurements' time stamp, and is equal to the sampling rate) that corresponds to the largest time delay (travelling time) obtained from modal analysis.

5.3.2 Travelling time interpolation

The travelling time will not be (in general) an exact multiple of the estimation step. Interpolation to the correct travelling time has to be applied[4]. The interpolation is applied in the modal domain. The use of interpolation during estimation with long lines adds damping that helps prevent excessive error build-up that otherwise would be present, which would increase in error magnitude as the estimation time increases (the error adds up when history terms are calculated). When interpolation is not used, the noise adds over time, making the estimated waveforms useless if the estimation time is too long (more than a few cycles). The half-step interpolation formula (3.4) is modified as follows

$$v_{(T-(1-\delta)\Delta t)} = v_{(T-\Delta t)} + \delta[v_{(T)} - v_{(T-\Delta t)}] \tag{5.7}$$

where $T-(1-\delta)\Delta t$ is the actual modal travelling time ($0.0 < \delta < 1.0$), T is an integer number of time-steps and $0 \leq [T-(\tau/\Delta t)] < 1$. Equation 5.7 is used on all voltages and currents before they are included in (5.3) to calculate the history terms.

5.4 OBSERVABILITY

For a review of the existing observability analysis method for TSE with NIS, please refer to section 4.1.2. In the case of distributed parameter lines, at least two measurements are required (one at each line end). The use of $\mathbf{V}$ is not enough with long lines, because it will indicate a node with one current measurement related to a distributed parameter line as observable, ignoring the fact that another measurement is required on the other end as well [which is necessary to calculate the history terms (5.3)]. A developed subroutine reviews if measurements are included on both sides of transmission lines, before the first estimation step (see Fig. 5.2), and serves as observability information. This subroutine identifies the line ends (buses) that are unobservable owing to lack of measurement at the other end. Therefore, the subroutine finds unobservable islands that contain measurements. These measurements, without a pair at the other line end, have to be discarded before the estimation can proceed.

5.5 APPLICATION EXAMPLES

Figure 5.3 presents a one-line diagram of test system 1, known as the 9 bus Anderson-Farmer test system [Anderson and Farmer, 1996]. This system has seven long transmission lines; the

[4]This is another difference with simulation, the EMTDC/PSCAD manual recommends to use travelling time interpolation only when $\tau/\Delta t$ is small (e.g., if the approximated travelling time is 3 steps when the real value is 2.667 steps). Because, its use adds additional damping at high frequencies (if not used line length is artificially modified).

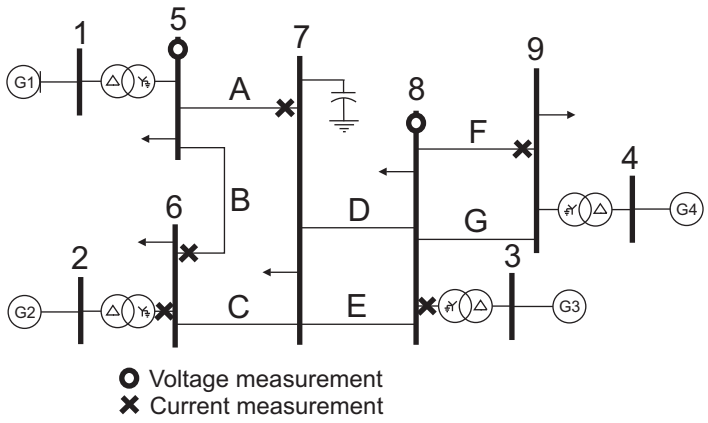

Figure 5.3 Test system 1, the 9 bus Anderson-Farmer.

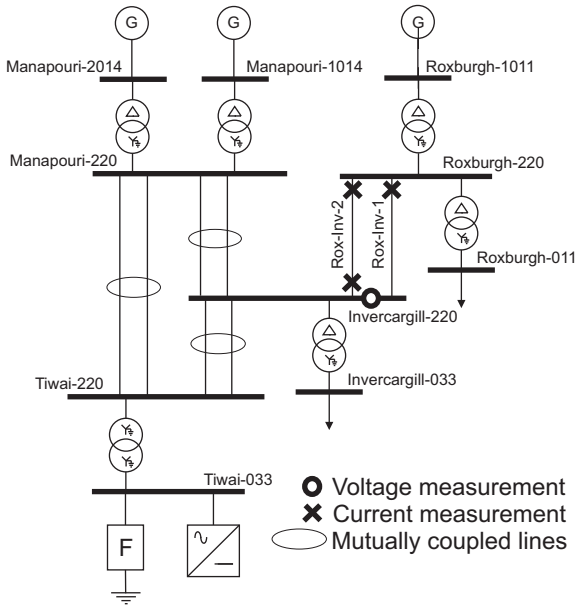

Figure 5.4 Test system 2, the reduced lower South Island New Zealand.

length of lines A and C is 600 km, and the rest are 500 km long. All lines are 500 kV (60 Hz) with the same geometry and characteristics (conductor numbers and type as well as ground resistivity). All system information is presented in [Anderson and Farmer, 1996]. The only assumptions made here are the transformer connections (indicated in Fig. 4.1, all Ynd11) and the generator voltages (23 kV).

Test system 2 is the reduced lower South Island New Zealand system, presented in figure 5.4 [Watson and Arrillaga, 2003b]. This system has eight transmission lines (220 kV, 50 Hz, the last three numbers after the bus name indicate bus voltage in kilovolts). The lengths of lines Rox-Inv-1 and Rox-Inv-2 are 132.20 km and 129.8 km respectively. The system has a non-linear load (24 pulse converter) and passive harmonic filters at the Tiwai-033 busbar.

5.5.1 Test system 1

To obtain measurements, test system 1 was modelled in EMTDC/PSCAD and DIgSILENT's PowerFactory software. The lines were modelled as distributed parameter with frequency dependence (untransposed and transposed), and their parameters were calculated from their geometry. Each software has its own routine to calculate line parameters, and their results are not identical; furthermore, PowerFactory uses J. Marti's model for frequency dependence, while the phase model (universal line model) is available in EMTDC/PSCAD (for EMTDC/PSCAD simulations, the phase model was used). A fault lasting 20 ms was simulated at line C, located 1 km from bus 6. The simulation results were saved (a simulation time-step of 50 μs used), and then noise was added before its use in estimation (noise is added as explained in section 3.1.1).

For estimation, only line and transformer data is introduced (the location of the fault and its parameters are unknown). Transformers are modelled as ideal (using NIS with trapezoidal rule); lines are represented using the Bergeron model with losses. Due to numerical oscillation created by ideal transformer model inductances, half-step interpolation is applied during the entire estimation time. The reason behind numerical oscillation in estimation are explained in chapter 3. The interpolation is applied as presented in section 3.2.

To measure the estimation accuracy, the normalised root mean square error (NRMSE) for each phase of each bus is calculated (see appendix A). The estimation starts at 0.975 s (the fault starts at 1 s) and ends at 1.06 s.

5.5.1.1 Noise

On the basis of results from EMTDC/PSCAD, lines were modeled as frequency-dependent and untransposed. The measurements are as indicated in figure 4.1. The fault is a-g (phase A-to-ground) at line C. A Monte Carlo simulation (5000 cases) was used to obtain figures 5.5, 5.6, and 5.7. Each Monte Carlo case used a new random vector for each measurement noise. In figure 5.5, the mean NRMSE is presented for each phase (observable buses only) for different noise standard deviations. Because lines are untransposed, its geometry is used as input to calculate travelling times and impedances for estimation. Complex depth approximation of Carson's ground return equation and complex penetration depth for conductors' internal impedance formulas are used (at 60 Hz) [Martinez-Velasco et al., 2010].

In figure 5.5, the error increases as the noise standard deviation increases. The error due to the model used is observable when no noise is added; this is the case when the noise standard deviation is zero. In this particular scenario, Monte Carlo simulation is not required.

The largest error is obtained at buses that are estimated through current measurements (i.e.,

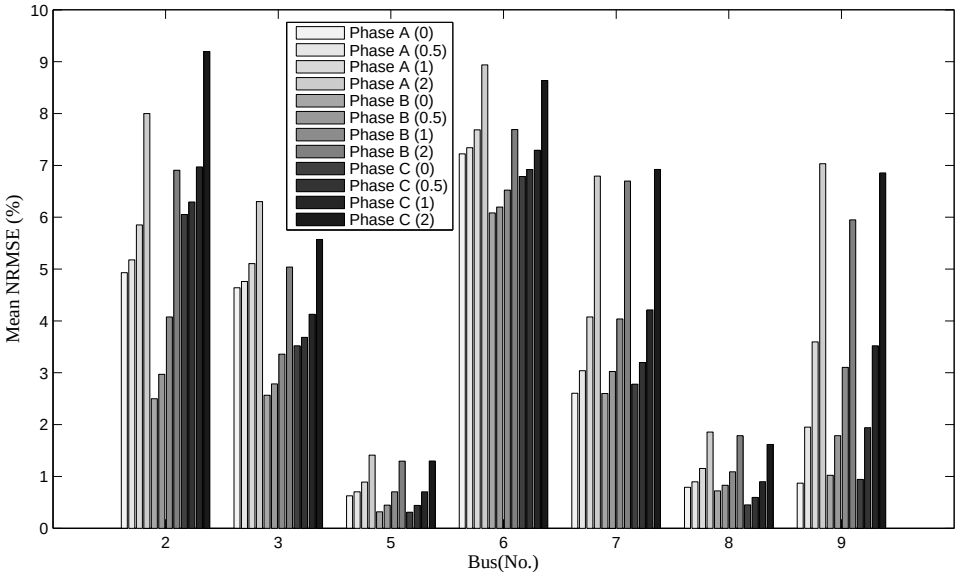

Figure 5.5 Mean NRMSE for observable buses after 5000 estimations (untransposed lines); fault is a-g. Number in parentheses indicates noise standard deviation in percentage of pre-fault peak value.

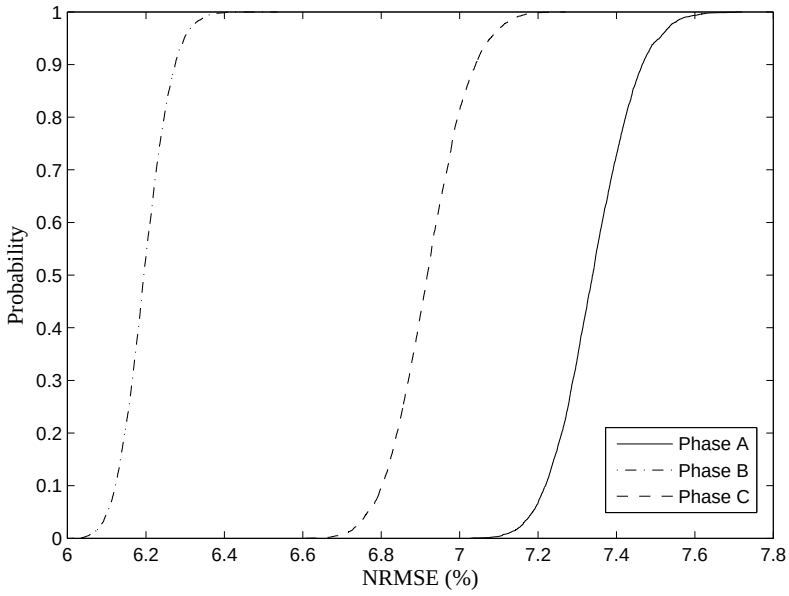

Figure 5.6 Probability curves for NRMSE at bus 6 after 5000 estimations; fault is a-g. Noise standard deviation is 0.5 % of pre-fault peak value.

no direct voltage measurement is available), see buses 2, 3, 6, 7, and 9. The error increases as a bus gets closer to fault location (and no direct voltage measurement is available); see the results for buses 6, 7, and 9. This is explained by a larger fault current magnitude at the associated current measurements, and has been observed previously in TSE with lumped parameters (e.g. see results in table 4.1).

Figures 5.6 and 5.7 show the change in probability curves for bus 6 between two different noise standard deviations. Bus 6 was chosen because it presents the largest error for the estimated

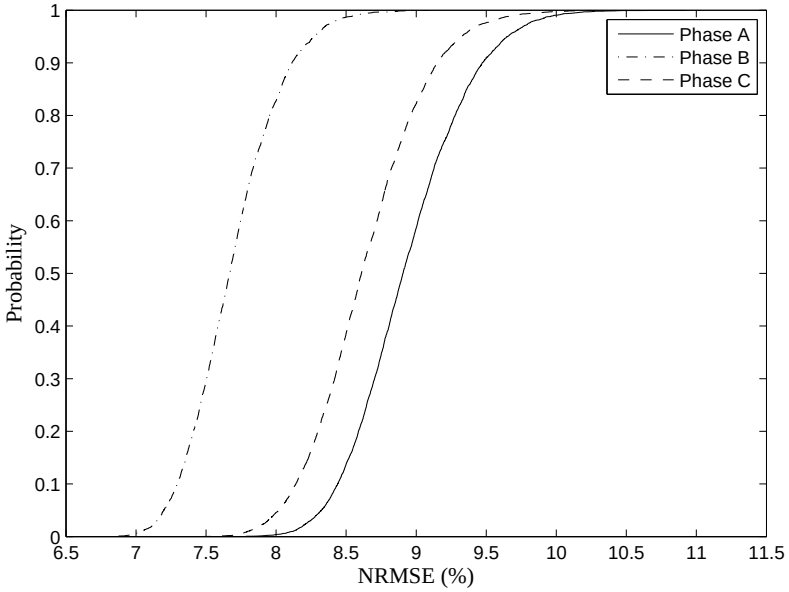

Figure 5.7 Probability curves for NRMSE at bus 6 after 5000 estimations; fault is a-g. Noise standard deviation is 2 % of pre-fault peak value.

voltage obtained from a transmission line measurement (see Fig. 4.1). The estimated voltages at buses 2 and 3 are obtained from transformer measurements.

In figure 5.8, the difference between the actual (from simulation) and estimated (no noise added) voltages is presented in p.u., and the base voltage is $500\times\sqrt{2}/\sqrt{3}$ kV. The difference is small before the fault. This is due to the initial condition estimation. Then at the fault start (1.0 s), a spike appears and repeats itself but its magnitude decreases over time (the effect of travelling time interpolation). Finally at the fault's end (1.02 s), a new spike appears and again repeats itself by decreasing in magnitude over time. This explains the smaller change in the mean NRMSE for bus 6 in figure 5.5, compared to buses 7 and 9 (also estimated from line current measurements).

5.5.1.2 Fault type

On the basis of the results from EMTDC/PSCAD, lines are modelled as frequency-dependent and untransposed. The measurements are as indicated in figure 4.1. The noise standard deviation is 1 % of the pre-fault peak value.

Figure 5.9 was obtained after a Monte Carlo simulation (5000 cases), and the mean NRMSE is presented for each observable bus phase for three different fault types (all at the same location and duration, previously indicated for test system 1).

From figure 5.9, it is clear that the phases with largest error are the ones located closer to the fault and estimated from current measurements (see bus 6). They are the phases carrying the

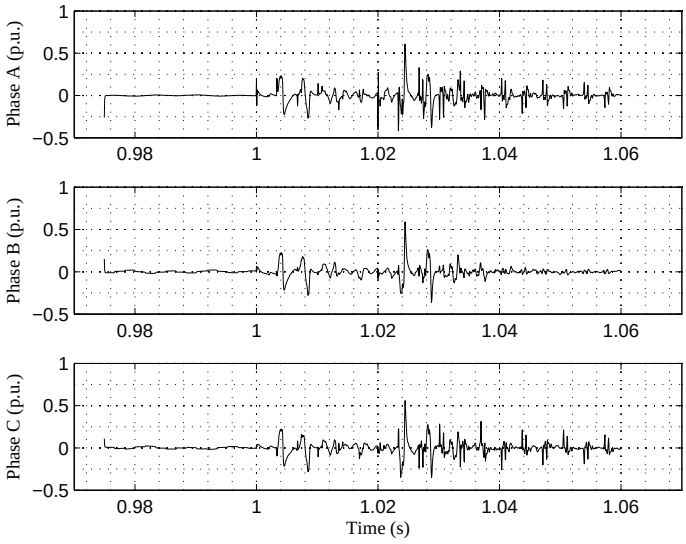

Figure 5.8 Voltage difference at bus 6, between actual (EMTDC/PSCAD result) and estimated (without noise) voltages. Fault is a-g.

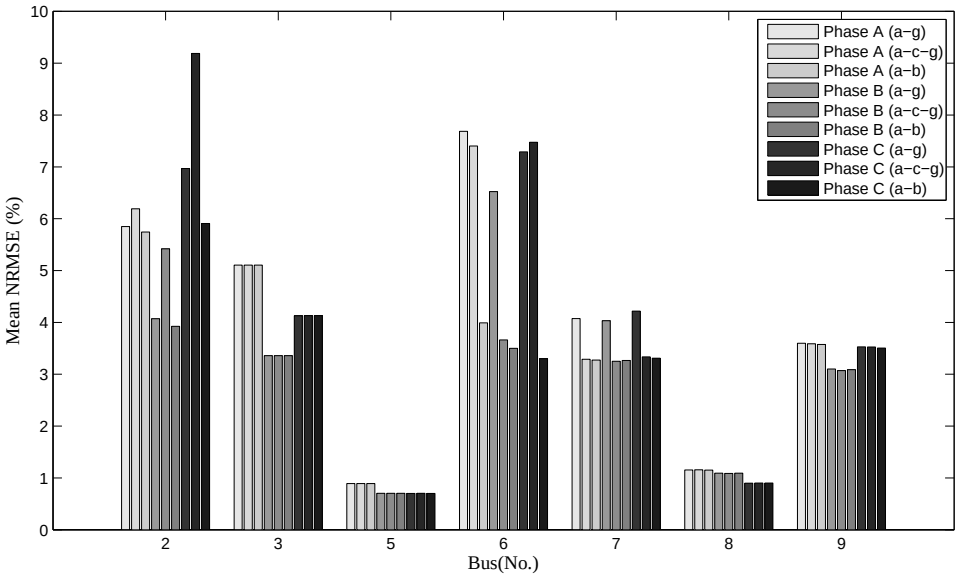

Figure 5.9 Mean NRMSE per bus after 5000 estimations (untransposed lines); noise standard deviation 1 % of pre-fault peak value. Fault type is indicated.

largest fault currents, such as line B's phase A in the a-g fault.

5.5.1.3 Fault type (transposed lines)

Using results obtained from PowerFactory, lines were modelled as frequency-dependent and transposed. The measurements are as indicated in figure 4.1. The noise standard deviation for each measurement is 1 % of the pre-fault peak value. Monte Carlo simulation (1000 cases) was

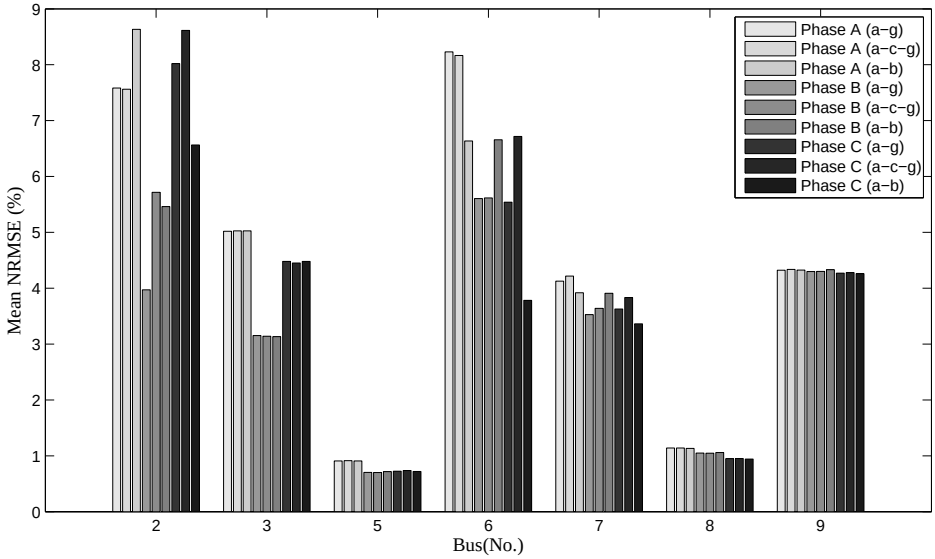

Figure 5.10 Mean NRMSE per bus after 1000 estimations (transposed lines); noise standard deviation 1 % of pre-fault peak value. Fault type is indicated.

used to obtain figure 5.10. In figure 5.10, the mean NRMSE is presented for each observable bus phase of three different fault scenarios. Because the lines are transposed, zero and the positive sequence impedance and admittance (obtained from PowerFactory) are used to calculate travelling times and impedances for estimation.

The same conclusions as from figure 5.9 can be obtained from figure 5.10. Again, buses closer to the fault and estimated by current measurements present the largest error, and again faulted phases present the largest error, per fault type.

5.5.1.4 Voltage sag

On the basis of the measurements obtained from PowerFactory, the voltage sags on a per-phase basis had been calculated. Table 5.1 shows the difference in residual voltage and sag duration for voltage sags detected during an a-g fault. The differences are calculated after the RMS voltage is obtained from actual (results from simulation) and estimated (estimated after measurements with 1 % of pre-fault peak value standard deviation noise) waveforms[5]. The base voltage is the nominal RMS line-to-ground voltage. A sag is defined as a reduction in RMS voltage of more than 0.1 p.u. that lasts at leasts half cycle (the nominal frequency). NA in the table means no

[5]The true RMS value is calculated over one cycle (fundamental frequency) as $|V| = \sqrt{\left(\sum_{n=1}^{N}[v(n)]^2\right)/N}$, the value is calculated from the first available cycle in estimation and updated with every new step. The values in table 5.1 are calculated from the difference in the minimum values obtained from the entire waveforms, i.e., the sag residual voltage difference is $|V|_{min} - |\hat{V}|_{min}$ where $|\hat{V}|_{min}$ is the minimum RMS value obtained from the estimated waveform. The sag duration difference is $t_1 - t_2$ where t_2 is the sag duration obtained form the estimated RMS waveform.

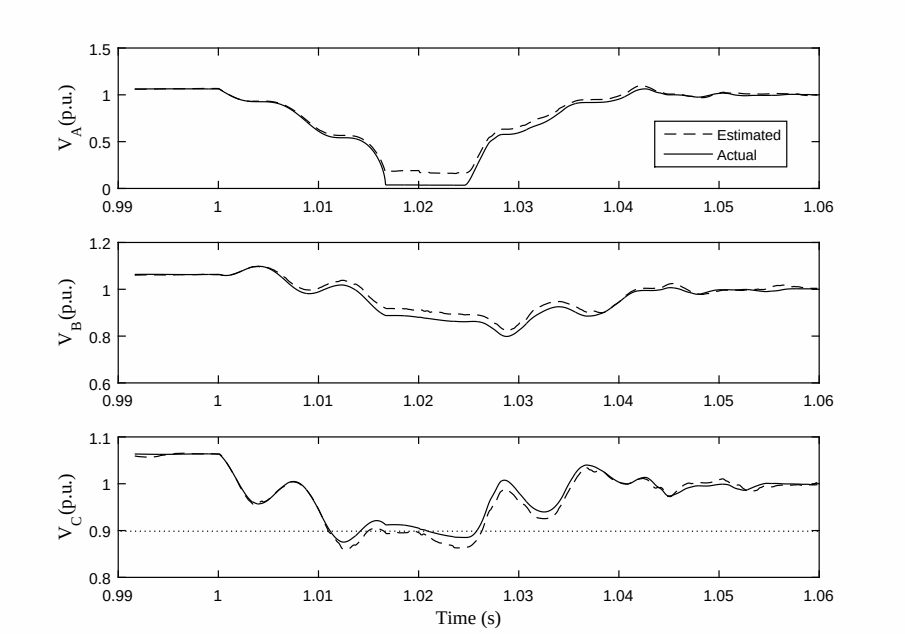

Figure 5.11 RMS voltage at bus 6.

Table 5.1 Difference in residual voltage and sag duration for voltage sags present during the a-g fault.

	Residual voltage (p.u.)			Duration (ms)		
Bus	A	B	C	A	B	C
2	0.0189	NA	-0.0111	0.45	NA	0.80
6	-0.1253	-0.0226	0.01582	0.80	7.15	-9.91
7	-0.0063	NA	NA	1.05	NA	NA

sag is detected. Further, bus 6 phase C of the actual waveform does not present a sag (voltage is less than 0.9 p.u. for 5 ms), see phase C in figure 5.11.

The results in table 5.1 show how good the estimated voltage waveforms are. These results again highlight the largest estimation error in the bus closest to the fault (bus 6).

5.5.2 Test system 2

Test system 2 (figure 5.4) was modelled in PowerFactory. A single-phase-to-ground fault at bus Roxburgh-011 was simulated (a-g lasting 30 ms, and clear after disconnection of bus Roxburgh-011). Lines are untransposed and simulated with frequency dependence (simulation time-step 50 μs).

For the following estimations, the same measurements are used, all with 1 % of the pre-fault peak value standard deviation noise (noise was generated only once). Only lines and transformers were

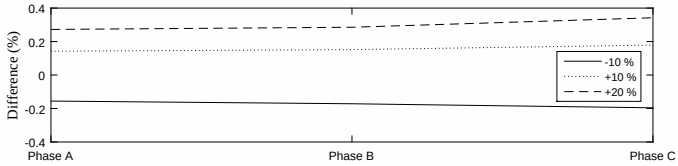

(a) Variation applied to resistance values.

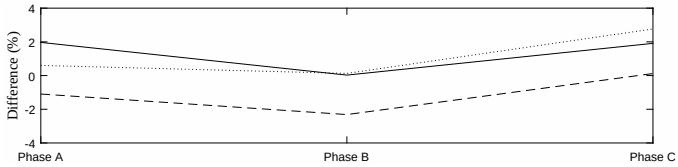

(b) Variation applied to reactance values.

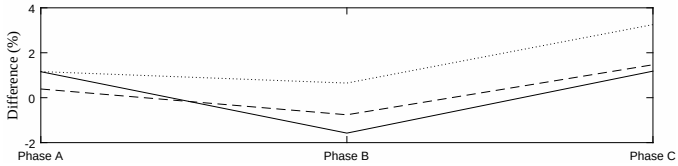

(c) Variation applied to susceptance values.

Figure 5.12 Difference in NRMSE at bus Roxburgh-220 with parameters variation.

included as input. The fault location and its parameters are unknown. The lines impedance and admittance matrices (obtained from PowerFactory) are used to calculate travelling times and equivalent impedances in estimation. The estimation starts at 0.475 s (fault starts at 0.5 s) and ends at 0.6 s.

5.5.2.1 Line parameters

Estimation was conducted using voltage measurement at Invercargill-220 and current at line Rox-Inv-1 (see figure 5.4). Only buses Roxburgh-220 and Invercargill-220 are observable. Figure 5.12 was obtained by changing the resistance, reactance, and susceptance magnitudes in the line impedance and admittance matrices.

The estimation of line voltages using the Bergeron model is not severely affected by small changes in line resistance; see figure 5.12 (a). It is, however, affected by deviations in reactance and susceptance values; see figures 5.12 (b) and (c). This is to be expected as the resistance value is smaller than the characteristic impedance, and this impedance and the travelling times are calculated from the inductance and capacitance (reactance and susceptance).

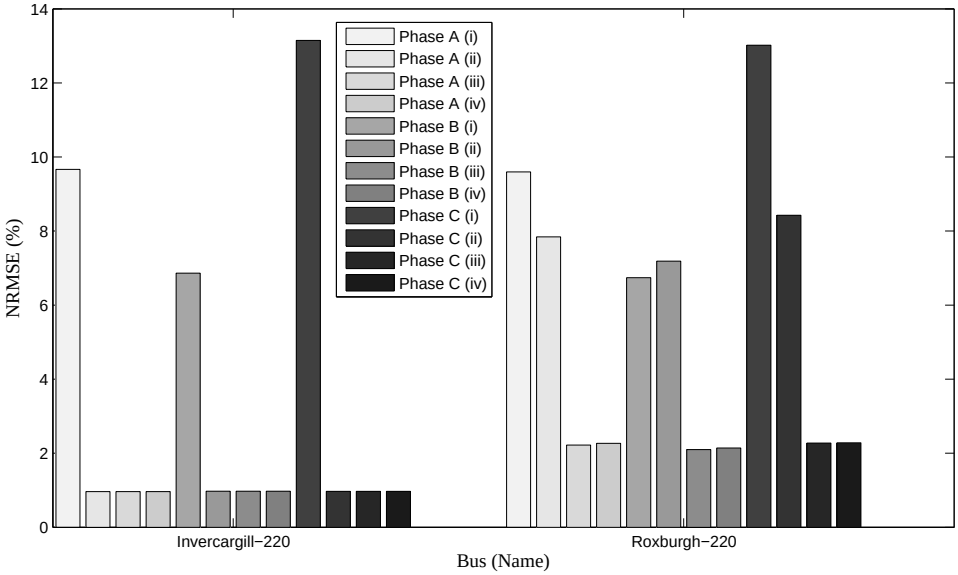

Figure 5.13 Observable buses NRMSE; noise standard deviation 1 % of the pre-fault peak value. (i) Current measurements at line Rox-Inv-2. (ii) Current measurement at line Rox-Inv-1 plus voltage measurement at Invercargill-220. (iii) Current measurements at line Rox-Inv-2 plus voltage measurement at Invercargill-220. (iv) All four measurements.

5.5.2.2 Measurements

Accuracy is investigated, using different combinations of measurements, for Roxburgh-220 and Invercargill-220 voltage estimation. The available measurements are the voltage at Invercargill-220, and the currents at lines Rox-Inv-1 and Rox-Inv-2 (see figure 5.4).

From the three possible measurement combinations to estimate distributed parameter line voltages (see section 5.3), it is possible to further subsume them into two cases: currents only and current plus voltage. Figure 5.13 presents these two cases (i and ii) and two more cases where now the number of measurements is greater than the number of observable buses (iii and iv). The worst possible scenario to estimate, long transmission line voltages using Bergeron's model, is when the only available measurements are the currents at both ends of the line. The best estimation is obtained when the number of measurements is greater than the number of observable buses.

5.5.2.3 Harmonics

Estimation was performed using voltage measurement at Invercargill-220 and current measurement at line Rox-Inv-1 (see figure 5.4). Only buses Roxbourgh-220 and Invercargill-220 are observable. The results are used to investigate if it is possible to estimate harmonic content from the estimated voltage waveforms. Figures 5.14 and 5.15 are presented. Both were obtained after FFT (Fast Fourier Transform) was separately applied to 1 cycle of the actual and

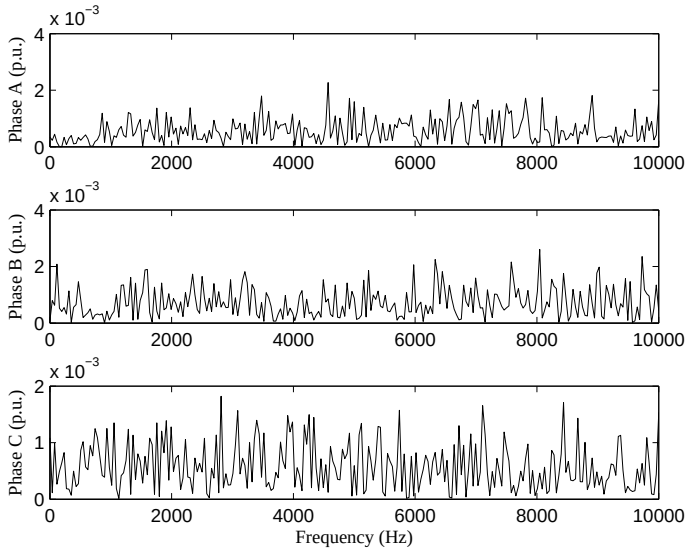

Figure 5.14 Frequency spectrum magnitude difference, between actual and estimated voltages at bus Invercargill-220 (pre-fault).

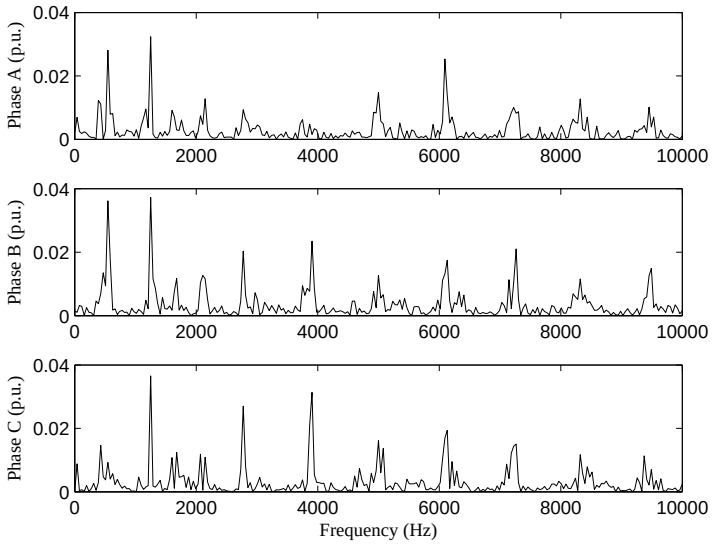

Figure 5.15 Frequency spectrum magnitude difference, between actual and estimated voltages at bus Roxburgh-220 (pre-fault).

estimated waveforms (pre-fault period), and then the resulting magnitudes subtracted. The magnitude difference is in p.u., the base is the maximum magnitude in the actual case.

Figure 5.14 presents the frequency domain magnitude difference of each phase voltage at bus Invercargill-220, while figure 5.15 presents the same difference for Roxburgh-220. It is possible to conclude that the first few harmonics magnitudes (including the fundamental) can be extracted from both buses. However the difference increases with the frequency, in particular for Roxburgh-220 (no direct voltage measurement). Similar results can be obtained for the fault and post-fault

Table 5.2 Harmonic magnitude error and angle difference at Invercargill-220 (pre-fault).

	Magnitude (%)			Angle (|rad|)		
Harmonic	A	B	C	A	B	C
1st	0.37	0.09	0.36	0.0010	0.0021	0.0025
21st	1.81	2.52	3.49	0.0253	0.0301	0.0348
23rd	1.42	7.06	4.42	0.0173	0.1015	0.0018

Table 5.3 Harmonic magnitude error and angle difference at Roxburgh-220 (pre-fault).

	Magnitude (%)			Angle (|rad|)		
Harmonic	A	B	C	A	B	C
1st	6.74	0.17	3.48	0.0326	0.0124	0.0210
21st	0.50	8.96	10.66	0.1053	0.0607	0.0053
23rd	2.97	19.68	6.44	0.0712	0.0881	0.0852

Table 5.4 Harmonic magnitude error and angle difference at Invercargill-220 (post-fault).

	Magnitude (%)			Angle (|rad|)		
Harmonic	A	B	C	A	B	C
1st	0.37	0.05	0.41	0.0016	0.0004	0.0021
21st	4.37	0.01	0.91	0.0551	0.0228	0.0037
23rd	4.28	9.54	5.78	0.0535	0.0340	0.0105

periods.

Tables 5.2, 5.3, 5.4, and 5.5 show the magnitude error and angular difference between harmonic magnitudes and phase angles for harmonics present at observable buses (the harmonics were estimated using least squares up to the 30th harmonic order [Ribeiro et al., 2014, pp.215-216], see appendix C)[6]. The fundamental can be extracted from both buses. However, the differences increase with higher harmonic frequencies, especially for Roxburgh-220 (no direct voltage measurement). Therefore, the extracted harmonic magnitudes cannot be trusted for higher harmonics. Similar results can be obtained for the fault period. The reason for this is the lack of frequency dependence in the model used in this work for transmission line voltages estimation.

[6]The magnitude error per harmonic is $|(|V_k| - |\hat{V_k}|)/|V_k|| \times 100$, while the phase angle difference is $|\delta_k - \hat{\delta_k}|$; where $|\hat{V_k}|$ and $\hat{\delta_k}$ are the harmonic magnitudes and angles obtained from estimated waveforms.

Table 5.5 Harmonic magnitude error and angle difference at Roxburgh-220 (post-fault).

	Magnitude (%)			Angle (|rad|)		
Harmonic	A	B	C	A	B	C
1st	0.61	0.95	4.42	0.0032	0.0199	0.0145
21st	9.1	5.8	0.39	0.2732	0.1499	0.0515
23rd	12.8	29.8	42.1	0.2008	0.2482	0.1101

5.6 CONCLUSION

To estimate transient voltage waveforms in long transmission lines, the line parameters' distributed nature has to be taken into account. This chapter has presented the first TSE to incorporate a transmission line model with distributed parameters. It is based on the classical Bergeron model with losses that is used for electromagnetic transient simulation. The equations required to extend the TSE algorithm were presented and discussed, as well as the way in which the addition affects the TSE initial condition requirements and observability analysis.

The TSE algorithm was tested on two transmission systems; both systems include transmission lines modelled with distributed parameters and frequency dependence. The presented results indicate that TSE performs well, despite the lack of frequency dependence modelling in the estimation. The obtained estimated voltages are a good approximation to the actual voltages, as indicated by the calculated error and the application of estimated waveforms in voltage sag and harmonic content calculations. In particular it has been shown that the fundamental harmonic voltage magnitude difference between the actual and estimated values is small. The magnitude error increases with harmonic order. The phase angle error is negligible for the fundamental and harmonics. A future enhancement for TSE is the inclusion of a frequency-dependent transmission line model.

Chapter 6

CONCLUSION

In this chapter conclusions are presented and future work on TSE with NIS is recommended.

6.1 CONCLUSION

The inclusion of distributed parameters models was demonstrated, for TSE with NIS, using the Bergeron model with losses. This improvement in TSE with NIS allows its application to transmission systems. The error in the estimation results was presented for two transmission test systems, being acceptable in presence of noise, unbalance and harmonics.

The application of TSE with NIS to non-linear elements was tested on a simple circuit with a surge arrester. The piecewise linear method is best suited, that the compensation method, for its implementation in TSE with NIS.

The possibility to have an unobservable island containing measurements, in TSE with NIS for distribution systems (lumped parameters), was demonstrated. An improved observability analysis capable to identify the nodes forming the unobservable island was proposed and tested. And, a virtual measurement was introduced in TSE as a possible solution for unobservable islands, its application was investigated and under given conditions the unobservable island becomes observable.

Interpolation has been applied in TSE with NIS to eliminate numerical oscillations (half-step interpolation), in estimation for single-phase and three-phase (with lumped and distributed parameters) circuits. And, linear interpolation was used to better approximate waves travelling times in transmission lines resulting in damping added to the model against numerical oscillation created by noise build-up.

In TSE with NIS the most important elements to be measured (and modelled in the estimation) are series elements rather than shunt elements. The reason for this is in the estimation model itself. The series elements (transmission lines, transformers, circuit breakers) have a large impact

since thorough its modelling, for current measurements, information spreads between nodes. Shunt elements main effect is on the node (singular) they are connected to.

Transient state estimation is still under development; this work advanced its state of the art but more work is required before its implementation to identify failure causes using field measurements.

6.2 FUTURE WORK

Future work required to achieve the goal of a transient state estimation that works in any system with any failure, can be classified in three categories: transient model, estimation model and implementation.

The transient model category refers to the need to accurately represent the elements during a transient. Based on the previous work the following is recommended:

- Include a frequency-dependent model for transmission lines. The results obtained in chapter 5 are acceptable but it is clear that part of the error is created by the model, especially in buses estimated by current closer to a fault. For simulation, it is accepted that it is better to include the frequency dependence in transmission lines.
- Improve transformer model. So far, transformers had been represented considering only leakage reactance. Copper loses (series resistance) and saturation (non-linear reactance) need to be included and tested. It is also recommended to try other models (e.g. UTC model) to represent transformers.
- Include time-varying elements. The need to model circuit breaker operations is extremely important for TSE, a brief discussion on the topic was presented in section 3.3.

Keep in mind that with more advanced models there is also the need for more information, which comes with a higher chance of error in the model parameter and the difficulty to obtain such parameters.

The estimation model refers to problems in the estimation solution. It can be improved in the following ways:

- To implement a procedure to recognise faulted elements. The estimation fails if a current measured element contains a fault (e.g. fault located at the middle of a transmission line). A procedure is needed to recognise such condition during the estimation and perhaps also locate the fault (if at all possible).

- To improve the observability analysis. There is the need to detect changes in the system and its effect on observability, contrary to other PQSE techniques TSE is not applied to a instant in time picture of the system. The system topology changes during the transient and this can affect observability, subject to measurements location and type.

- To explore the application of virtual measurement with distributed parameter elements. The work done on virtual measurement in this thesis is applicable to a node with lumped parameters elements connected to it.

The utilization of tools common to PQSE techniques, to be applied in the items above, need to be investigated for TSE with NIS. Tools like: topology processor, bad data detection, measurement equipment optimal placement, and parameter and structural error processing. Most of these tools are limited to situations where the number of measurements is higher than the number of state variables.

The implementation refer to problems that can happen when the estimation is used with field measurements. Some examples are:

- Unsynchronized measurements. It is possible to have field instruments recording at different sampling rates. TSE with NIS needs to be modified to accommodate such condition.

- Incorrect time stamp. The effect of error in the time stamp (or lack of it) needs to be investigated and solutions need to be proposed.

- Incorrect measurement assignment. If a measurement is incorrectly assigned (to an element) the parameters used on the measurement matrix will not correspond to it. The result is an erroneous estimation. A solution to review the correct measurement assignment is needed. Keep in mind that direction is as important as location for currents.

So far, the utilization of field measurements has not been reported for TSE. This is an important area of opportunity.

Appendix A

NORMALISED ROOT MEAN SQUARE ERROR

The normalised root mean square error (NRMSE) for the voltage of phase A of bus k is

$$\mathrm{NRMSE}_{k,\mathrm{A}} = \left(\sqrt{\frac{\sum_{i=1}^{\mathrm{N}} (v_{k,\mathrm{A}(i)} - \hat{v}_{k,\mathrm{A}(i)})^2}{\mathrm{N}}} \right) / V_{LNp} \tag{A.1}$$

where v and $\hat{v}$ are the true (obtained from the simulation and before noise addition) and estimated voltages, respectively; N is the number of time steps used to calculate the error (could be one cycle or the entire estimation time); and V_{LNp} is the nominal bus voltage (peak value line to neutral).

Thus, the average NRMSE value for bus k is

$$\mathrm{NRMSE}_k = \frac{\mathrm{NRMSE}_{k,\mathrm{A}} + \mathrm{NRMSE}_{k,\mathrm{B}} + \mathrm{NRMSE}_{k,\mathrm{C}}}{3}. \tag{A.2}$$

Equation A.1 is an approximation of the estimation error standard deviation, divided by a base value.

Appendix B

KILLINCHY DISTRIBUTION SYSTEM DATA

The Killinchy distribution system in South Canterbury, New Zealand. Its one-line diagram is presented in figure 4.1, the element parameters are in tables B.1, B.2, and B.3.

Table B.1 Load data.

Load	Bus	P, kW	Q, kVAr
1	4	38.801138	9.724482
2	5	23.280683	5.834689
3	10	460.763516	115.478222
4	11	567.466646	142.220548
5	13	58.201707	14.586723
6	14	77.602276	19.448964
7	15	11.640341	2.917345

Table B.2 Transformer data.

Transformer	Ratio HV/LV (V)	Configuration	X. p.u. (Base 100 MVA)
TXR1	11000/400	Dyn11	0.05
TXR2	11000/400	Dyn11	0.05

Table B.3 Line data.

Line	Length, km	R^+, Ω/km	Xl^+, Ω/km	Xc^+, Ω×km	R^0, Ω/km	Xl^0, Ω/km	Xc^0, Ω×km
1	1.606	0.4803	0.4452	1.5113999×10^5	0.628	1.787	3.7828285×10^5
2	1.274	0.986	1.1366	7.5569995×10^4	2.4632	6.2799	1.8914142×10^5
3	0.529	2.464	0.81	1.5113999×10^5	2.76	3.478	3.78285×10^5
4	0.87	0.2733	0.3532	3.0227998×10^5	0.421	1.695	7.5656570×10^5
5	1.471	0.5466	0.7064	1.5113999×10^5	0.842	3.39	3.7828285×10^5
6	0.107	2.734	0.824	3.0227998×10^5	3.03	3.492	7.5656570×10^5
7	0.123	3.42	0.652	6.7336959×10^3	4.436	2.39	7.7016667×10^5
8	0.319	4.2566	1.0321	3.0227998×10^5	5.5432	5.1537	7.565657×10^5
9	1.07	0.5466	0.7064	1.5113999×10^5	0.842	3.39	3.7828285×10^5
10	0.406	0.446	0.378	3.0227998×10^5	0.594	1.711	7.5656570×10^5
11	0.954	1.9006	1.0914	1.034355939×10^5	2.344	5.109	2.5368189×10^5
12	0.079	0.5466	0.7064	1.5114386×10^5	0.842	3.39	3.7828285×10^5
13	0.083	0.5466	0.7064	1.5114386×10^5	0.842	3.39	3.7828285×10^5
14	5.149	0.986	0.1366	5.2911353×10^3	2.4632	6.2799	2.5218857×10^5

Appendix C

PHASOR ESTIMATION BY LEAST-SQUARES

Consider any signal $v(t)$ defined as

$$v(t) = A_0 e^{(-t/\tau)} + \sum_{k=1}^{K} A_k \cos(k\omega t + \delta_k) \tag{C.1}$$

expanding the cosine after transformation to the discrete-time (t, used in this thesis, is replaced by n)

$$v_{(n)} = A_0 - A_1 n + \sum_{k=1}^{K} B_k \sin(k\Omega n) + \sum_{k=1}^{K} C_k \cos(k\Omega n) \tag{C.2}$$

where $\Omega = \omega \Delta t$ and ω is the system nominal frequency (50 or 60 Hz)[1].

To completely define the phasors for all K harmonics and the DC decaying component, it is necessary to find the values for all the constants in (C.2). To do so the number of samples (or measurements is N, and the window time is $N\Delta t$) taken from the waveform over one cycle must be greater than $2K + 2$. The estimation problem to be solved is

$$\mathbf{z} = \mathbf{H}\mathbf{x} + \mathbf{w} \tag{C.3}$$

where the state variables are

$$\mathbf{x} = [A_0 \quad A_1 \quad B_1 \quad C_1 \quad \ldots \quad B_K \quad C_K]^T$$

[1]The assumption that the fundamental frequency is equal to the system nominal frequency is one limitation of phasor estimation by least-squares. The reality is that the fundamental will be close to, but not equal to, the nominal frequency.

the measurement matrix is

$$\mathbf{H} = \begin{bmatrix} 1 & 0 & 0 & 1 & \dots & 0 & 1 \\ 1 & 1 & \sin(\Omega) & \cos(\Omega) & \dots & \sin(K\Omega) & \cos(K\Omega) \\ \vdots & & & & \vdots & & \\ 1 & N-2 & \sin((N-2)\Omega) & \cos((N-2)\Omega) & \dots & \sin(K(N-2)\Omega) & \cos(K(N-2)\Omega) \\ 1 & N-1 & \sin((N-1)\Omega) & \cos((N-1)\Omega) & \dots & \sin(K(N-1)\Omega) & \cos(K(N-1)\Omega) \end{bmatrix}$$

Because $N > 2K + 2$, $\left(\mathbf{H}^T\mathbf{H}\right)^{-1}$ exists.

In the particular case when only the fundamental phasor is of interest, $\mathbf{H}$ must only contain the third and fourth columns of those shown above (and at least two samples per period are required). Finally, to compensate for the phase angle rotation, the estimated phasor (known from the real and imaginary part B and C, respectively) is multiplied by the phasor

$$e^{-j\Omega(l-1)}$$

where l is the number of time steps difference between the estimation window first step and an arbitrary reference (usually the zero time for all waveforms).

Appendix D

LIST OF PUBLICATIONS

Journal papers The following is a list of papers published/under review in journals during the work course of this thesis

1 A. Castellanos-Escamilla and N.R. Watson, *Observability and virtual measurements for transient state estimation of distribution networks*, under review.

2 A. Castellanos-Escamilla and N.R. Watson, *Transient state estimator for smart transmission grids*, under review.

REFERENCES

[Abur and Exposito, 2004] Abur, A. and Exposito, A. G. (2004). *Power System State Estimation: Theory and Implementation*. Marcel Dekker.

[Alsaç et al., 1998] Alsaç, O., Vempati, N., Stott, B., and Monticelli, A. (1998). Generalized state estimation. *IEEE Transactions on Power systems*, 13(3):1069–1075.

[Anderson and Farmer, 1996] Anderson, P. M. and Farmer, R. G. (1996). *Series Compensation of Power Systems*. PBLSH! Inc.

[Anton and Busby, 2003] Anton, H. and Busby, R. C. (2003). *Contemporary Linear Algebra*. John Wiley & Sons, Inc.

[Arrillaga et al., 2000] Arrillaga, J., Watson, N. R., and Chen, S. (2000). *Power System Quality Assessment*. John Wiley & Sons.

[Beides and Heydt, 1991] Beides, H. M. and Heydt, G. T. (1991). Dynamic state estimation of power system harmonics using Kalman filter methodology. *IEEE Transactions on Power Delivery*, 6(4):1663–1669.

[Bennett, 1993] Bennett, S. (1993). *A History of Control Engineering 1930-1955*. Peter Peregrinus Ltd. on behalf of the Institution of Electrical Engineers.

[Branin, 1967a] Branin, F. H. (1967a). Computer methods of network analysis. *Proceedings of the IEEE*, 55(11):1787–1801.

[Branin, 1967b] Branin, F. H. (1967b). Transient analysis of lossless transmission lines. *Proceedings of the IEEE*, 55(11):2013–2013.

[Clements, 1990] Clements, K. A. (1990). Observability methods and optimal meter placement. *International Journal on Electric Power & Energy Systems*, 12(2):88–93.

[Dommel, 1969] Dommel, H. W. (1969). Digital computer solution of electromagnetic transients in single and multiphase networks. *IEEE Transactions on Power Apparatus and Systems*, 88(4):388–399.

[Dommel, 1987] Dommel, H. W. (1987). *Electromagnetic Transients Program (EMTP) Theory Book*. Bonneville Power Administration, Portland, OR, U.S.A.

[Du et al., 1996] Du, Z.-P., Arrillaga, J., and Watson, N. (1996). Continuous harmonic state estimation of power systems. *Generation, Transmission and Distribution, IEE Proceedings*, 143(4):329–336.

[Espinosa-Juarez and Hernandez, 2007] Espinosa-Juarez, E. and Hernandez, A. (2007). A method for voltage sag state estimation in power systems. *IEEE Transactions on Power Delivery*, 22(4):2517–2526.

[Farzanehrafat, 2014] Farzanehrafat, A. (2014). *Power Quality State Estimation*. PhD thesis, University of Canterbury, Christchurch, New Zealand.

[Farzanehrafat and Watson, 2013] Farzanehrafat, A. and Watson, N. R. (2013). Power quality state estimator for smart distribution grids. *IEEE Transactions in Power Systems*, 28(3):2183–2191.

[Gao et al., 2003] Gao, W., Solodovnik, E., Dougal, R., Cokkinides, G., and Sakis-Meliopoulos, A. P. (2003). Elimination of numerical oscillations in power system dynamic simulation. In *Eighteenth Annual IEEE Applied Power Electronics Conference and Exposition, APEC'03*, pages 9–13, Miami Beach, U.S.A.

[Grainger and Stevenson, 1994] Grainger, J. J. and Stevenson, W. D. (1994). *Power System Analysis*. McGraw-Hill, Inc.

[Handschin, 1971] Handschin, E. (1971). Real-time data processing using state estimation in electric power systems. In *Proceedings of the symposium on real time control of electric power systems*, pages 29–61, Baden, Switzerland. Brown, Boveri & Company Limited.

[Heydt, 1989] Heydt, G. T. (1989). Identification of harmonic sources by a state estimation technique. *IEEE Transactions on Power Delivery*, 4(1):569–576.

[Heydt, 1991] Heydt, G. T. (1991). *Electric Power Quality*. Starts in a circle publications.

[IEEE, 2007] IEEE (2007). Recommended practice for the design of reliable industrial and commercial power systems. Std. 493-2007.

[Jazwinski, 1970] Jazwinski, A. H. (1970). *Stochastic Processes and Filtering Theory*. Academic Press.

[Kanao et al., 2005] Kanao, N., Yamashita, M., Yanagida, H., Mizukami, M., Hayashi, Y., and Matsuki, J. (2005). Power system harmonic analysis using state-estimation method for Japanese field data. *IEEE Transactions on Power Delivery*, 20(2):970–977.

[Kuffel et al., 1995] Kuffel, P., Kent, K., and Irwin, G. (1995). The implementation and effectiveness of linear interpolation within digital simulation. In *International Conference on Power Systems Transients, IPST'95*, Lisbon, Portugal.

[Marti and Lin, 1989] Marti, J. R. and Lin, J. (1989). Suppression of numerical oscillations in the EMTP. *IEEE Transactions on Power Systems*, 4(2):739–747.

[Martinez-Velasco et al., 2010] Martinez-Velasco, J. A., Ramirez, A. I., and Davila, M. (2010). *Power System Transients: Parameter Determination*, chapter 2. Overhead lines. CRC Press.

[Matair et al., 2000] Matair, S. S., Watson, N. R., Wong, K. P., Pham, V. L., and Arrillaga, J. (2000). Harmonic state estimation: a method for remote harmonic assessment in a deregulated utility network. In *Proceedings of International Conference on Electric Utility Deregulation and Restructuring and Power Technologies, DRPT 2000*, pages 41–46, London, England.

[Meliopoulos et al., 1994] Meliopoulos, A. P. S., Zhang, F., and Zelingher, S. (1994). Power system harmonic state estimation. *IEEE Transactions on Power Delivery*, 9(3):1701–1709.

[Monticelli, 1999] Monticelli, A. (1999). *State Estimation in Electric Power Systems, A Generalized Approach*. Kluwer's Power Electronics and Power Systems Series.

[Monticelli and Wu, 1985] Monticelli, A. and Wu, F. F. (1985). Network observability: theory. *IEEE Transactions on Power Apparatus and Systems*, 104(5):1042–1048.

[Najjar and Heydt, 1991] Najjar, M. and Heydt, G. T. (1991). A hybrid nonlinear - least squares estimation of harmonic signal levels in power systems. *IEEE Transactions on Power Delivery*, 6(1):282–287.

[Ribeiro et al., 2014] Ribeiro, P. F., Duque, C. A., daSilveira, P. M., and Cerqueira, A. S. (2014). *Power Systems Signal Processing for Smart Grids*. John Wiley & Sons, Inc.

[Schweppe, 1970] Schweppe, F. C. (1970). Power system static-state estimation, part iii: Implementation. *IEEE Transactions on Power Apparatus and Systems*, 89(1):130–135.

[Schweppe and Handschin, 1974] Schweppe, F. C. and Handschin, E. J. (1974). Static state estimation in electric power systems. *Proceedings of the IEEE*, 62(7):972–982.

[Schweppe and Rom, 1970] Schweppe, F. C. and Rom, D. B. (1970). Power system static-state estimation, part ii: Approximate model. *IEEE Transactions on Power Apparatus and Systems*, 89(1):125–130.

[Schweppe and Wildes, 1970] Schweppe, F. C. and Wildes, J. (1970). Power system static-state estimation, part i: Exact model. *IEEE Transactions on Power Apparatus and Systems*, 89(1):120–125.

[Smith, 2012] Smith, H. L. (2012). A brief history of feedback control. [Online] http://arri.uta.edu/acs/history.htm.

[Soliman et al., 1990] Soliman, S. A., Christensen, G. S., Kelly, D. H., and El-Naggar, K. M. (1990). A state estimation algorithm for identification and measurement of power system harmonics. *Electric Power System Research*, 19(3):195–206.

[Sorenson, 1970] Sorenson, H. W. (1970). Least-squares estimation: from Gauss to Kalman. *IEEE Spectrum*, 7(7):63–68.

[Stagg et al., 1970] Stagg, G. W., Dopazo, J. F., Klitin, O. A., and Vanslyck, L. S. (1970). Techniques for the real-time monitoring of power systems operations. *IEEE Transactions on Power Apparatus and Systems*, 89(4):545–555.

[Thomason, 1934] Thomason, J. L. (1934). Impulse generator circuit formulas. *Transactions of the American Institute of Electrical Engineers*, 53(1):169–176.

[Wang et al., 2005] Wang, B., Xu, W., and Pan, Z. (2005). Voltage sag state estimation for power distribution systems. *IEEE Transactions on Power Delivery*, 20(2):805–812.

[Watson, 2010] Watson, N. R. (2010). Power quality state estimation. *European Transactions on Electric Power*, 20(1):19–33.

[Watson and Arrillaga, 2003a] Watson, N. R. and Arrillaga, J. (2003a). Harmonics in large systems. *Electric Power Systems Research*, 66(1):15–29.

[Watson and Arrillaga, 2003b] Watson, N. R. and Arrillaga, J. (2003b). *Power Systems Electromagnetic Transients Simulation*. The Institution of Engineering and Technology.

[Watson and Farzanehrafat, 2013] Watson, N. R. and Farzanehrafat, A. (2013). Identification of the sources of transient disturbances. In *International Conference on Power Systems Transients, IPST2013*, pages 21–25, Vancouver, Canada.

[Watson and Farzanehrafat, 2014] Watson, N. R. and Farzanehrafat, A. (2014). Three-phase transient state estimation algorithm for distribution networks. *IET Generation, Transmission & Distribution*, 8(10):1956–1666.

[Watson et al., 2012] Watson, N. R., Farzanehrafat, A., and Perera, S. (2012). Power quality state estimation: a new concept. In *EEA conference & exhibition 2012*, Auckland, New Zealand.

[Watson and Irwin, 1998] Watson, N. R. and Irwin, G. D. (1998). Electromagnetic transient simulation of power systems using root-matching techniques. *Generation, Transmission and Distribution, IEE Proceedings*, 145(5):481–486.

[Watson and Yu, 2008] Watson, N. R. and Yu, K. K. C. (2008). Transient state estimation. In *13th International Conference on Harmonics and Quality of Power, ICHQP 2008*, Wollongong, Australia.

[Wu, 1990] Wu, F. F. (1990). Power system state estimation: a survey. *International Journal of Electrical Power & Energy Systems*, 12(2):80–87.

[Yu, 2005] Yu, K. K. C. (2005). *Harmonic State Estimation and Transient State Estimation*. PhD thesis, University of Canterbury, Christchurch, New Zealand.

[Yu and Watson, 2004] Yu, K. K. C. and Watson, N. R. (2004). Influence of transformer configuration on measurement placement in harmoninc state estimation. In *International Conference on Power Systems Technology, POWERCON 2004*, pages 176–181, Singapore.

[Yu and Watson, 2005] Yu, K. K. C. and Watson, N. R. (2005). Identification of fault locations using transient state estimation. In *International Conference on Power Systems Transients, IPST'05*, pages 19–23, Montreal, Canada.

[Yu and Watson, 2007] Yu, K. K. C. and Watson, N. R. (2007). An approximate method for transient state estimation. *IEEE Transactions on Power Delivery*, 22(3):1680–1687.